ARMY RESEARCH LABORATORY

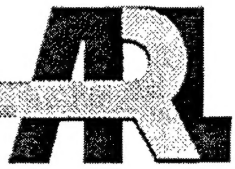

Comprehensive Visualization of Interface Defeat-Based Ballistic Impact Damage in a Titanium Carbide (TiC) Ceramic Target Disk

by William H. Green, Joseph M. Wells,
and Nevin L. Rupert

ARL-TR-2565 September 2001

The findings in this report are not to be construed as an official Department of the Army position unless so designated by other authorized documents.

Citation of manufacturer's or trade names does not constitute an official endorsement or approval of the use thereof.

Destroy this report when it is no longer needed. Do not return it to the originator.

Army Research Laboratory
Aberdeen Proving Ground, MD 21005-5069

ARL-TR-2565 September 2001

Comprehensive Visualization of Interface Defeat-Based Ballistic Impact Damage in a Titanium Carbide (TiC) Ceramic Target Disk

William H. Green, Joseph M. Wells, and Nevin L. Rupert
Weapons and Materials Research Directorate, ARL

Abstract

This study was initiated to demonstrate the feasibility of applying the state-of-the-art nondestructive testing methodology known as x-ray computed tomography (CT) to a ballistic damage assessment. Specifically desired is the capture, digitization, and display, in both two-dimensional (2-D) and three-dimensional (3-D) formats, of the actual mesocracking damage created in bulk ceramic targets following an interface defeat or dwell ballistic impact experiment. Dwell involves the delay, and interface defeat involves the prevention, of penetration by a long rod penetrator into the ceramic. In each mechanism, the penetrator material contacting the ceramic front face flows laterally. These mechanisms occur at or near the impacted front surface of a highly confined armor ceramic material and may result in considerable subsurface or interior damage. This study also reports on the development of a new capability to graphically represent the full assemblage of networked interior mesocracks by an isolated 3-D point cloud or wireform model which aids significantly in the visualization and understanding of the entire mesocracking damage network. Practical limits of image spatial resolution with this technique (≈400 μm for large volume samples) preclude the nondestructive characterization of the detailed microcracking damage at this time.

Acknowledgments

The authors would like to acknowledge the most professional support of George Hauver for sharing both his TiC armor ceramic disk sample and his insight and knowledge of interface defeat. Also, we would like to sincerely thank Drs. J. LaSalvia, A. Wereszczak, K. Doherty, J. Beatty, and A. Dietrich for their comments and efforts in reviewing this manuscript.

INTENTIONALLY LEFT BLANK.

Contents

List of Figures

List of Tables

INTENTIONALLY LEFT BLANK.

1. Introduction

Bless et al. (1992) achieved interface defeat with a titanium diboride (TiB_2) ceramic tile with a loss of ceramic to only a depth of 5.5 mm. Hauver et al. (1994) subsequently demonstrated the phenomenon of interface defeat using a highly confined target disk with several ceramics, including silicon carbide (SiC), titanium carbide (TiC), TiB_2, and tungsten carbide (WC). Lundberg et al. (2000) and LaSalvia et al. (2000) have recently reported on the transition between interface defeat and penetration. While the actual penetration of the projectile into the ceramic is very limited with the occurrence of interface defeat, there is, nevertheless, considerable subsurface internal damage in the target ceramic ahead of the ceramic boundary. This damage consists mainly of a comminuted zone of pulverized ceramic containing both microcracks and voids and, frequently, a larger network of considerable mesocracking. The mesocracks are of conical, radial, and lateral (laminar) orientation and are generally between about 10^2–10^3 μm in width. Similar subsurface cracking damage has also been described by Shockey et al. (1990) using destructive sectioning.

1.1 Intrinsic Mesocracking Damage

Ballistic evaluations frequently concentrate on in-situ flash x-ray diagnostics and post-mortem penetration (e.g., DOP, V_{50}, etc.) measurements, all of which are extrinsic to the internal damage of the target material. Characterization of the internal impact damage in ceramic targets is normally limited to impact surface fractography and random through-thickness sectioning for polishing and ceramographic examination. The latter is seldom done in sufficient amount to capture a detailed understanding of the intricate and complex nature of the intrinsic three-dimensional (3-D) mesocracking portion of the ballistic damage.

Such mesocracks seriously reduce the capability of the ceramic material in resisting penetration from subsequent impacts (Hauver et al. to be published). Indeed without lateral confinement, the ceramic with developing mesocracks would shatter under a single ballistic impact and would not achieve the condition of interface defeat at all. If the mesocracking can be reduced, modified, or eliminated, the structural integrity of the ceramic and its intrinsic resistance to penetration can be improved substantially. First, however, one needs to be able to accurately observe and measure the nature and extent of this mesocracking damage nondestructively. Thus, our objective was to develop a methodology that allows the detection, measurement, and the 3-D visualization of the resulting mesocracking damage. Destructive sectioning for microscopic examination of either the micro- or mesocracked areas also can be utilized to further evaluate the intrinsic ceramic damage. It was felt that the availability of this tool would prove

useful in the selection of destructive sectioning locations and in the evaluation of the ballistic confinement design as well. This tool may then lead to an improved understanding of the impact damage that limits ballistic performance. Subsequently, it may also assist in the optimization of the intrinsic capability of the target ceramic material and their confinement designs to increase dwell (LaSalvia et al. 2000), resist penetration and, ultimately, to better fully defeat the impacting penetrator.

1.2 Ballistic Testing Approach

The resistance of a ceramic target material to ballistic penetration is known to be influenced by the design configuration of the target assembly, the severity of the projectile threat, and the structure/properties of the confined ceramic target material (Figure 1).

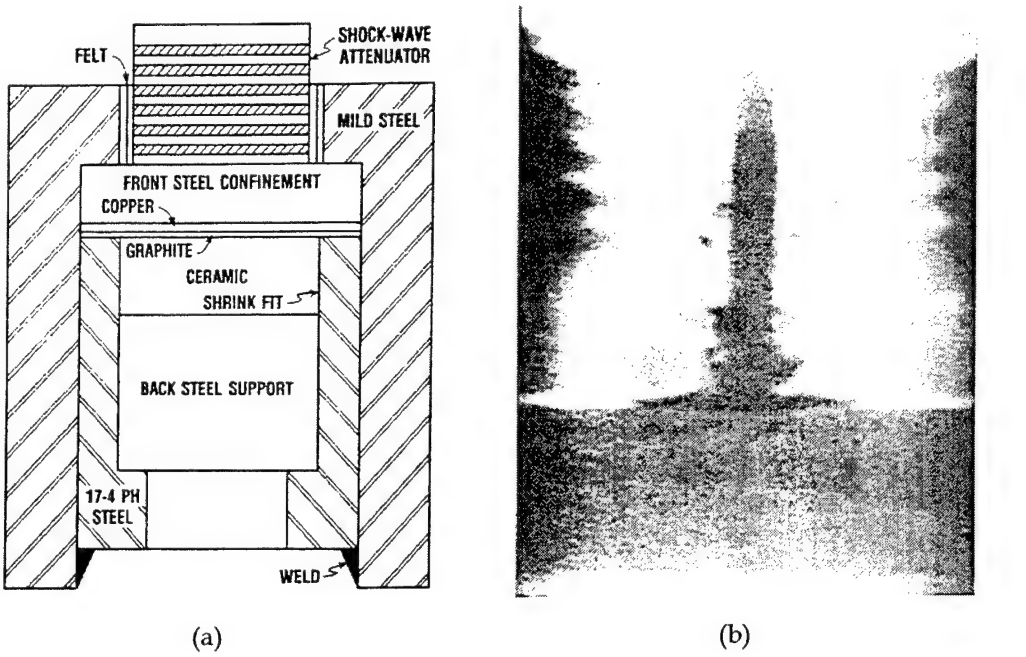

Figure 1. Depictions of (a) schematic of heavy constraint ballistic test fixture and (b) flash x-ray of the penetrator experiencing interface defeat at the front surface of the TiC disk. Not to scale (Hauver et al. to be published).

The heavy constraint apparatus used by Hauver et al. (1994) for confining the TiC ceramic sample disk during the ballistic impact testing is shown schematically in Figure 1(a). A high-speed flash radiograph showing the interface defeat of the impacting penetrator with lateral flow at the front surface of the TiC disk is shown in Figure 1(b). The penetrator was a 90% W alloy short rod with a length-to-diameter ratio (L/D) = 20, and impacted the target at a contact velocity of about 1,600 m/s.

1.3 TiC Sample Description

The TiC ceramic sample utilized in this study was provided by George E. Hauver and is one-half of a 72-mm-diameter × 25-mm-thick ceramic target disk section (Figures 2[a] and [b]). A higher magnification view of the sample cross section containing the comminuted zone and the mesocracking is more clearly shown in Figure 3.

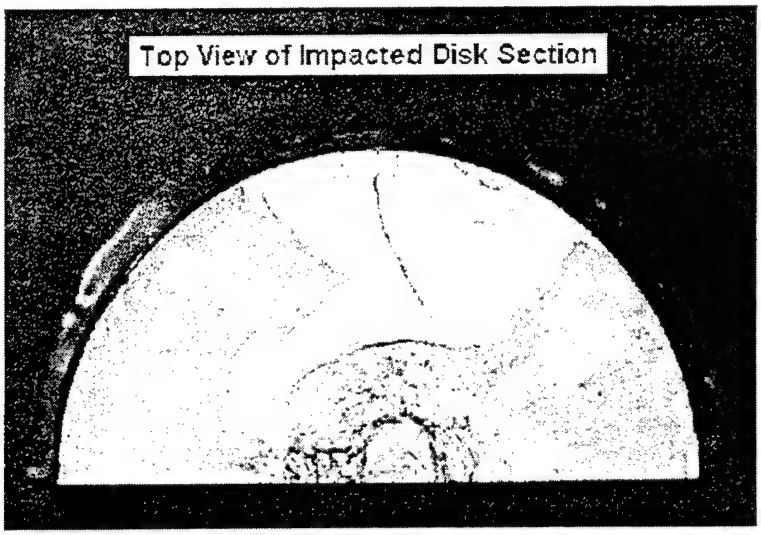

a. Macrophotograph of TiC ceramic half-disk, 72-mm in diameter, showing front (interface defeat) impact surface.

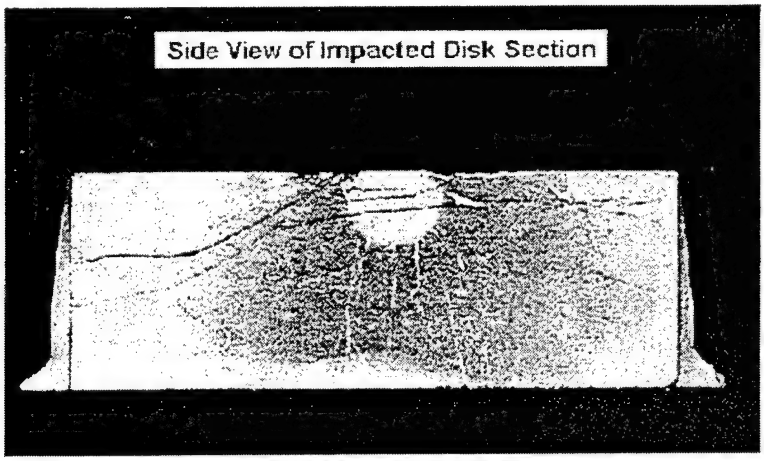

b. Macrophotograph of TiC ceramic half-disk, 25 mm thick, showing comminuted microdamaged zone (light circular area) and mesocracking through the thickness of cross section.

Figure 2. Macrophotograph of TiC ceramic half-disk showing impact surface and damaged zone.

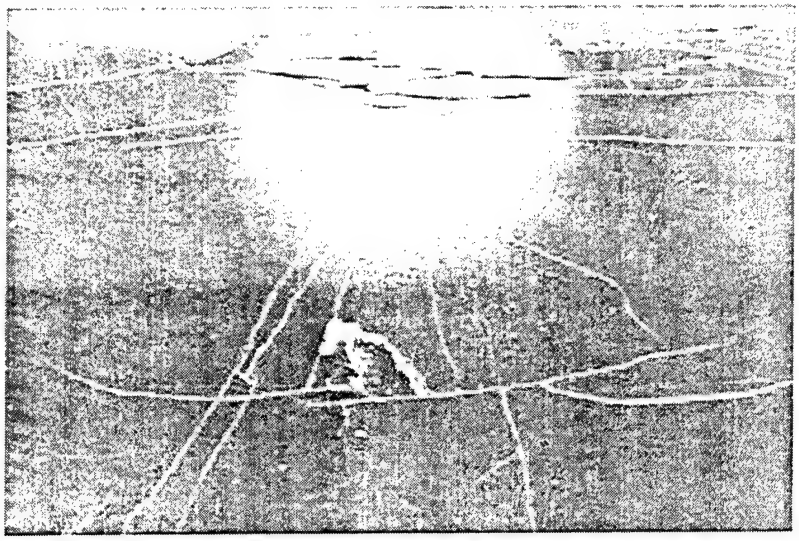

Figure 3. Closer view of the comminuted zone (light circular area) and the prominent mesocracking in TiC disk (LaSalvia et al. 2000).

2. X-ray Computed Tomography (CT) Method

2.1 Principles and Technique

Figure 4 schematically shows the rotate-only (RO) x-ray CT technique. The x-ray source and detector remain stationary. The object remains stationary relative to the turntable. The collimated horizontal fan beam "scans" a slice of the object, as the turntable rotates 360°. The height above the turntable and thickness of the slice are known. A set of attenuation line integrals is generated from the scan. The line integrals can be conceptually grouped into subsets referred to as "views." Each view corresponds to a set of ray paths through the object from a particular direction. The views are also referred to as "projections" or "profiles," while each individual datum within a given projection is referred to as a "sample," or often just a "data point."

A state-of-the-art scanner routinely collects millions of measurements per scan, each one accurately quantified and precisely referenced to a specific line of sight through the object of interest. The views from the scan are passed to the reconstruction algorithm for processing (Stanley 1985). The CT reconstruction process yields a two-dimensional (2-D) array of numbers corresponding to the cross section of the object. This 2-D array of numbers (i.e., densitometric gray levels) is the CT image.

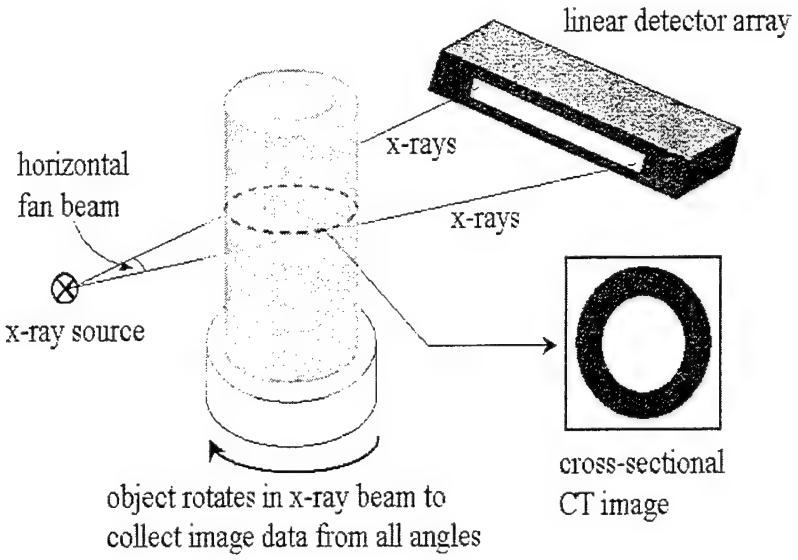

Figure 4. Schematic of RO CT scan technique.

2.2 3-D Volume Reconstruction

The excellent dimensional accuracy and the digital nature of CT images allow the accurate volume reconstruction of multiple adjacent slices. The slices are "stacked" to provide 3-D information throughout the entire object or a section of the object. Two ways of visualizing volumetric data are multiplanar reconstruction (MPR) and 3-D reconstruction. MPR (visualization) displays top, front, side, and oblique slices through the object. The orientation of the top slice is parallel to the cross-sectional image plane. The front slice is orthogonal to the top slice. The side slice is orthogonal to both the top and front slices. The oblique slice can be placed on any one of the other three slices. The MPR display is similar to an engineering drawing. However, each view (i.e., top, front, side, and oblique) is a slice with finite thickness through the object, not a 2-D projection. The top, front, and side slices can be moved anywhere in the reconstructed volume. The oblique slice can be rotated through 360°.

The volumetric data is displayed as a 3-D solid object in 3-D reconstruction, and the orientation of the solid in space can be changed to facilitate different views. The solid can also be "virtually" sectioned by only displaying part of the reconstructed volume, which creates a "virtual" cutting plane on the solid showing the x-ray density values on that plane. This plane may be orthogonal to the cross-sectional image plane. In effect, virtual sectioning shows the exposed surface as it would look if the object were actually destructively sectioned along that plane.

2.3 3-D Point Cloud Generation

As previously stated, a CT image is a 2-D array of densitometric gray levels (i.e., CT densities). For example, a 12-bit image would have 4,096 levels of gray from black to white, with darker (blacker) normally indicating less x-ray attenuation and lighter (whiter) indicating more attenuation. The field of image processing is much too large to discuss in detail here, but it is sufficient to state that different materials in an image can be visually delineated to a high degree using various image processing techniques based upon their attenuation characteristics. In fact, black (gray level = 0) and white (gray level = 4,095) images can be generated using appropriate contrast enhancement. This is normally done to accurately define material (white) boundaries. Any number of black and white (i.e., binary) images can be vertically stacked to generate a 3-D point cloud, in which the set of points in space defines the internal and external surfaces of the object. Furthermore, a point cloud can be "polygonized" or made into a wireform model.

3. Experimental Technique

3.1 CT Equipment

The TiC half-disk was examined using a customized ACTIS 600/420 CT system designed and constructed by Bio-Imaging Research (BIR), Inc. and installed at the U.S. Army Research Laboratory (ARL) at Aberdeen Proving Ground (APG), MD. It has a 420 keV x-ray tube with two focal spot sizes and a 160 keV microfocus x-ray tube with four focal spot sizes, the smallest being 10 μ. It also has a linear detector array (LDA) and an image intensifier (II) with a zoom lens and a charged-coupled device camera. CT scanning can be done using the LDA or the II. The system can scan in RO and offset-RO mode using either source and the LDA or the II, and in translate-rotate (TR) mode using the LDA and either source. It can also perform digital radiography (DR) scans using the LDA or II.

3.2 CT Technique and Image Resolution

The entire height of the TiC sample was scanned perpendicular to the impact face in TR mode with the sectioned surface resting on the turntable. The source-to-object distance (SOD) and source-to-image distance (SID), were 662.8 mm and 930.0 mm, respectively. The slice thickness and increment were 0.50 mm and 0.20 mm, respectively, resulting in overlapping scans. Overlapping scans generally improve MPR and 3-D solid images because they result in better quality attenuation data (i.e., better photon statistics) in the overlapping regions. Each slice was reconstructed to a 1,024 × 1,024 image matrix using 1,238 views. Scan time was about 25 min/slice with 183 slices required to scan the entire

sample. The scan configuration used the 420 keV tube with the LDA. The tube energy and current used were 350 keV and 2.5 mA, respectively, and the focal spot was 0.8 mm.

A second set of CT scans was also conducted parallel to the impact face in RO mode with the back face resting on the turntable. The SOD and SID were 747.6 mm and 950.0 mm, respectively. The slice thickness and increment were both 0.50 mm, resulting in contiguous scans. The scan configuration used the 420 keV tube with the LDA. The tube energy and current used were 415 keV and 2.0 mA, respectively, and the focal spot was 0.8 mm.

Table 1 lists approximate image resolution achieved for the different modes of image visualization.

Table 1. Summary of visualization modes and image spatial resolution for TiC mesocracking data.

Visualization Mode	View Description	Image Spatial Resolution
2-D CT Slice	Traditional cross section plane orthogonal to vertical axis	≈ 400 μm
MPR Pseudo 3-D	Arbitrary multiplanar slices	≈ 400 μm (500 μm in z direction)
3-D Solid (with or without cut sections)	Oblique view showing cracks within base TiC material	≈ 400 μm (500 μm in z direction)
3-D Point Cloud (polygon/wireform model)	3-D view of crack network only with base material removed	≈ 400 μm (500 μm in z direction)[a]

[a] Assumes point cloud is not significantly under sampled.

4. TiC Results

4.1 Digital Radiography and 2-D CT Slice

A digital radiograph in the through-thickness direction and three CT slices are shown in Figure 5. The vertical position of each slice is shown on the DR by dashed lines. The purely vertical streaking in the DR and the moiré fringe

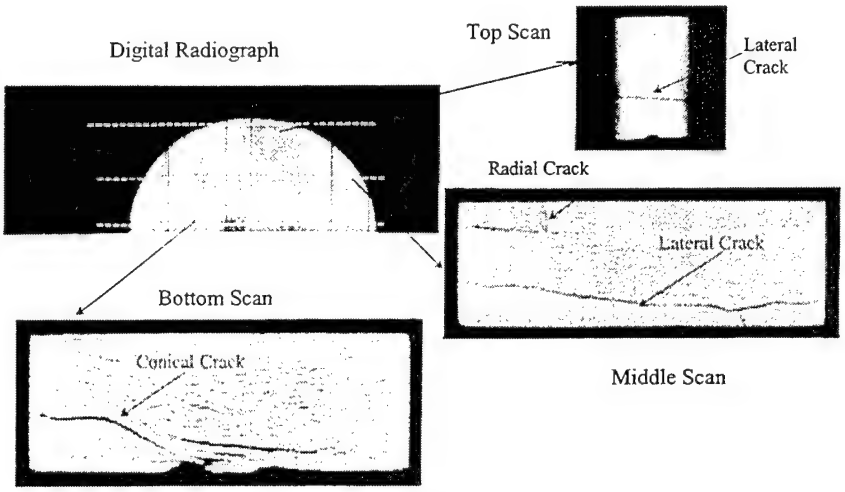

Figure 5. DR and 2-D CT slices in TiC sample.

pattern in the bottom CT slices are image artifacts. Mesocracking damage is readily apparent in both the DR and CT slices, even with the artifacts. The impact face is at the bottom of each slice.

4.2 MPR Visualization

Figure 6 is a MPR visualization of the entire sample with the top slice view parallel to the image plane. The top slice view is 18.18 mm from the sectioned surface; all the views show crack damage. The front slice and side slice views show the distribution of damage perpendicular to and in the through-thickness direction, respectively, for those slices. The oblique slice view shows an area of concentrated damage, which is comminuted ceramic material, in the immediate vicinity of the sectioned surface and additional cracking damage shaped roughly like a ring between the top and the sectioned surface. The oblique angle is 5° from the horizontal in the top slice view.

Figures 7(a)–(c) are top slice and front slice views with increasing distance into the sample interior moving away from the impact surface. The mesocracking damage in slices perpendicular to the through-thickness direction changes with distance into the sample interior.

A radial mesocrack is seen at the 5 o'clock position in the front slice views in Figures 7(a) and (b). Figures 8(a)–(c) are top slice and side slice views with different side slice locations. The side slice locations in the figures are 26.89 mm, 15.61 mm, and 5.64 mm to the left of the axis of the sample, respectively. The series of side slice views shows how both conical and lateral cracking damage in the thickness direction change with distance from the line of impact.

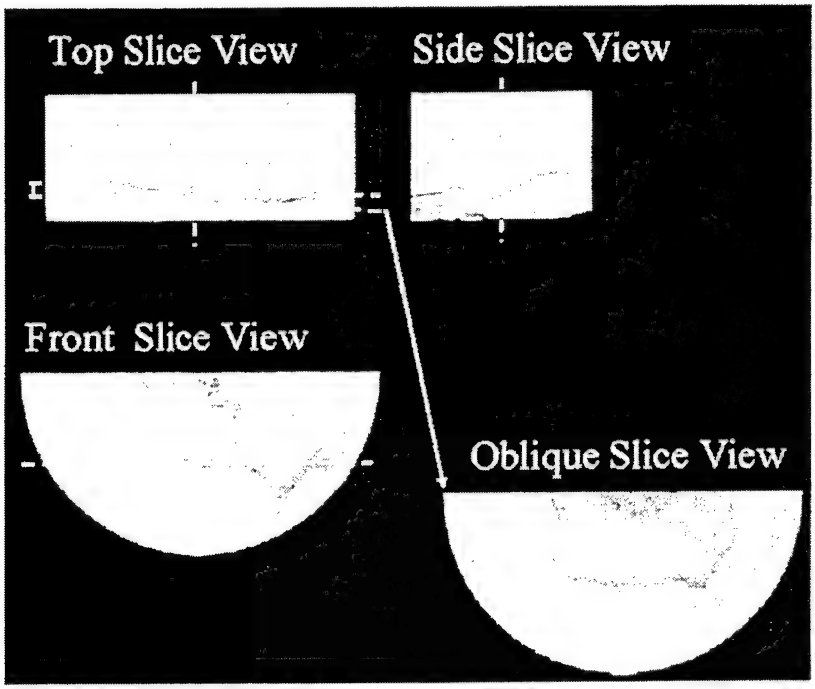

Figure 6. MPR visualization of TiC sample.

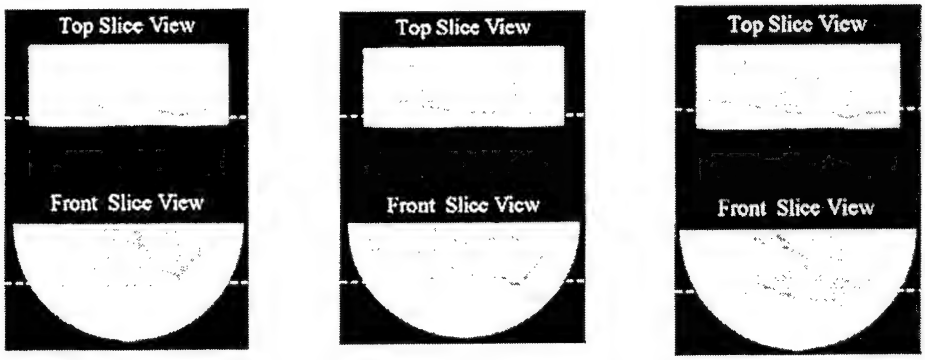

(a) 2.98 mm from impact face (b) 3.98 mm from impact face (c) 5.97 mm from impact face

Figure 7. Top and front slice views with different front slice distances from impact face into TiC sample interior.

4.3 3-D Solid Visualization

Figures 9(a)–(c) are 3-D solid visualizations showing different virtual surfaces. Figure 9(a) shows the entire sample and accurately reflects the damaged condition of the impact face. Figure 9(b) shows the sample with approximately one-half of it virtually cut off; conical and lateral cracking damage is readily apparent. Figure 9(c) shows the sample with two virtual cuts, the first

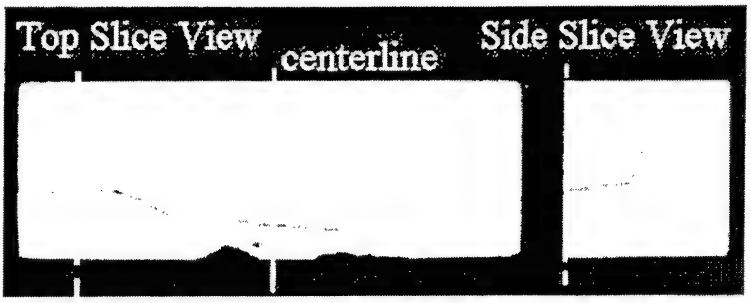

(a) 26.89 mm from axis

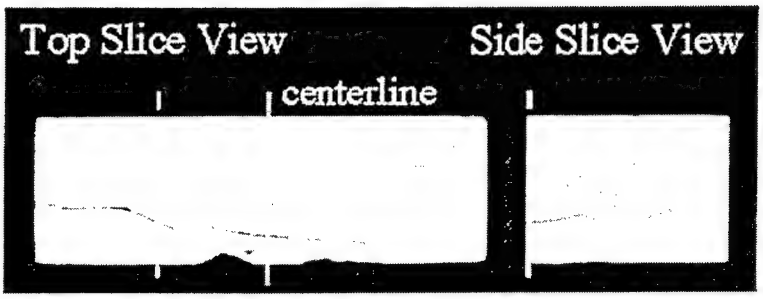

(b) 15.61 mm from axis

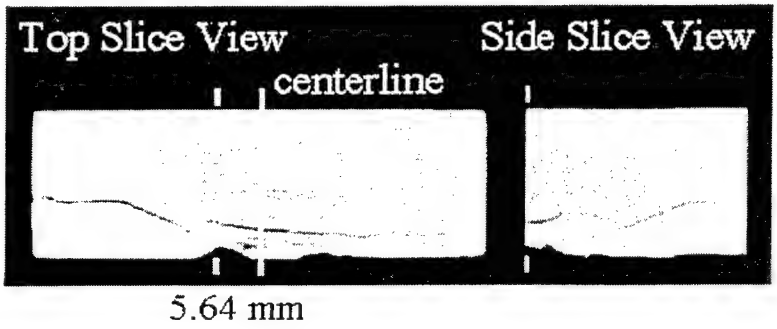

(c) 5.64 mm from axis

Figure 8. Top slice and side slice views with different side slice distances from axis (centerline) showing conical and laminar mesocracking.

being the same as in Figure 9(b). The sectioned surfaces appear as if the sample was actually cut at those surfaces. This is an effective way to visualize damage on sectioned planes in particular locations/directions while maintaining its registration to the entire original sample. The sample material is still represented in opaque bulk form and thus blocks access to contiguous damage features on adjacent slices not currently in view. A more comprehensive set of 3-D solid visualizations is presented in Appendix A.

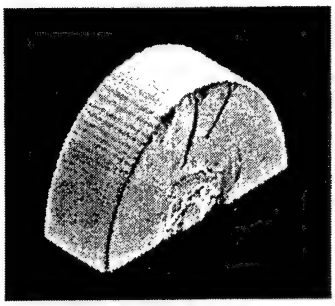

(a) Original sample

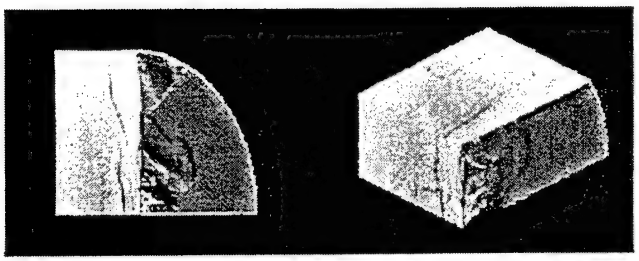

(b) One-half of the sample (c) Two-cut section

Figure 9. 3-D solid visualizations of TiC sample.

4.4 3-D Point Cloud and Wireform Visualization

It is difficult, therefore, to conceptualize the entire network of the mesocracking from these virtual surface views. It would be very tedious to look at hundreds or even thousands of these 2-D, MPR, or 3-D solid 3-D views to try to "get a complete picture" of the internal mesocracking. However, a 3-D point cloud provides the desired kind of information about the cracking pattern. The first step in obtaining the point cloud is to perform the required image processing to "clean up" undesirable image features or artifacts. DUP Technologies plug-in routines contained in the Adobe PhotoDeluxe Business Software were used to enhance the appearance of the CT scans. These routines do not add further detail beyond that present in the original scans. They do, however, allow the enhancement of sharpness in the scans by defining edges, reducing the dotted, grainy appearance of the scans, and removing moire patterns.

The moire fringe pattern removal routine also appeared to have the effect of removing very thin, faint crack damage. Figure 10 shows a CT slice near the sectioned surface of the sample to which this technique has been applied. The fringe pattern has been mostly removed with only a few vestiges of it remaining in and around the center of the image.

Figure 10. A preprocessed image.

The next step is to determine the best gray level to use to threshold and binarize (i.e., show only two gray levels or black and white) the images. This is done by "line profiling" the feature or features of interest in the image, as shown in Figure 11. Normally the full-width-half-maximum value, which is the gray level halfway between the minimum and maximums of the profile, is used. The result of binarizing the image in Figure 10, based on the profile in Figure 11, is shown in Figure 12 in which the crack damage along with some comminuted damage, are black and undamaged material is white.

Figure 11. Gray level line profile through a crack.

Figure 12. Preprocessed, thresholded, and binarized image.

Any number of binary images like the one shown in Figure 12 can be volumetrically combined to generate a 3-D point cloud describing "boundaries" of the cracking damage and comminuted ceramic material. In fact, the 51 binary images created from the RO CT slices throughout the volume of the sample were combined to generate a 3-D point cloud in order to describe the mesocracking and comminuted damage as they are located in the sample.

A systematic sampling technique was applied to decrease the amount of data and make the point cloud more visually informative, since the point cloud contained more points than were necessary for data analysis. Figure 13 shows the resulting point cloud, in which the x-direction is to the left and the z-direction is rotated 20° counterclockwise (i.e., out of the page) from vertical about the x-axis. The z-direction relative to the sample is from the back face to the impact face. Therefore, the point cloud is oriented such that the semicircular impact face, which is physically at the top of the image, is being viewed obliquely. Also, the sectioned edge along the diameter on the back face is physically at the bottom of the image. BIR ACTIS software was used to perform the line profiling, create binary images, and generate point cloud data. SURFACER software by SDRC/Imageware, Inc. was used to visualize the point cloud data.

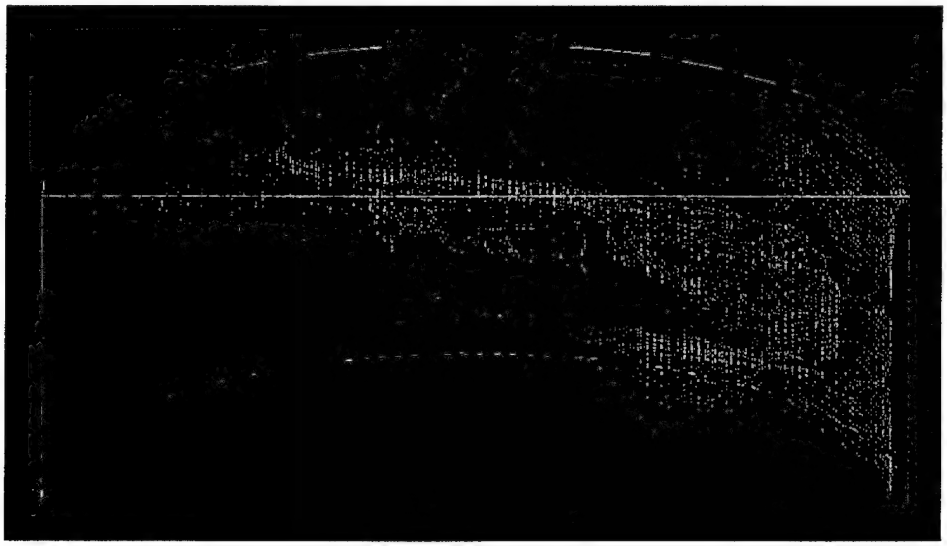

Figure 13. A 3-D point cloud (wireform) visualization of the entire mesocracking network.

While Figure 13 is a much more comprehensive image than those previously shown, it is the first static visualization of the *entire* TiC mesocracking damage pattern. This damage pattern is observed to be very asymmetrical with the largest damage volume (laminar and radial cracks) on the right hand side of this figure. In the upper center of the figure, an intermixing of mainly conical and laminar cracking is observed. Most of this cracking damage appears to be contiguous and perhaps interconnected, although distinct isolated cracking areas are observed in the lower center. A dynamic multi-axial rotating 3-D computer image reveals these features in a more comprehensible fashion, as shown in Appendix B.

5. Summary and Conclusions

We have demonstrated four different nondestructive methods (i.e., 2-D CT, MPR pseudo 3-D, 3-D solid, and 3-D point cloud or wireform) of visualization of the mesoscale cracking in a TiC ceramic target sample resulting from an interface defeat ballistic impact experiment. All four methods described herein allow increased visualization of the interior mesocracking at known depths within the sample. Normal digital x-rays provide no such flexibility of depth into the interior specimen thickness. The details of the complex and interwoven cracking patterns of the different constitutive cracking types are revealed with the point cloud image in a still complex yet more comprehensible perspective. The 3-D geometry and depth profile of such internal mesocracking damage has now become more easily visualized. Utilizing 3-D solid rotation software, one can further examine the point cloud mesocracking image from multiple orientations. While the image spatial resolution is insufficient to examine the microcracking damage directly, the described visualization techniques can assist in the selection of judicious locations for further destructive sectioning and subsequent high magnification ceramographic analysis. This microcracking has been considered recently by LaSalvia et al. (2000) through destructive examination and mechanistic modeling.

We have demonstrated also that the x-ray CT scanning technique is a viable and potentially useful tool in the detection and assessment of ballistic impact damage in brittle ceramic target materials. This tool may also be applied to assess damage resulting from configuration design changes as well as material modifications. While not yet able to separate the ensemble of each of the separate constituent cracking damage types, one can appreciate the convolution of their individual ensembles in the assymetrical overall mesocracking damage network. Further work is needed to develop the capability of deconvoluting the point cloud or wireform image into the constituent mesocracking types for semi-quantitative 3-D analysis. Such a deconvolution methodology would permit the individual cracking types to be independently assessed both geometrically as well as semi-quantitatively.

Finally, Grace (1997; 2000) has suggested that a combination of stress analysis and damage observations may point to possible ceramic failure mechanisms. It is thus desirable to eventually superimpose a computational volumetric stress analysis map over the volumetric mesocracking map (wireform) in order to examine damage correlations and to make comparisons to the explicit geometrical ballistic damage predictions of mechanistic mesodamage models as they become available.

6. References

Bless, S. J., M. Benyami, L. S. Apgar, and D. Eylon. "Impenetrable Ceramic Targets Struck by High Velocity Tungsten Long Rods." Proceedings of 2nd International Conference on Structures Under Shock and Impact, Portsmouth, UK, 16–18 June 1992.

Grace, F. I. "Elastic Response and Potential Damage Zones in Ceramic Target Materials For Interface Defeat Under Rod Impact Conditions." Presented at International Ceramic Working Group Meeting (DOD/DOE), Aberdeen Proving Ground, MD, 23–24 April 1997.

Grace, F. I. "Interface Defeat of Impacting Rods Against Ceramic Targets." Proceedings of Explomat 2000, June 2000.

Hauver, G. E., P. H. Netherwood, R. F. Benck, and L. J. Kecskes. "Enhanced Ballistic Performance of Ceramic Targets." 19th Army Science Conference, Orlando, FL, 20–24 June 1994.

Hauver, G. E., P. H. Netherwood, R. F. Benck, and E. J. Rapacki. "Interface Defeat of Long Rod Projectiles by Ceramic Armor." U.S. Army Research Laboratory, Aberdeen Proving Ground, MD, to be published.

LaSalvia, J. C., E. J. Horwath, E. J. Rapacki, C. J. Shih, and M. A. Meyers. "Microstructural and Micromechanical Aspects of Ceramic/Long-Rod Projectile Interactions: Dwell/Penetration Transitions." Proceedings of Explomat 2000, June 2000.

Lundberg, P., R. Renstrom, and B. Lundberg. "Impact of Metallic Projectiles on Ceramic Targets: Transition Between Interface Defeat and Penetration." *International Journal of Impact Engineering*, vol. 24, no. 3, pp. 259–275, March 2000.

Shockey, D. A., A. H. Marchand, S. R. Skaggs, G. E. Cort, M. W. Burkett, and R. Parker. "Failure Phenomology of Confined Ceramic Targets and Impacting Rods." *International Journal of Impact Engineering*, vol. 9, no. 3, pp. 263–275, 1990.

Stanley, J. H. "Physical and Mathematical Basis of CT Imaging." American Society for Testing and Materials CT Standardization Committee, E7.01.07, 1985.

INTENTIONALLY LEFT BLANK.

Appendix A. Virtual Sectioning of Titanium Carbide (TiC) Disk Using Three-Dimensional (3-D) Solid Visualization

INTENTIONALLY LEFT BLANK.

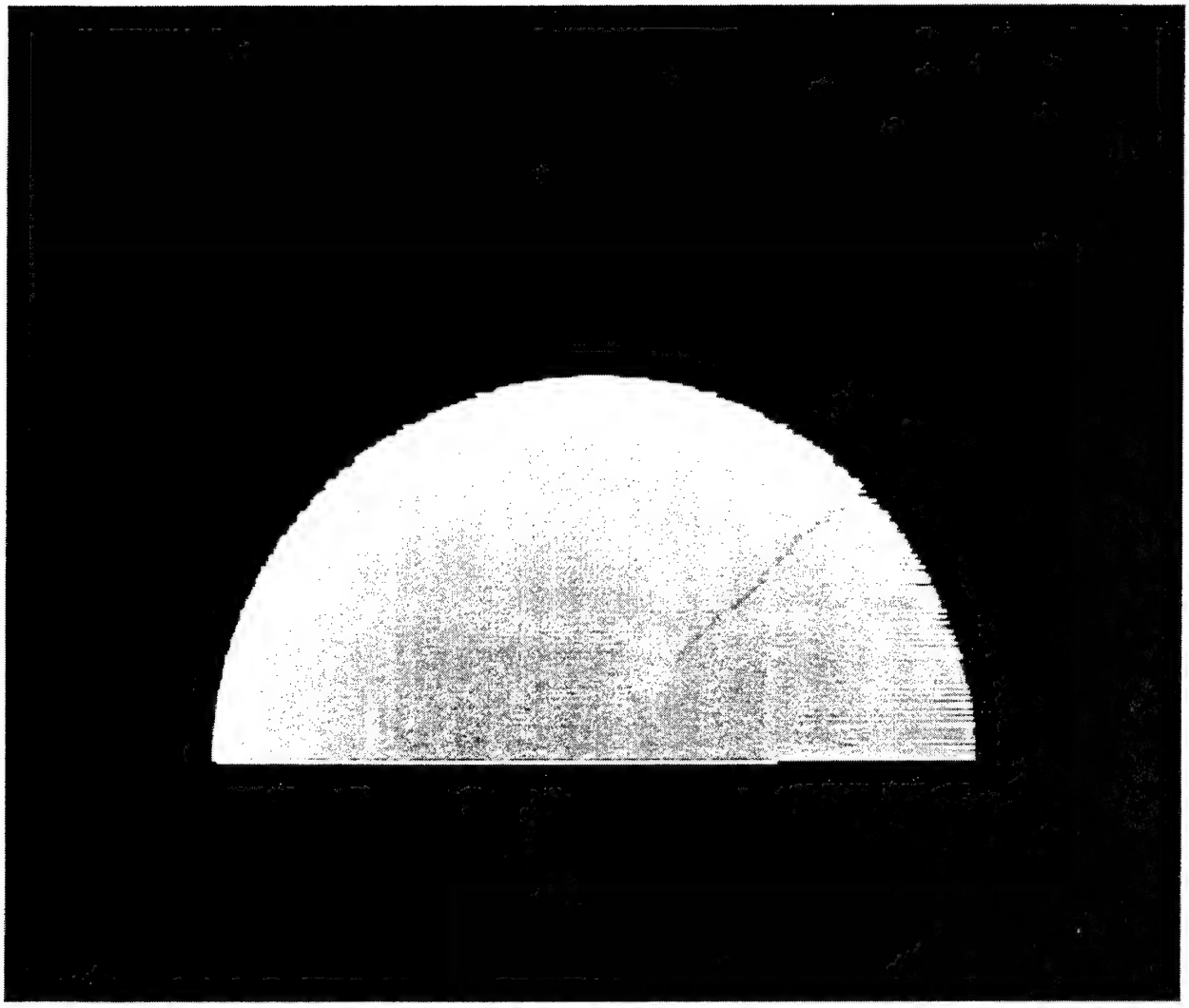

Figure A-1. 0.89 mm from bottom of disk with 65° rotation about X-axis.

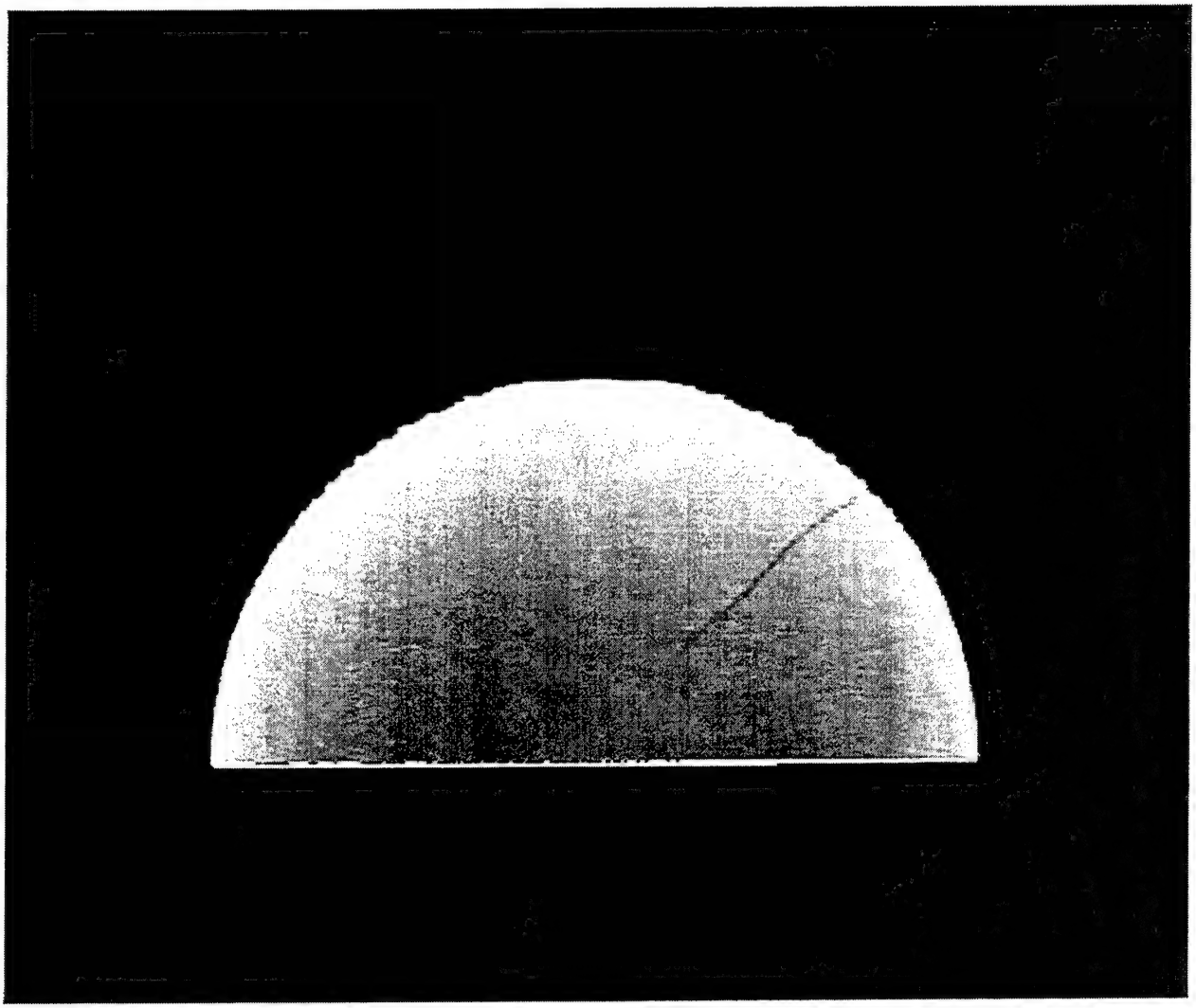

Figure A-2. 1.58 mm from bottom of disk with 65° rotation about X-axis.

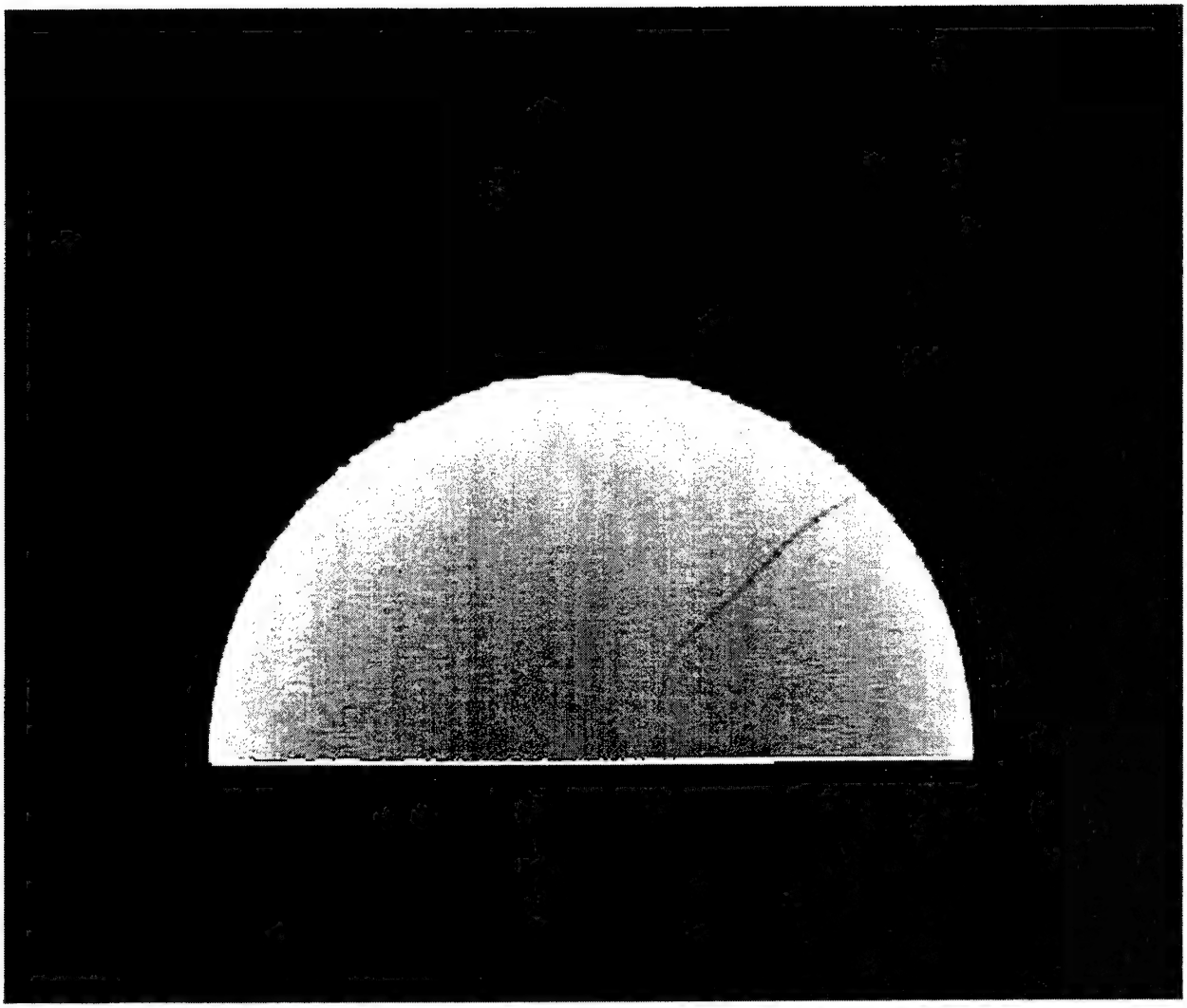

Figure A-3. 1.87 mm from bottom of disk with 65° rotation about X-axis.

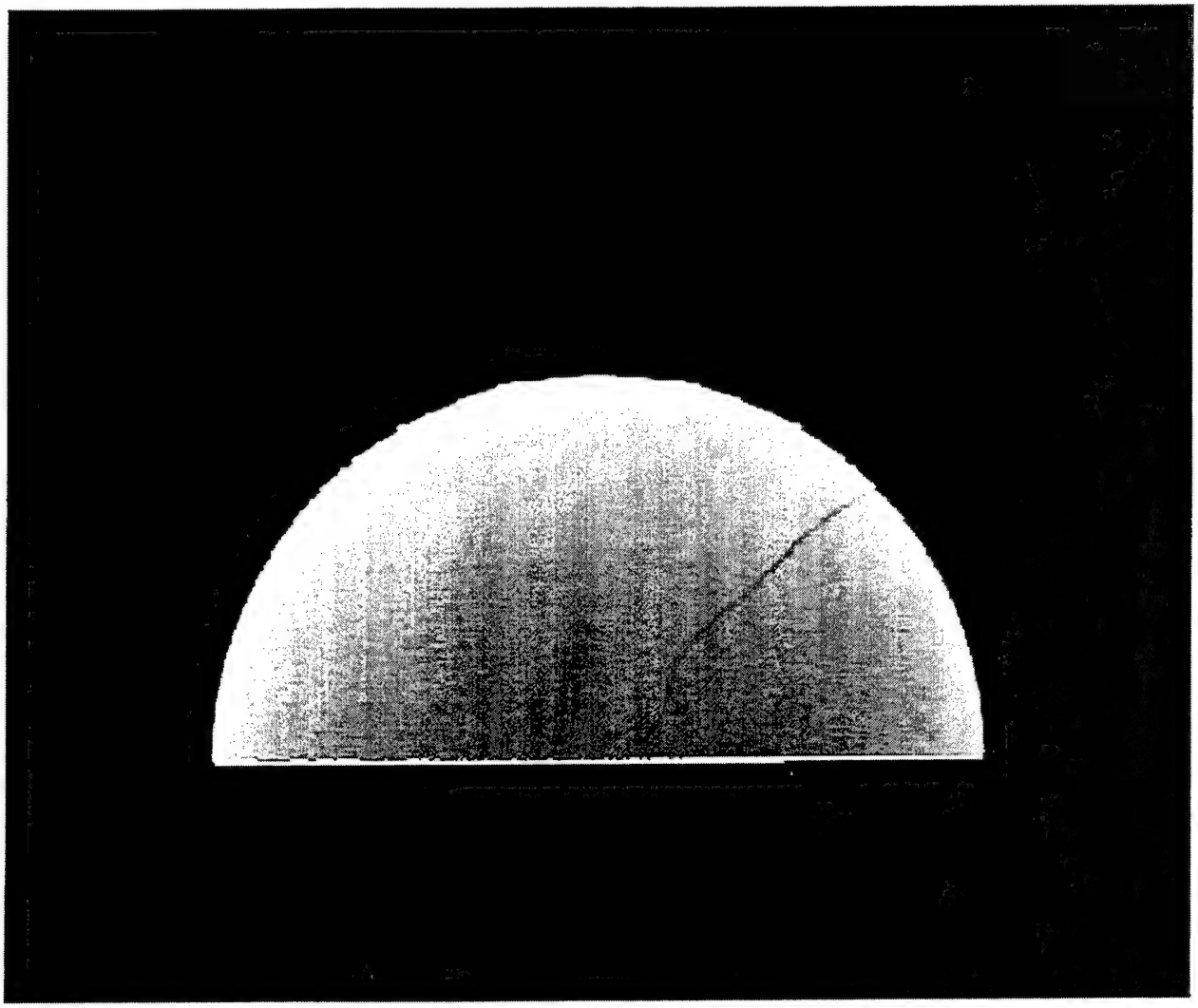

Figure A-4. 2.60 mm from bottom of disk with 65° rotation about X-axis.

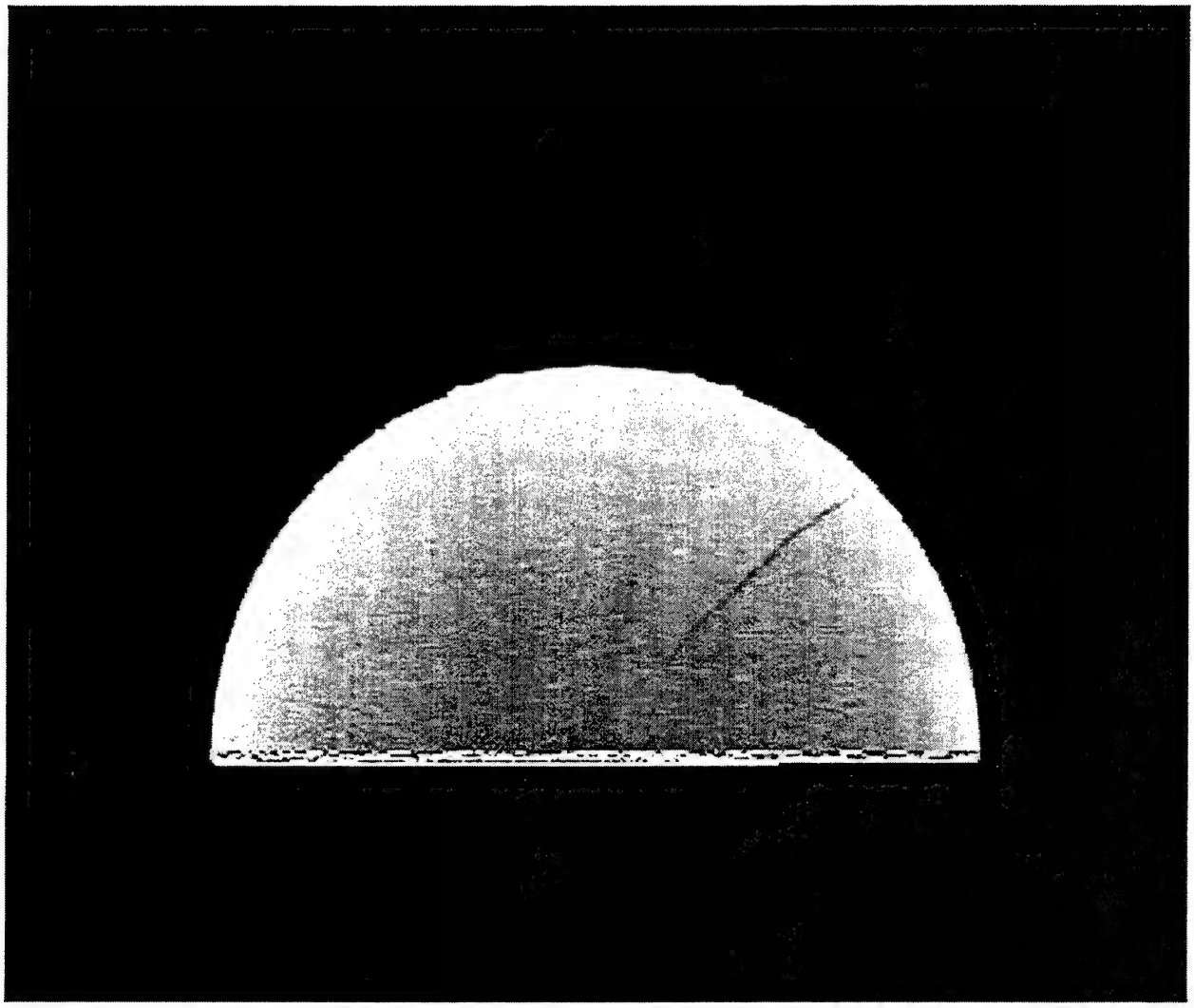

Figure A-5. 3.09 mm from bottom of disk with 65° rotation about X-axis.

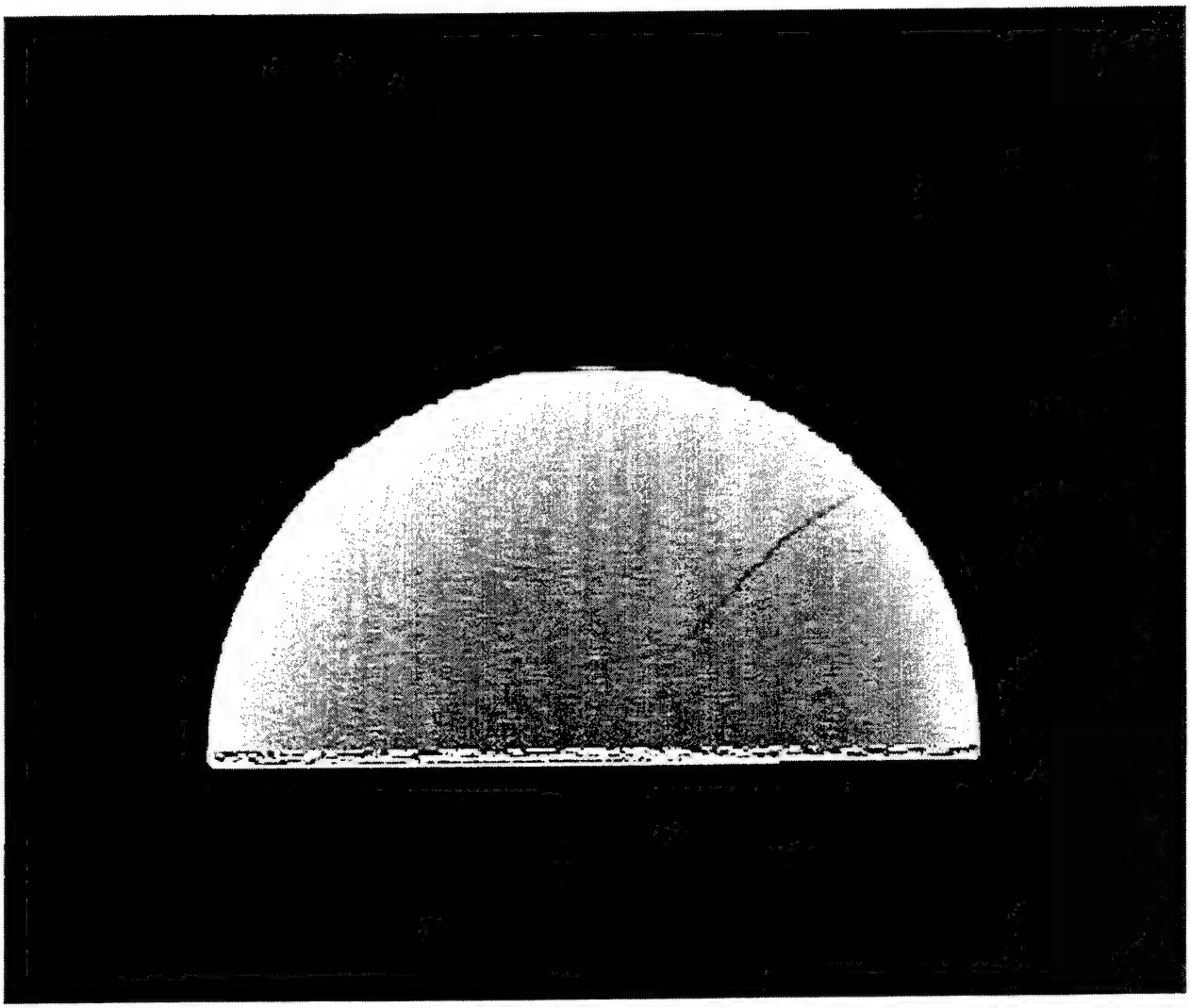

Figure A-6. 3.82 mm from bottom of disk with 65° rotation about X-axis.

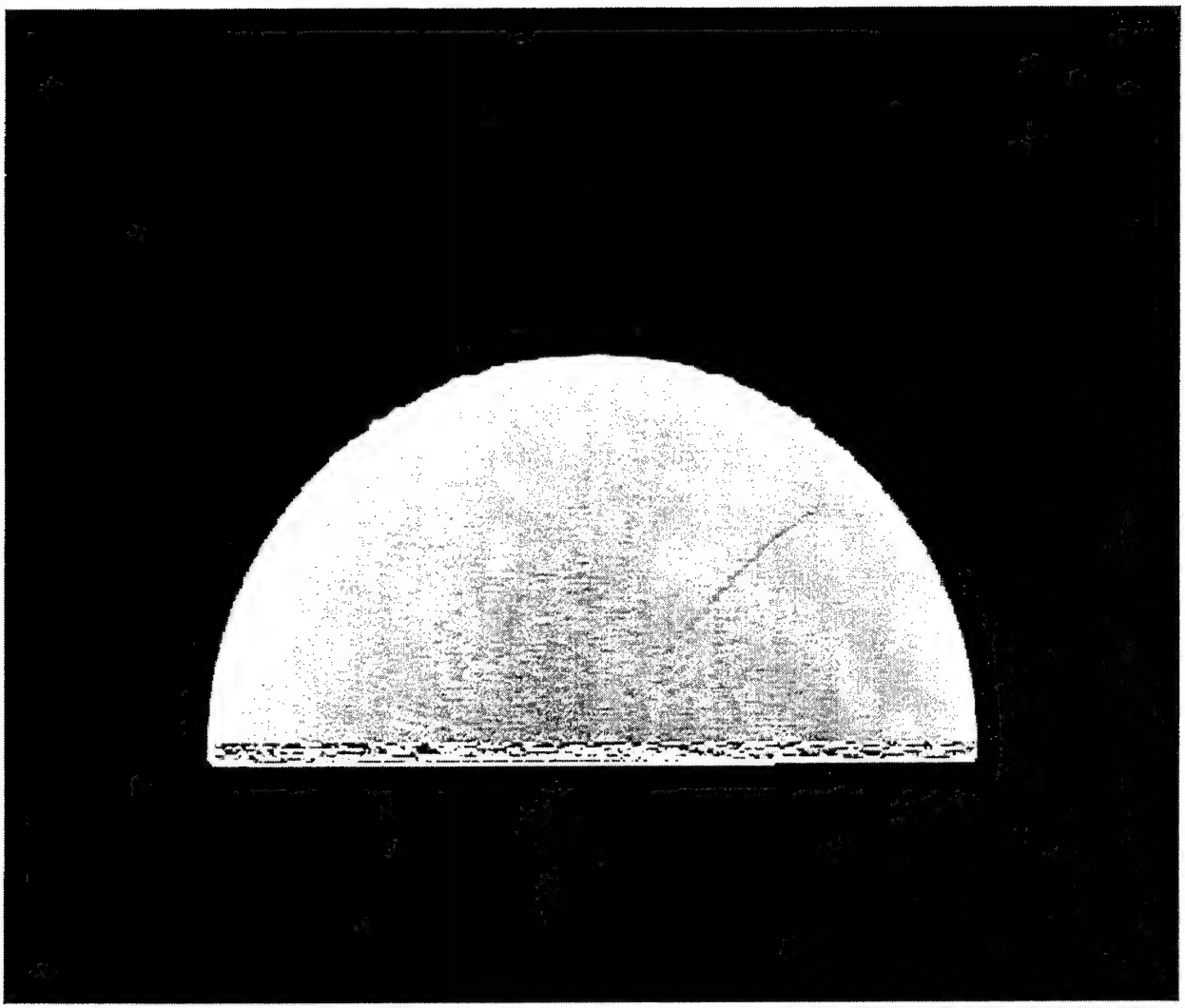

Figure A-7. 4.51 mm from bottom of disk with 65° rotation about X-axis.

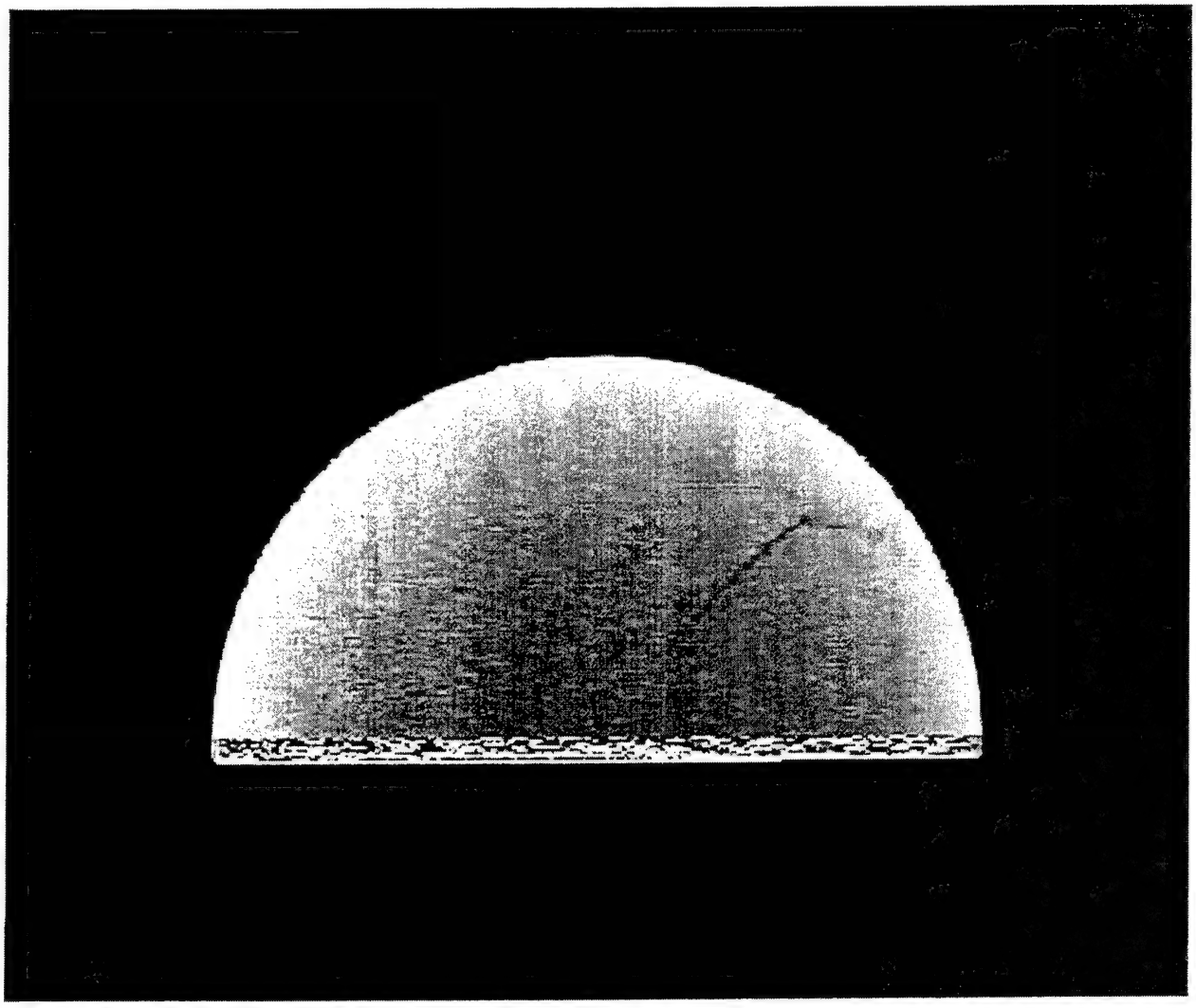

Figure A-8. 5.04 mm from bottom of disk with 65° rotation about X-axis.

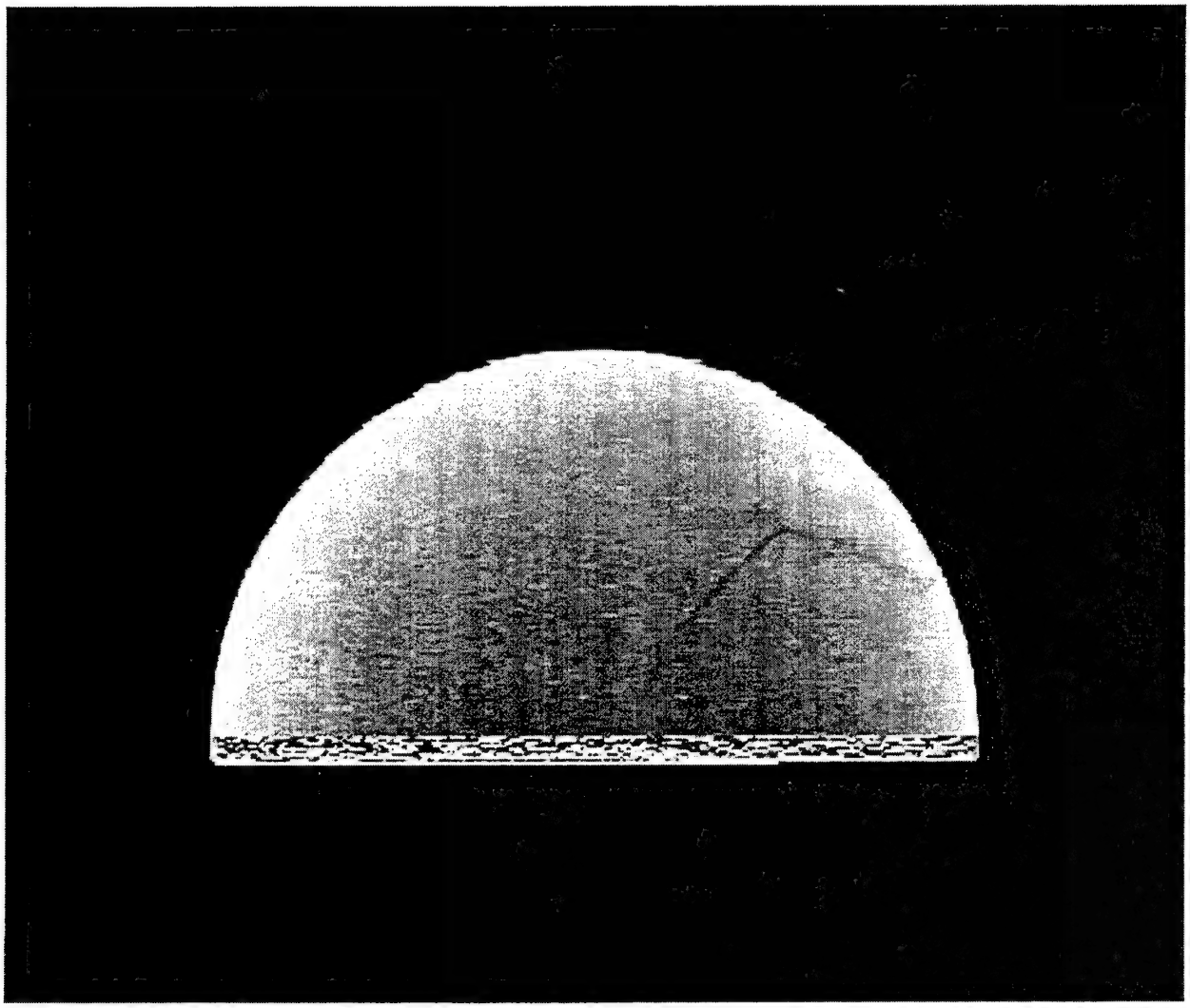

Figure A-9. 5.53 mm from bottom of disk with 65° rotation about X-axis.

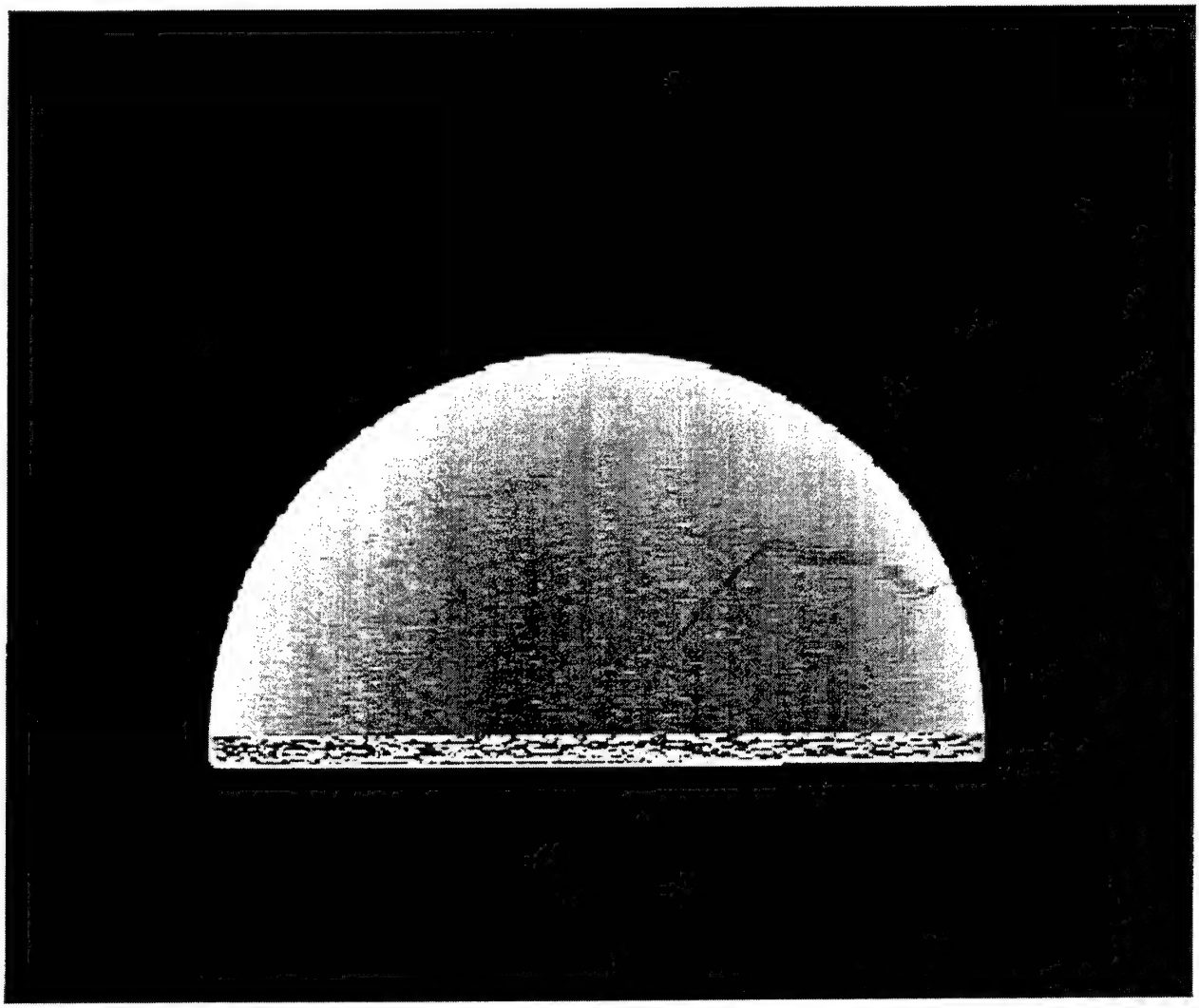

Figure A-10. 6.26 mm from bottom of disk with 65° rotation about X-axis.

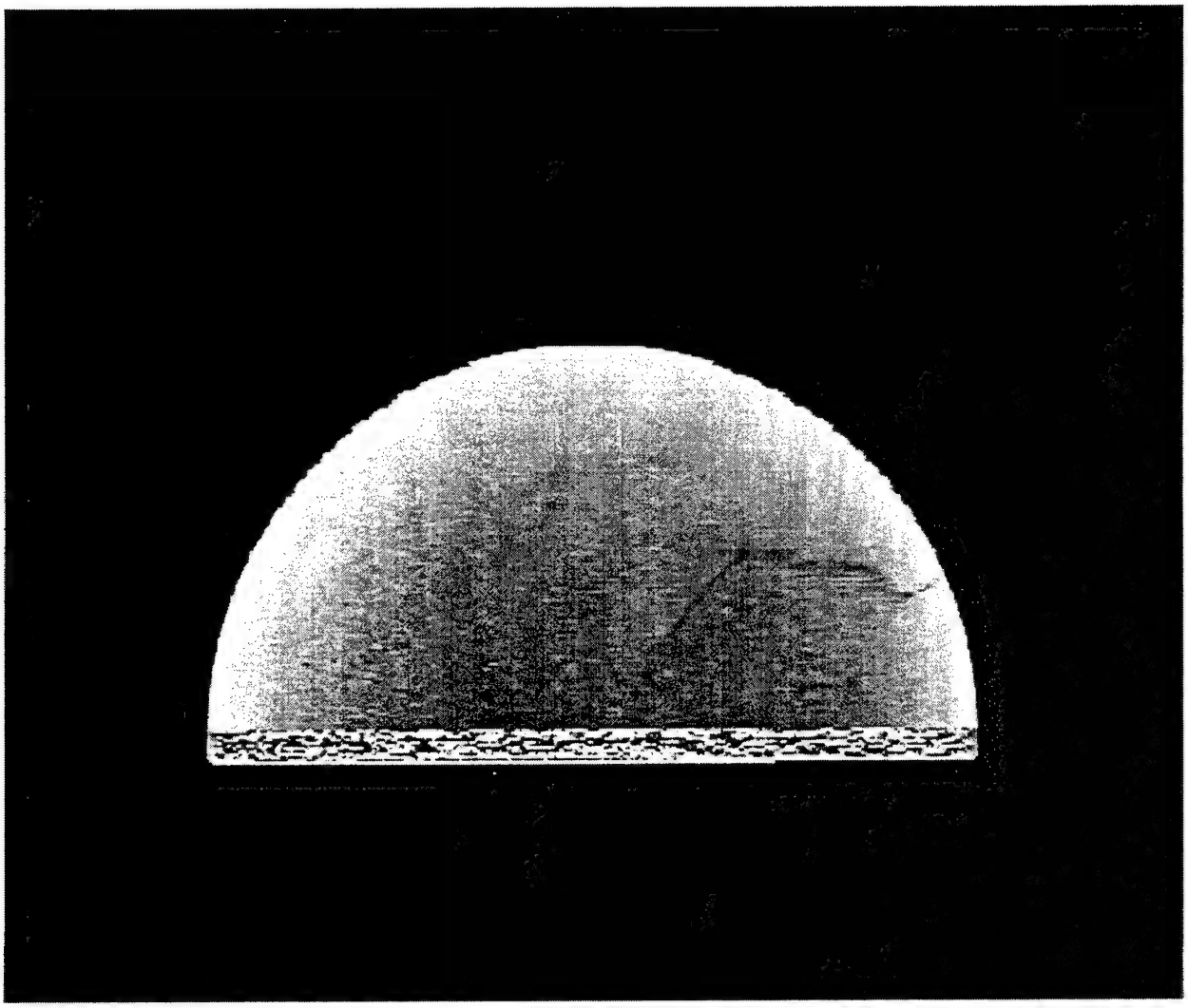

Figure A-11. 6.75 mm from bottom of disk with 65° rotation about X-axis.

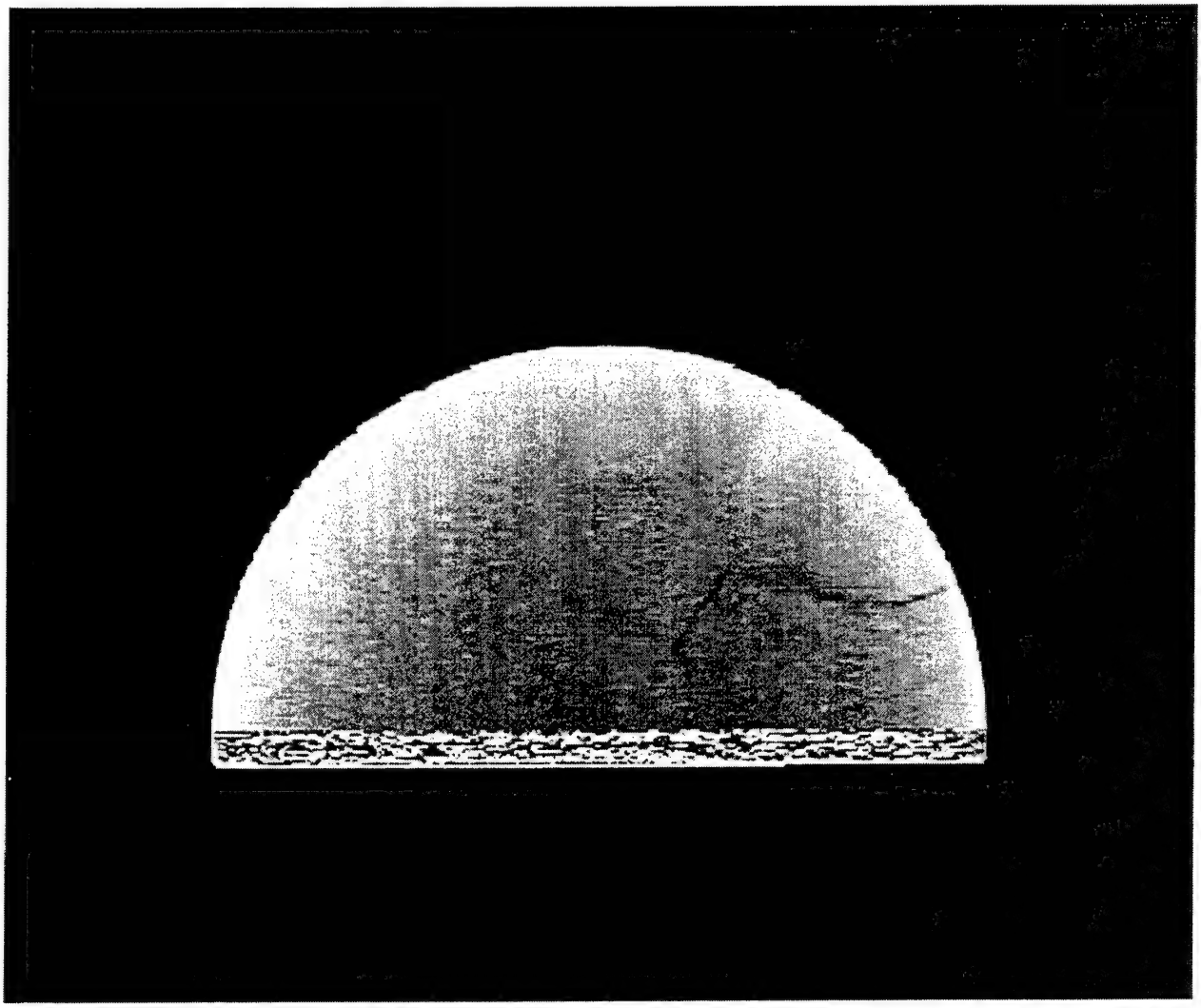

Figure A-12. 7.24 mm from bottom of disk with 65° rotation about X-axis.

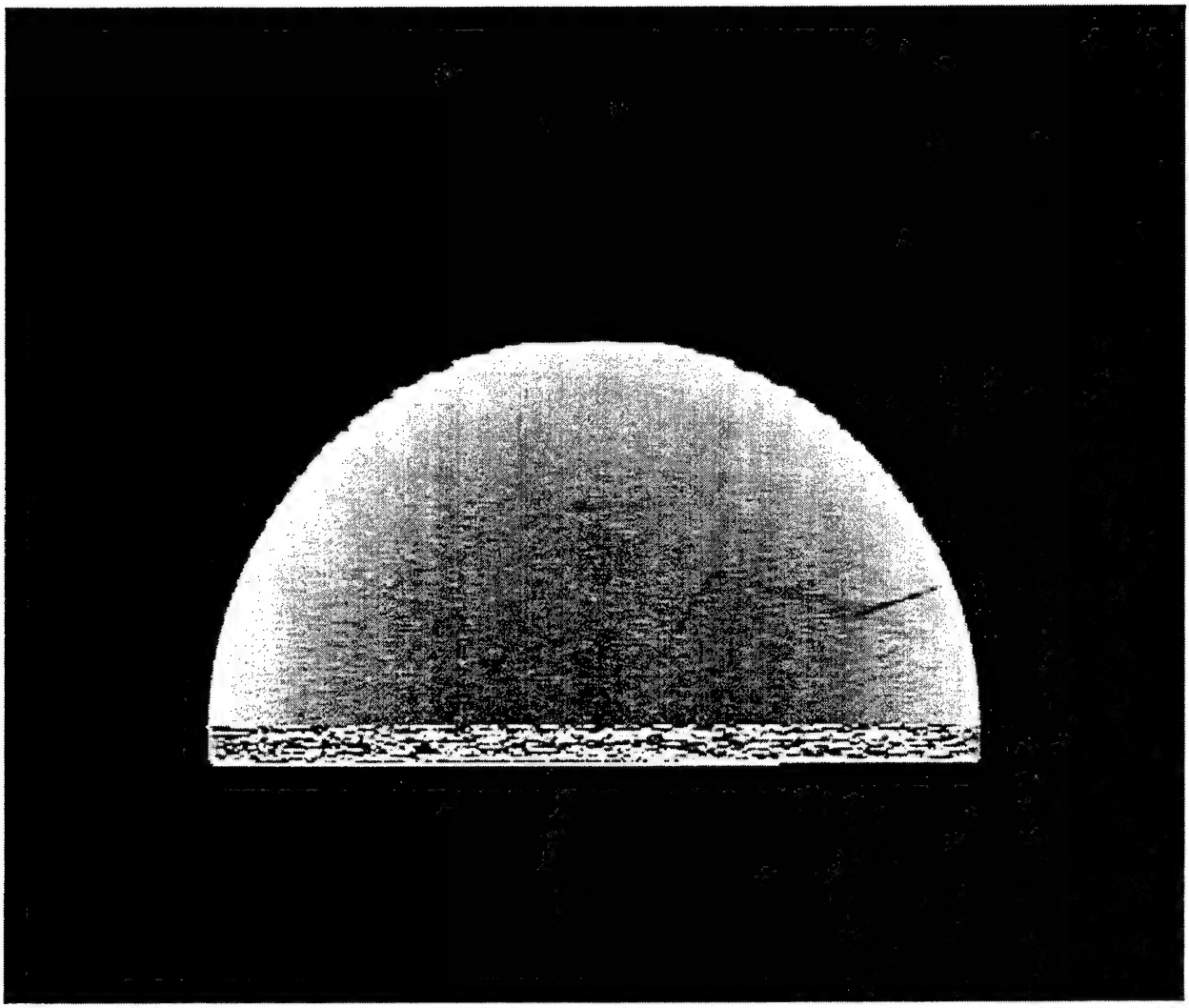

Figure A-13. 7.97 mm from bottom of disk with 65° rotation about X-axis.

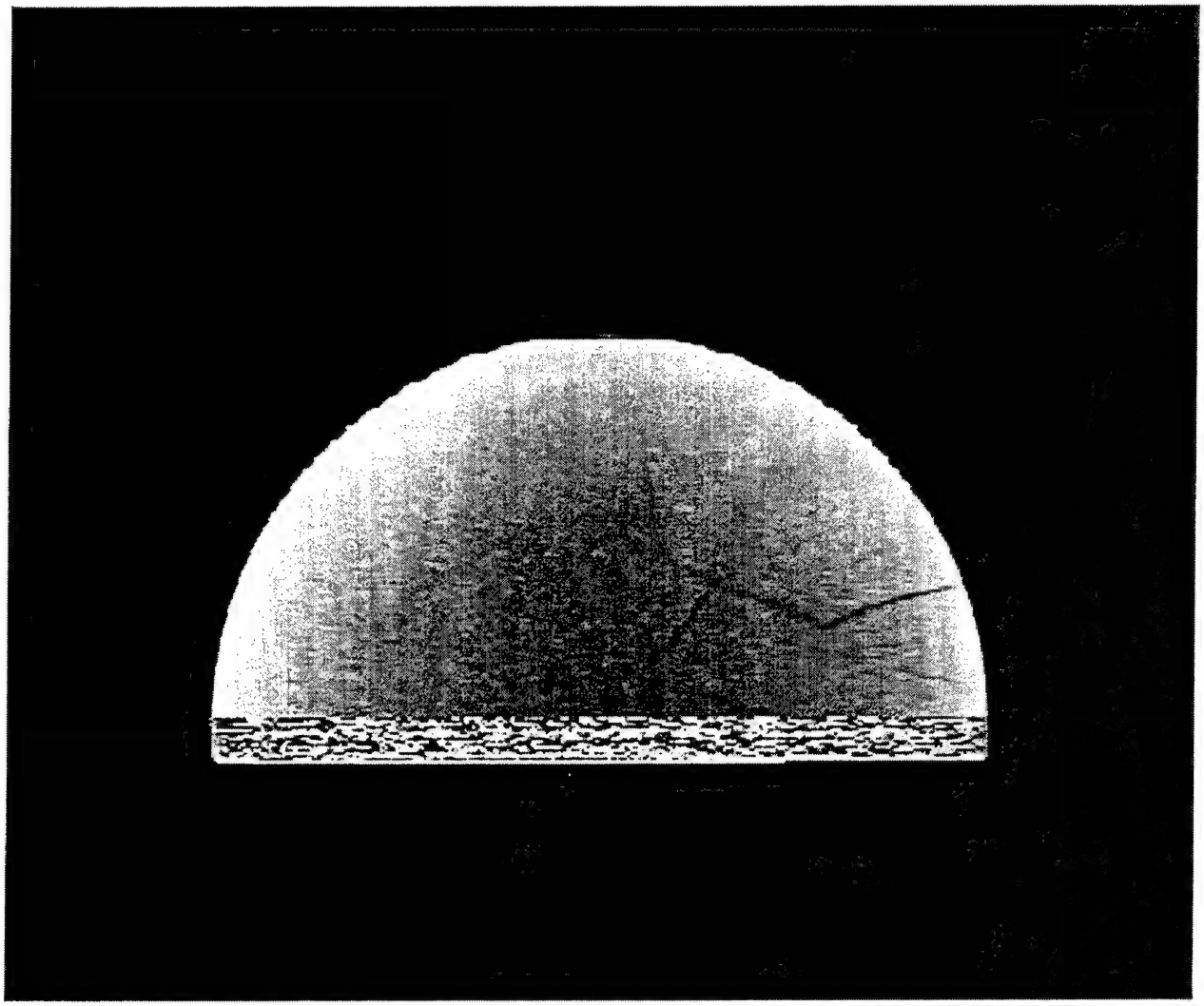

Figure A-14. 8.46 mm from bottom of disk with 65° rotation about X-axis.

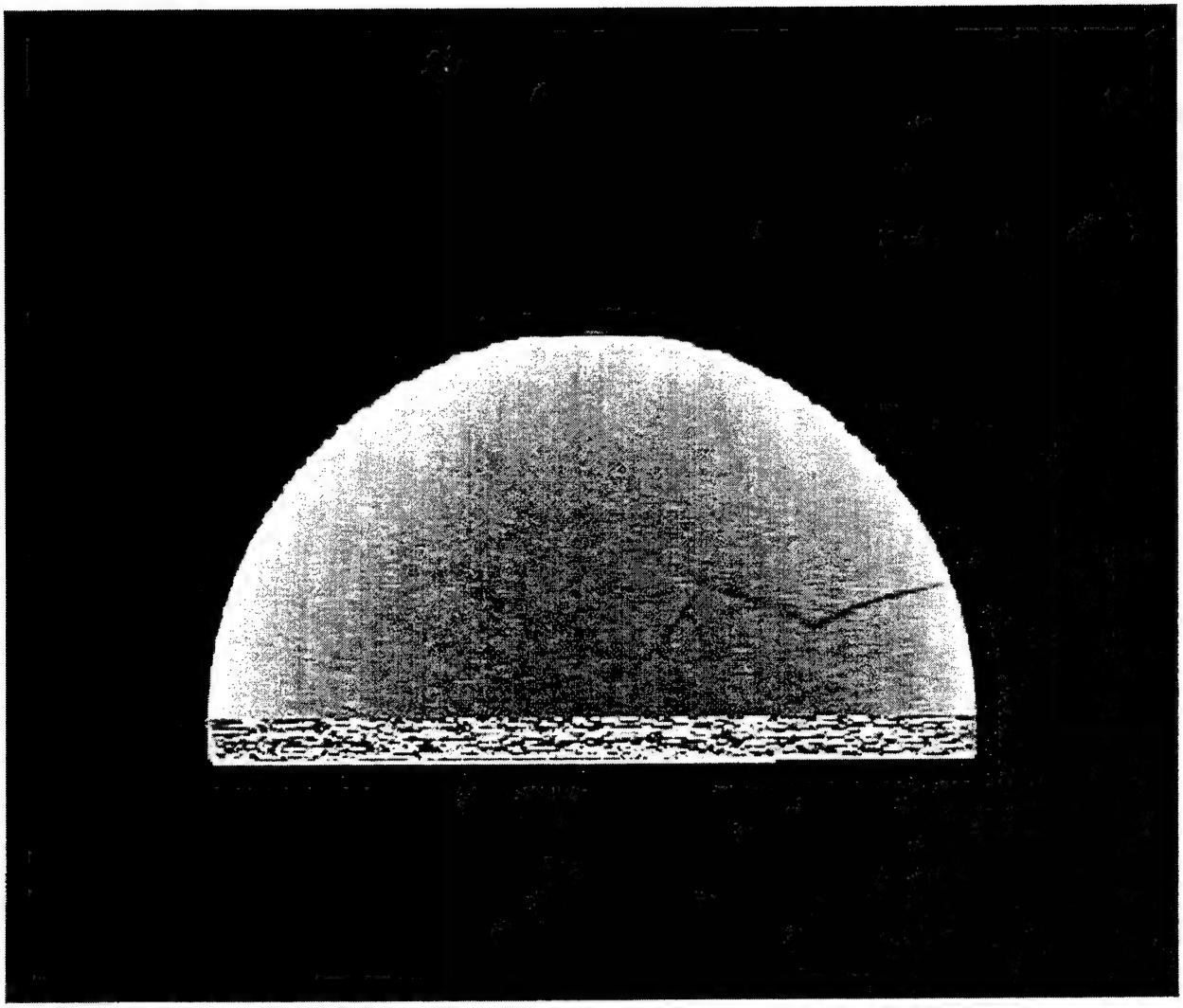

Figure A-15. 9.19 mm from bottom of disk with 65° rotation about X-axis.

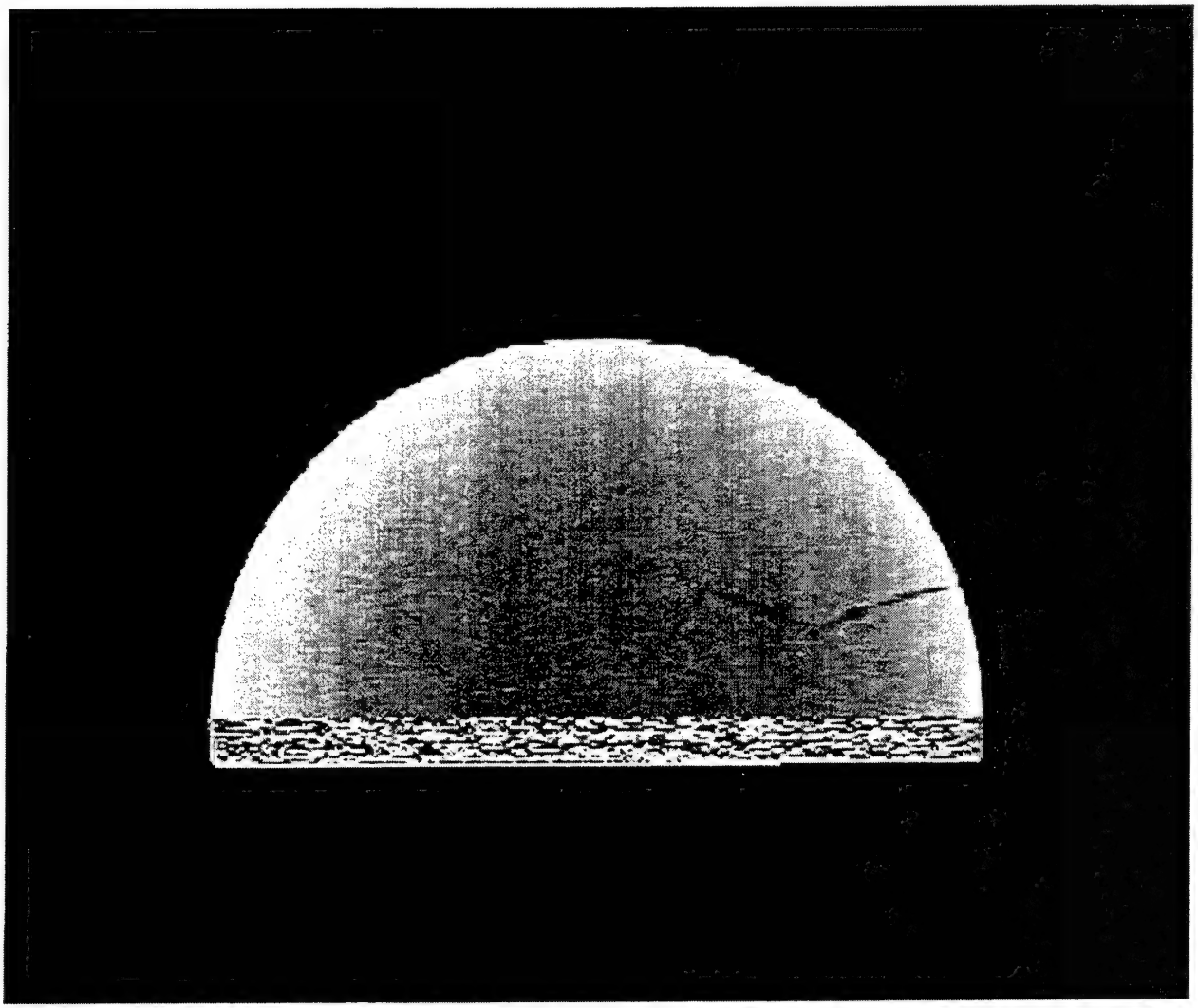

Figure A-16. 9.68 mm from bottom of disk with 65° rotation about X-axis.

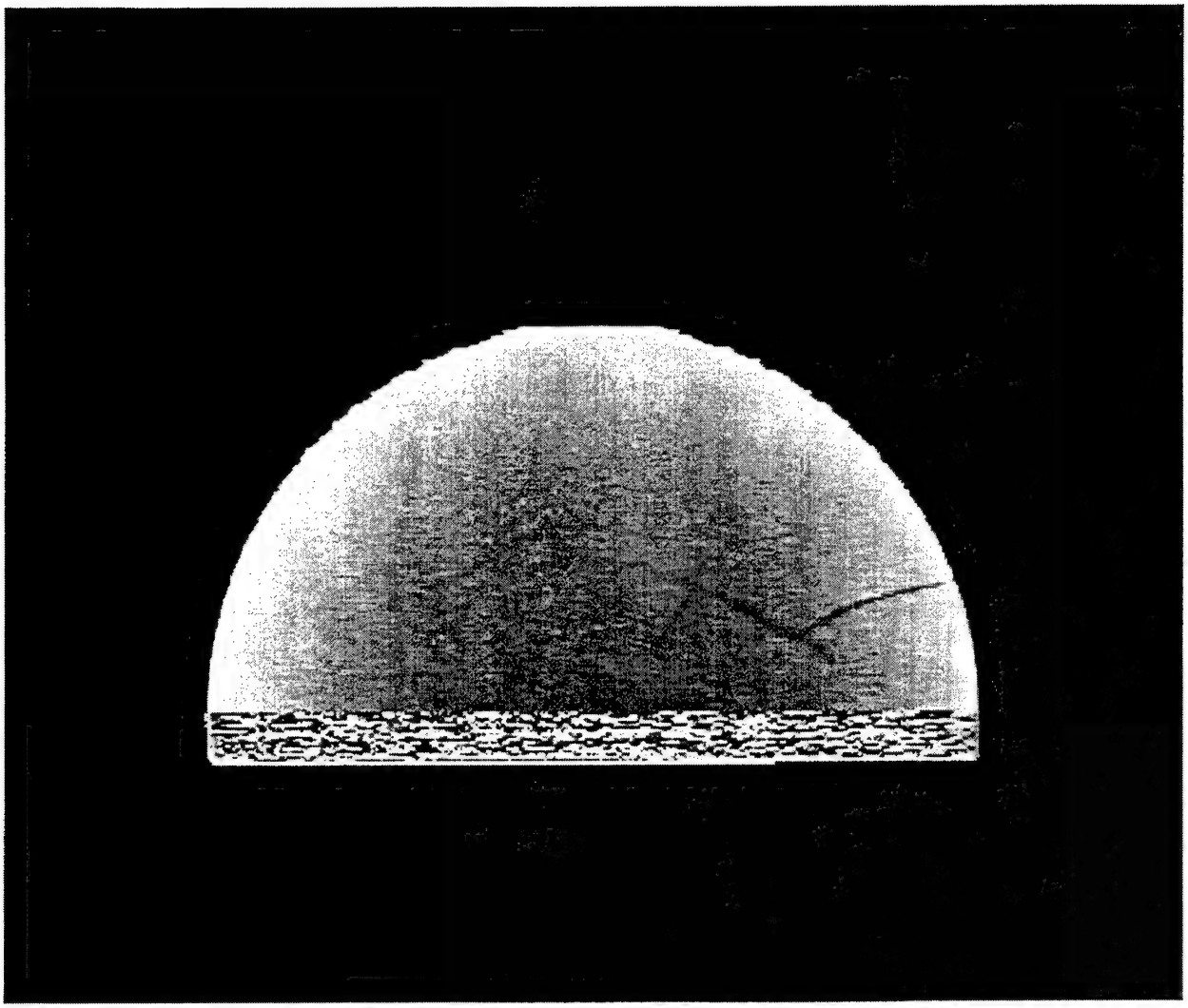

Figure A-17. 10.17 mm from bottom of disk with 65° rotation about X-axis.

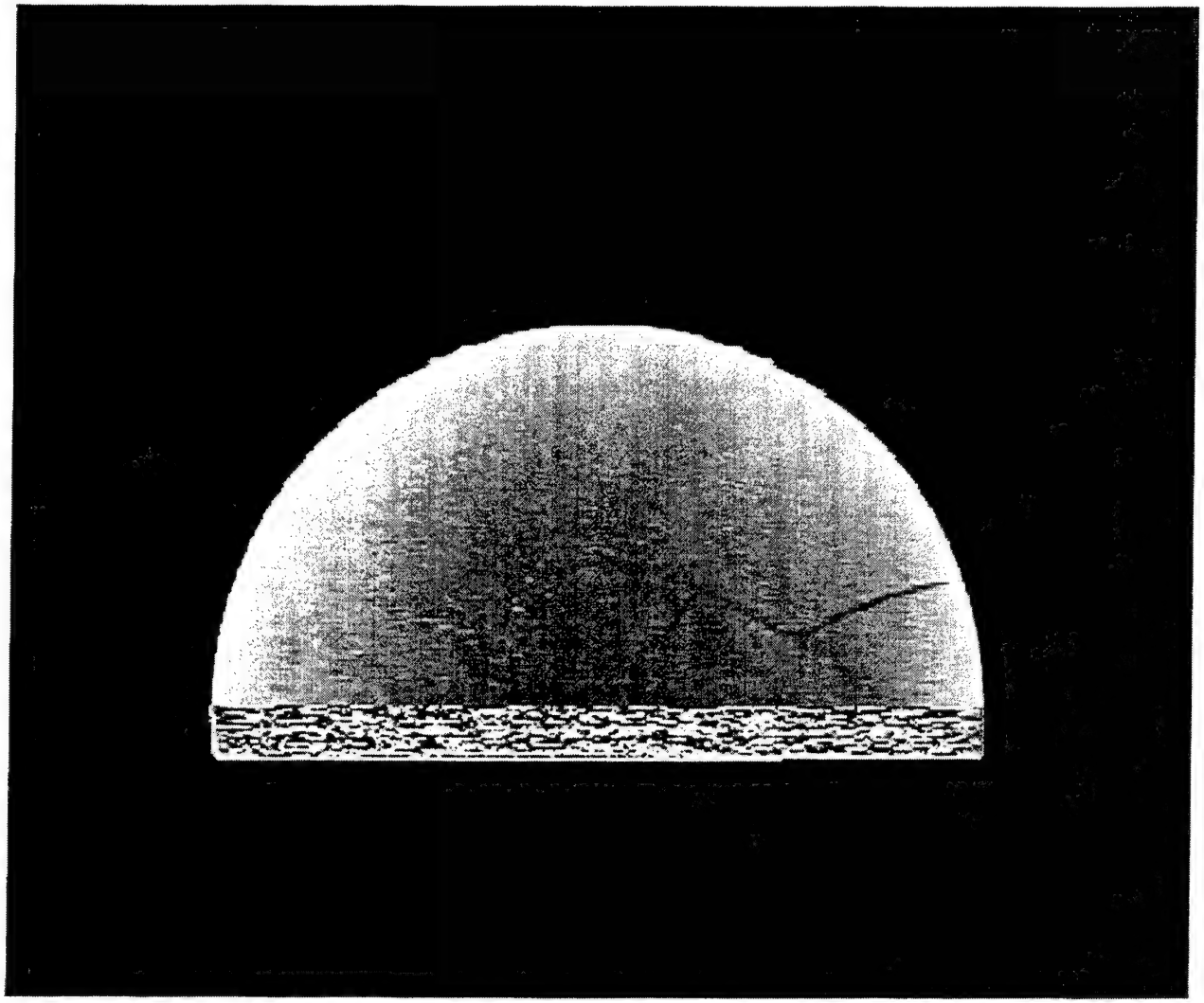

Figure A-18. 10.90 mm from bottom of disk with 65° rotation about X-axis.

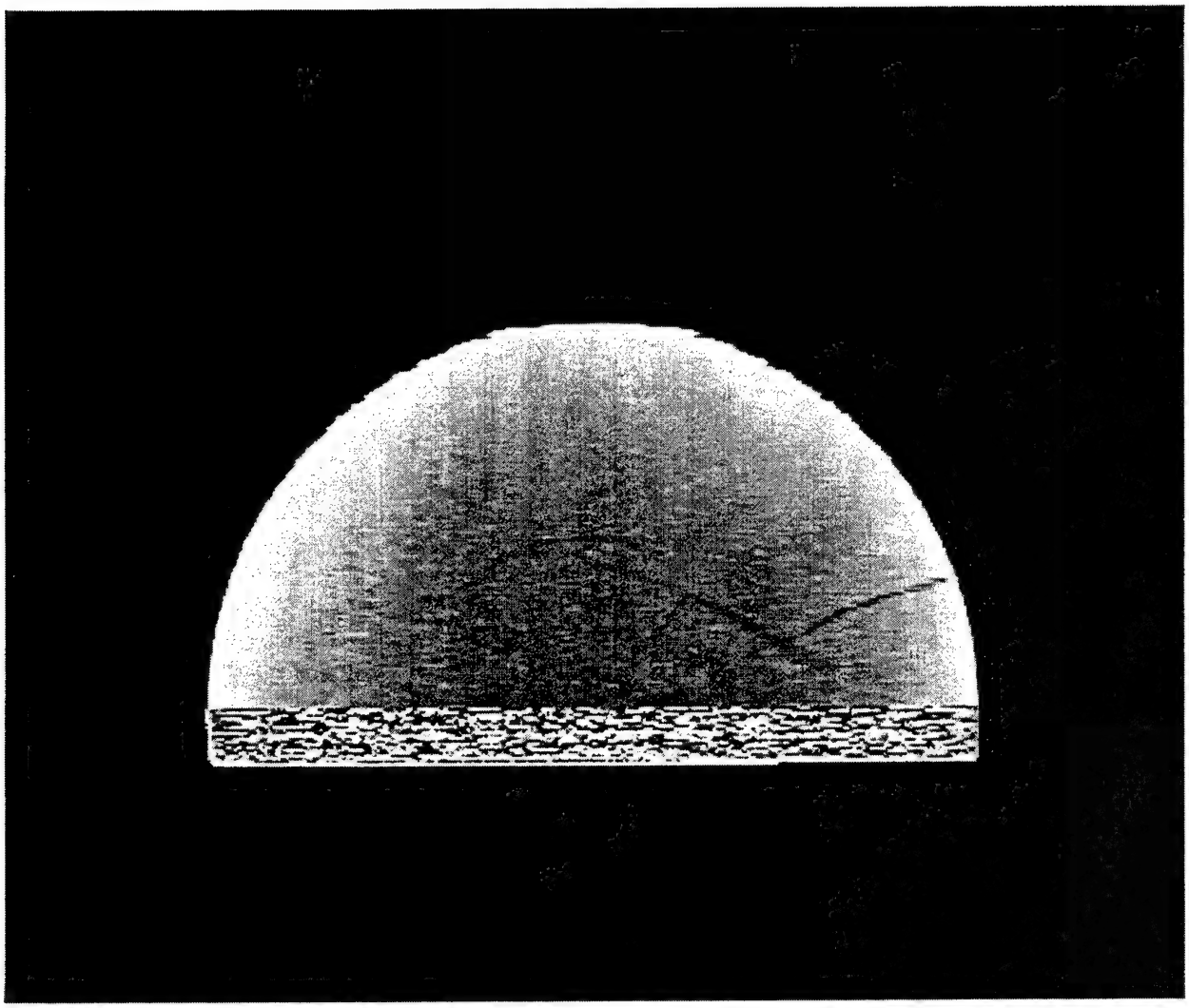

Figure A-19. 11.39 mm from bottom of disk with 65° rotation about X-axis.

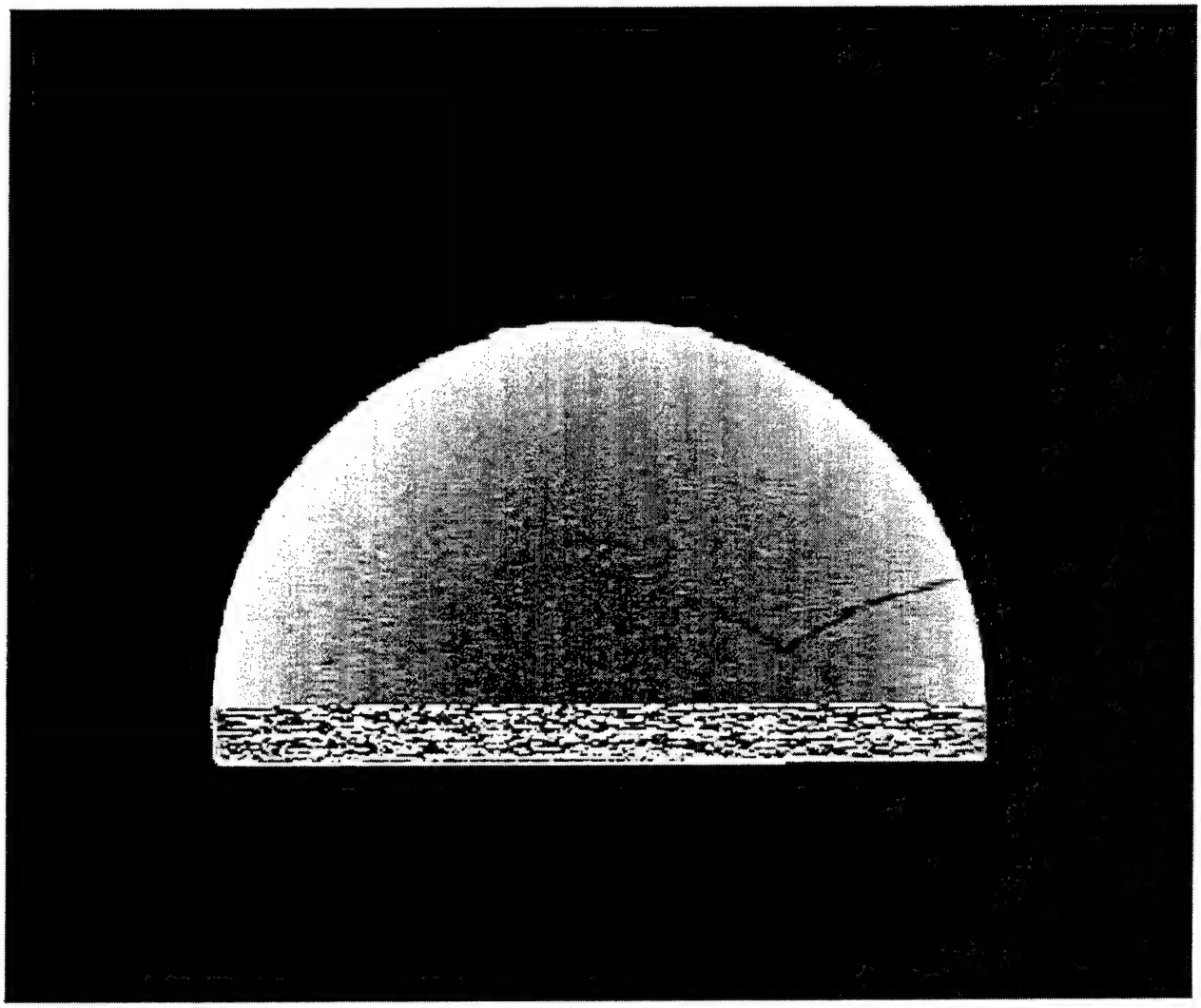

Figure A-20. 12.12 mm from bottom of disk with 65° rotation about X-axis.

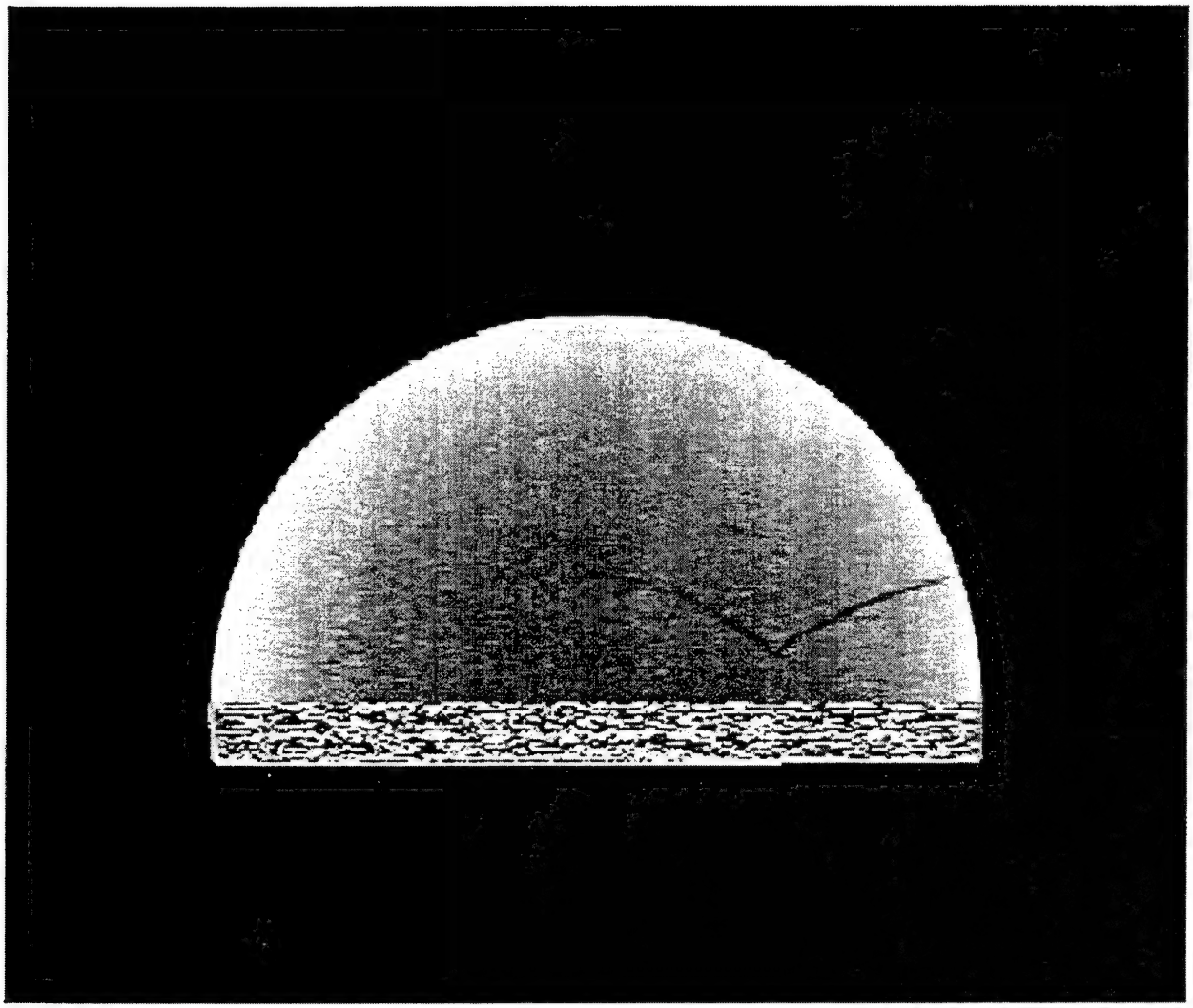

Figure A-21. 12.61 mm from bottom of disk with 65° rotation about X-axis.

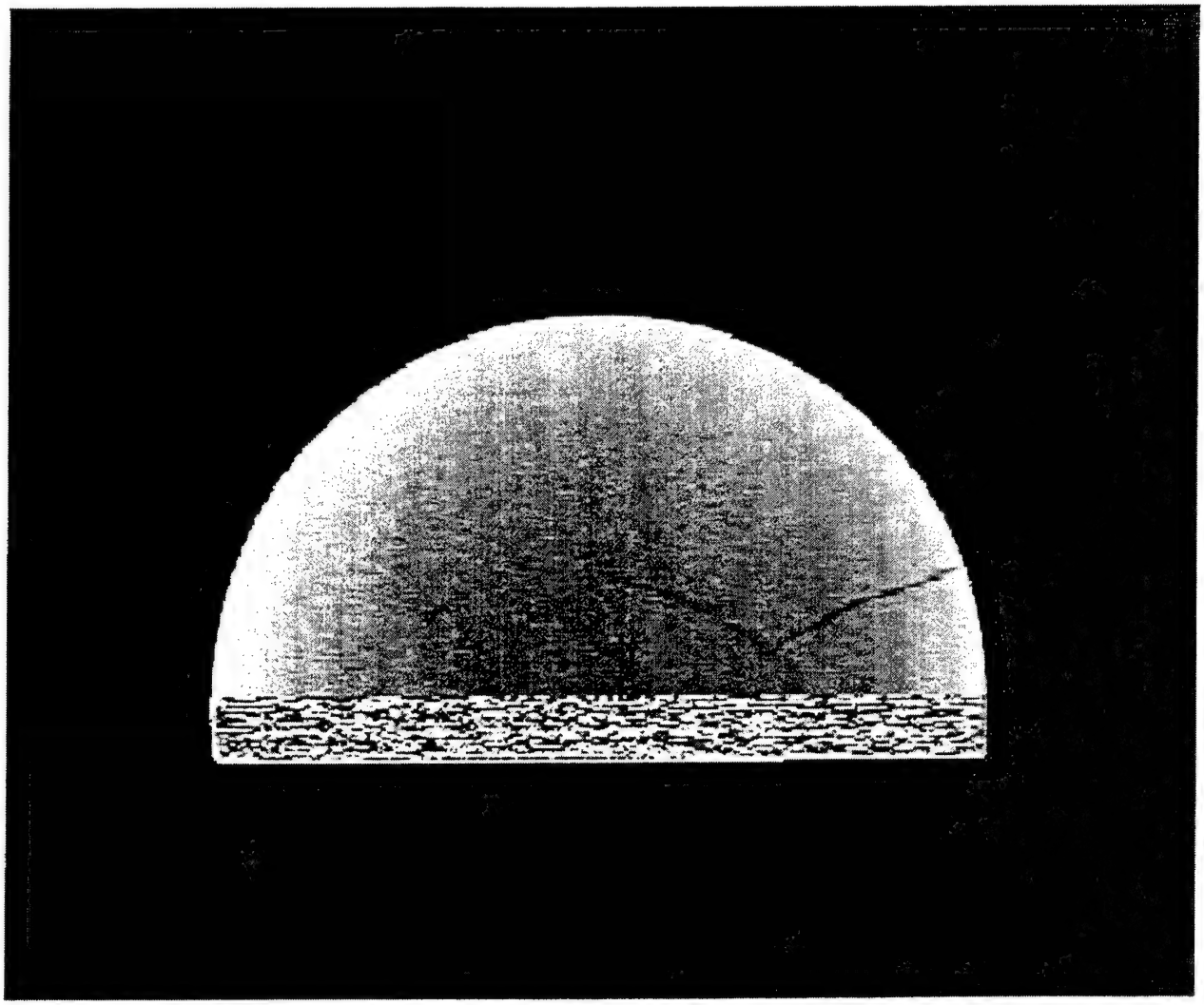

Figure A-22. 13.10 mm from bottom of disk with 65° rotation about X-axis.

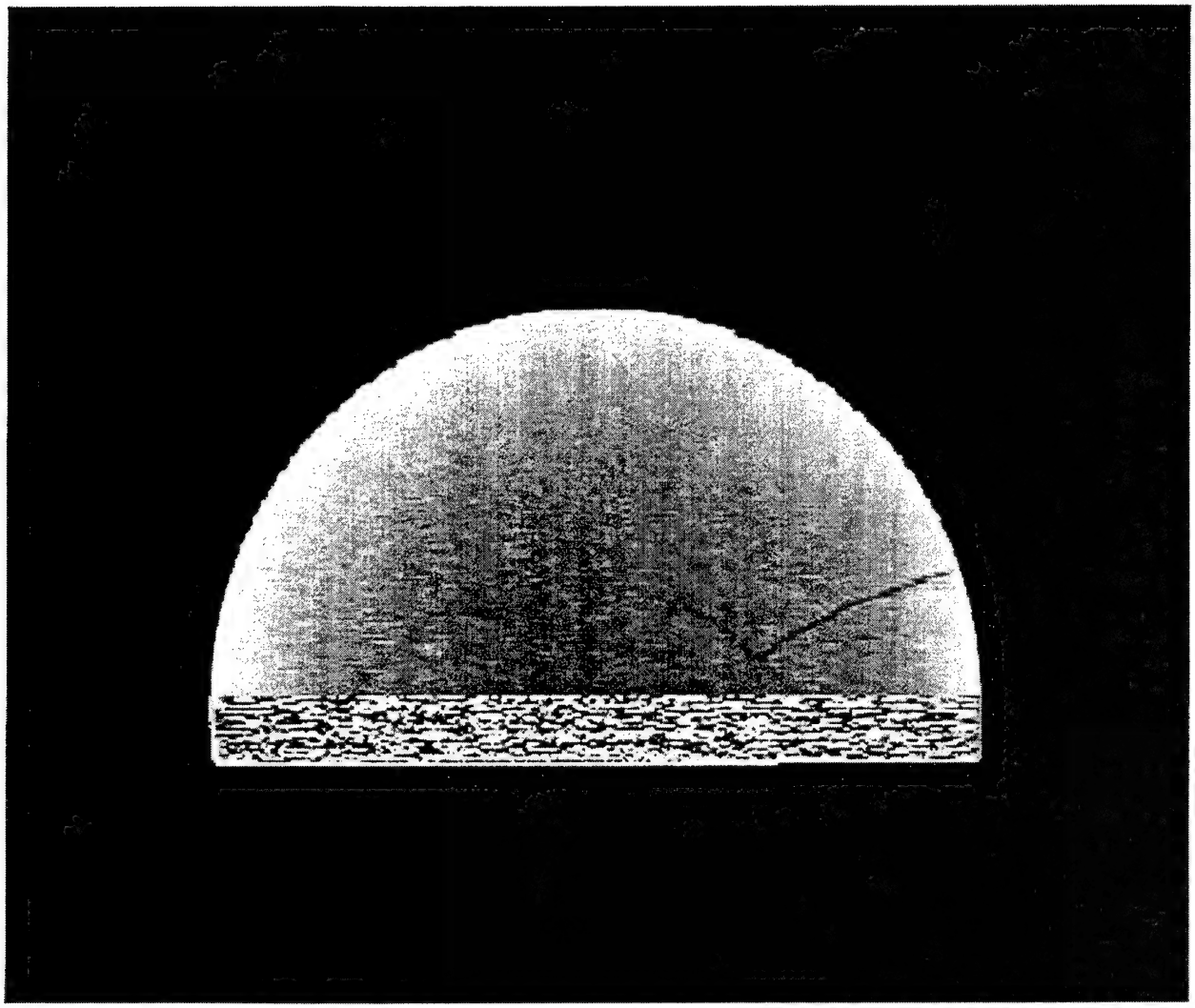

Figure A-23. 13.83 mm from bottom of disk with 65° rotation about X-axis.

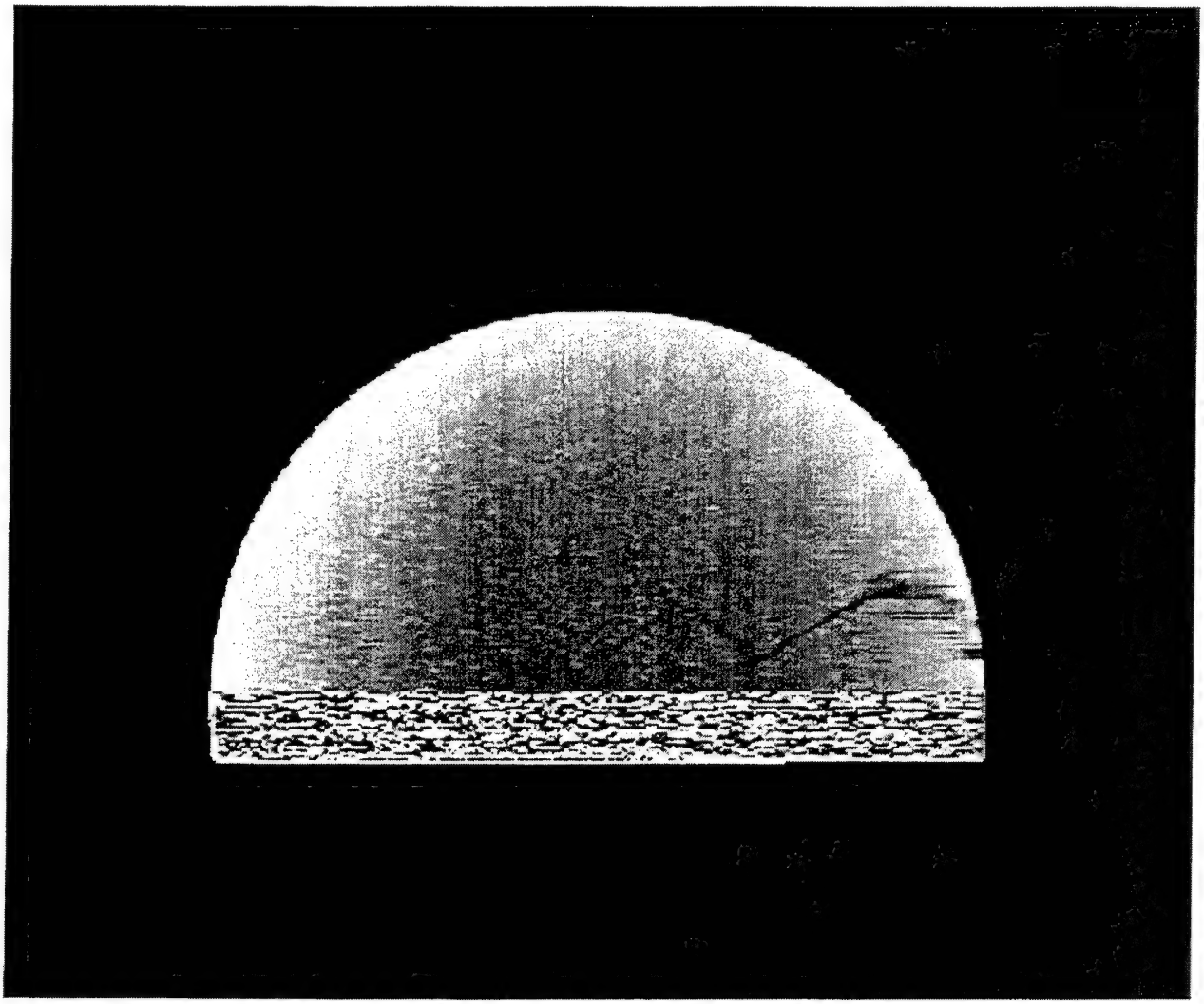

Figure A-24. 14.32 mm from bottom of disk with 65° rotation about X-axis.

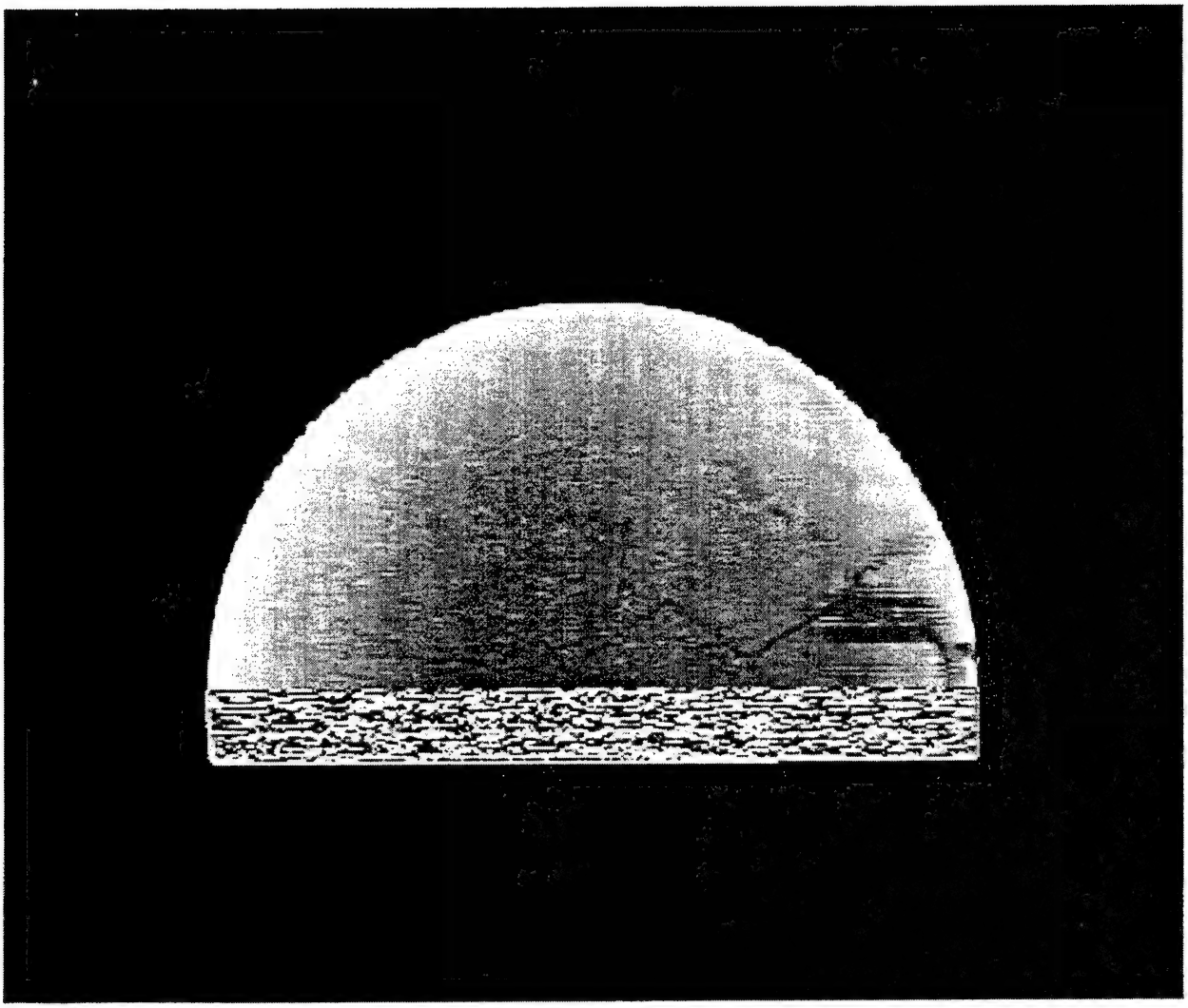

Figure A-25. 15.05 mm from bottom of disk with 65° rotation about X-axis.

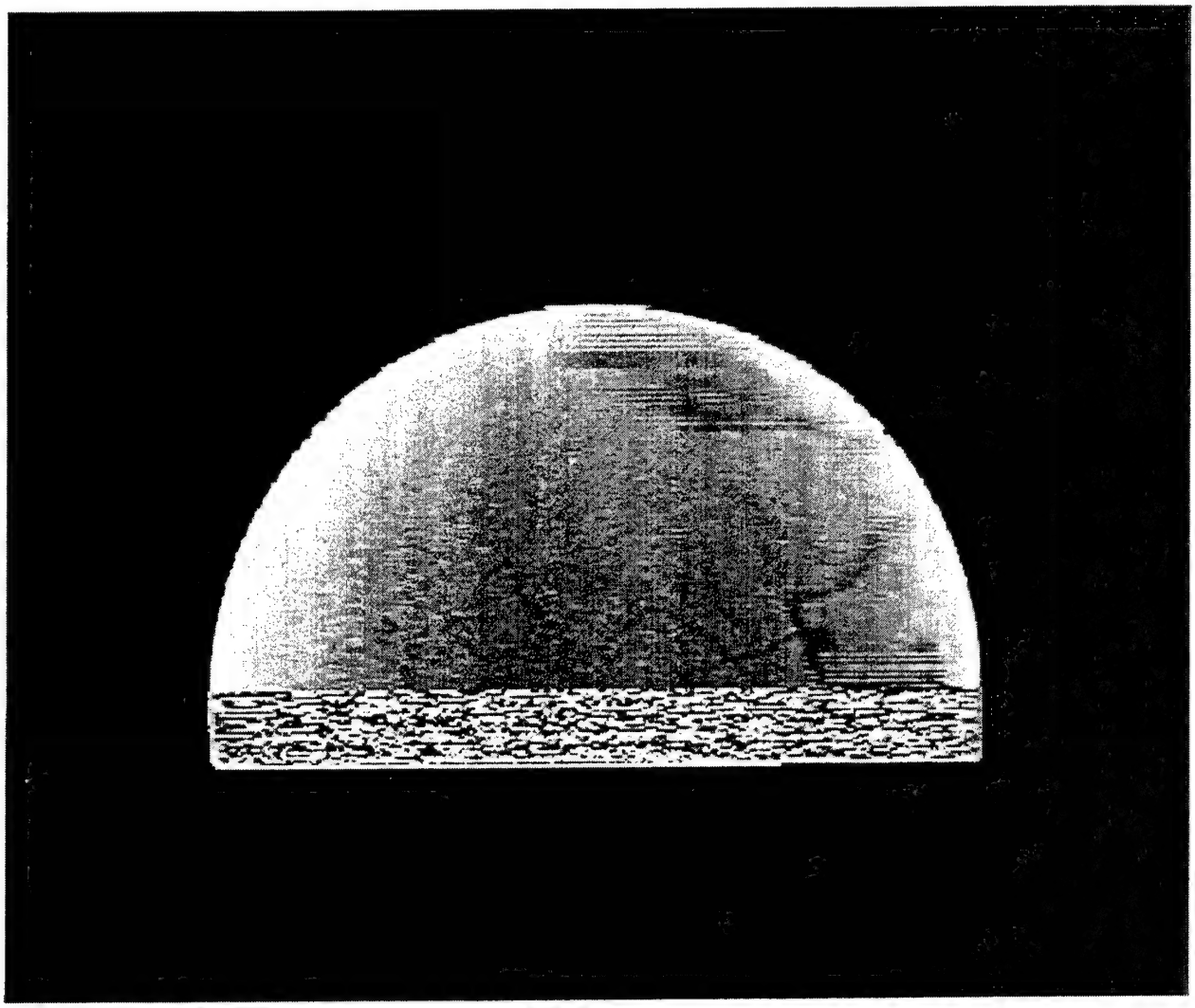

Figure A-26. 15.54 mm from bottom of disk with 65° rotation about X-axis.

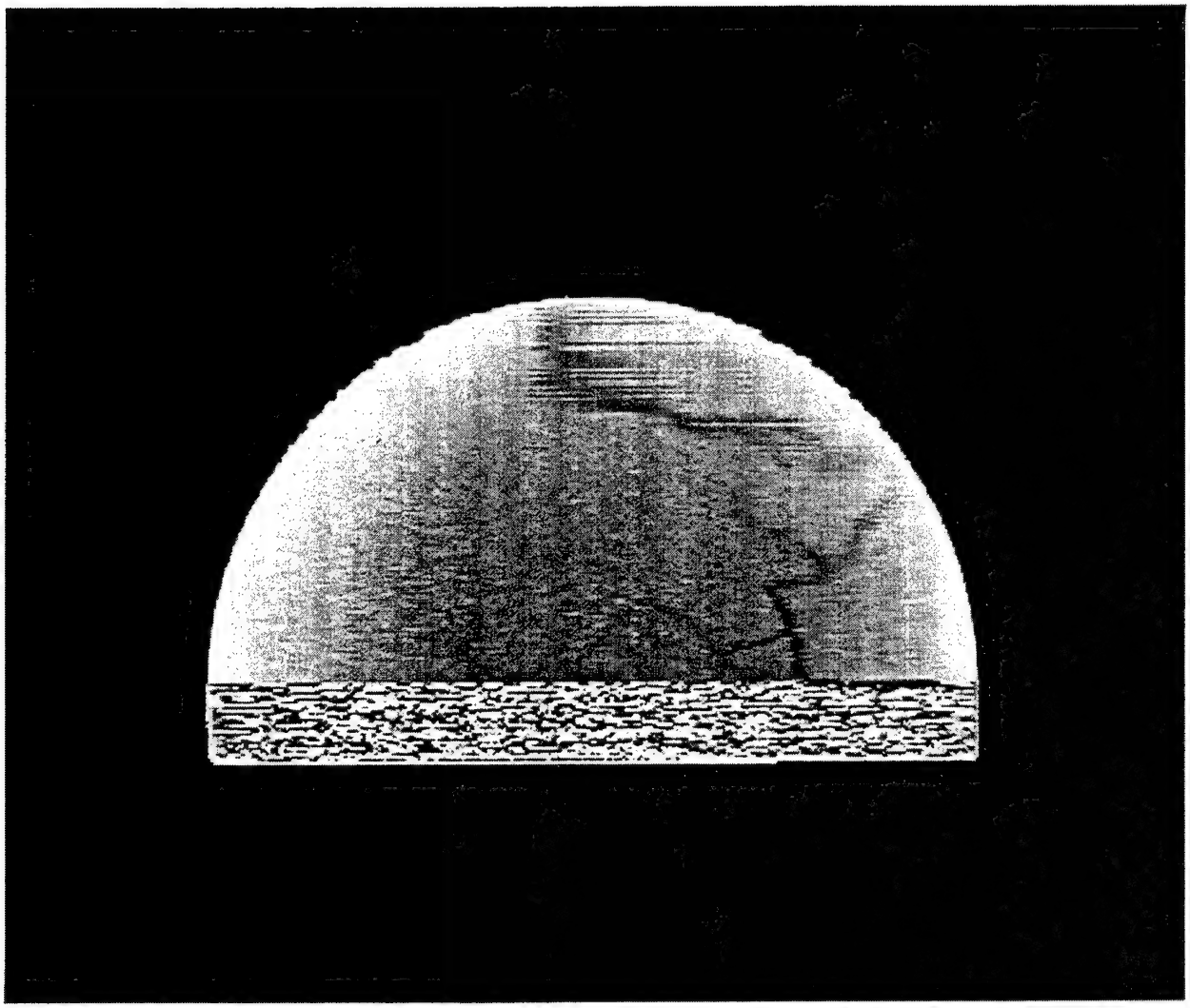

Figure A-27. 16.27 mm from bottom of disk with 65° rotation about X-axis.

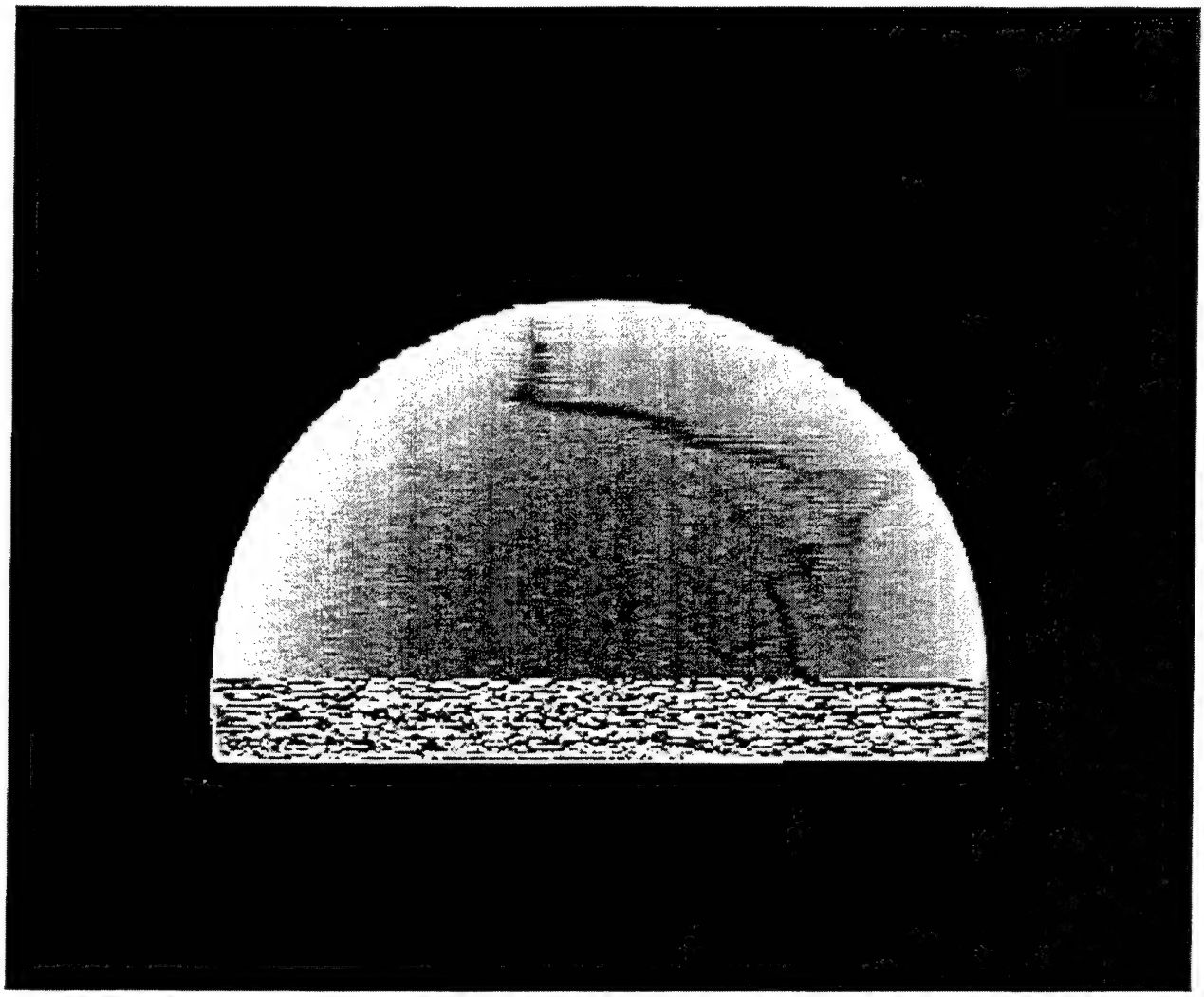

Figure A-28. 16.76 mm from bottom of disk with 65° rotation about X-axis.

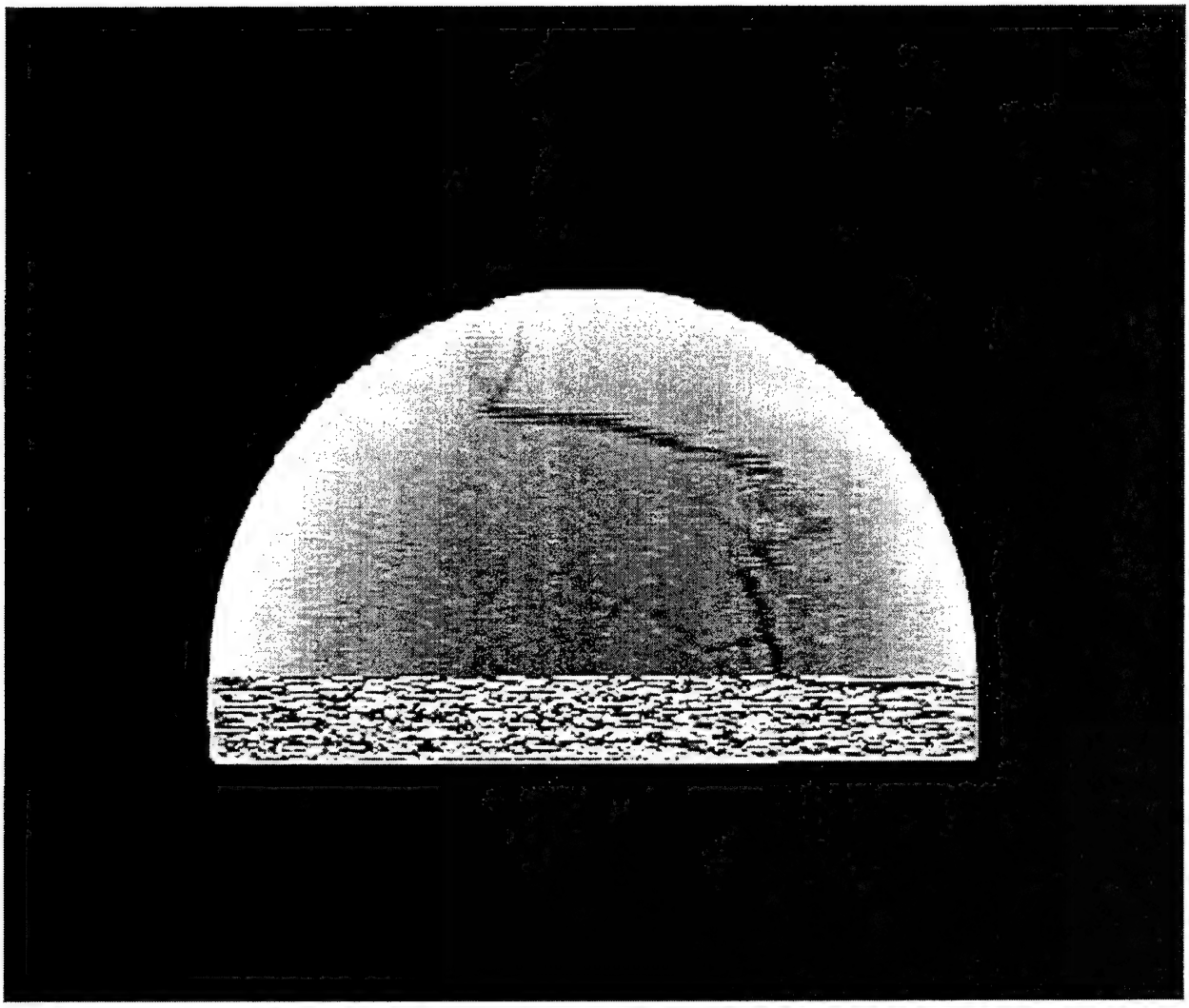

Figure A-29. 17.25 mm from bottom of disk with 65° rotation about X-axis.

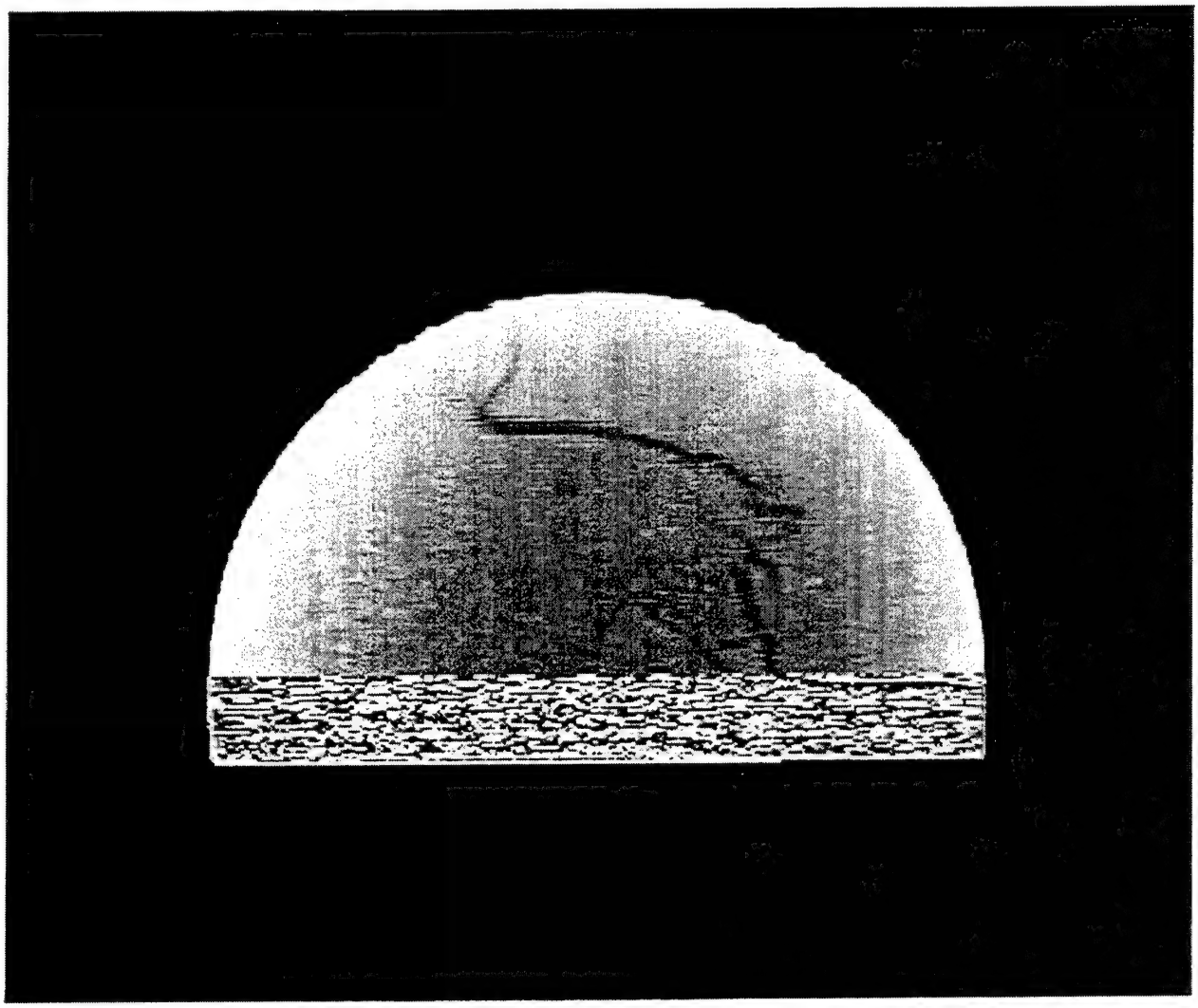

Figure A-30. 17.98 mm from bottom of disk with 65° rotation about X-axis.

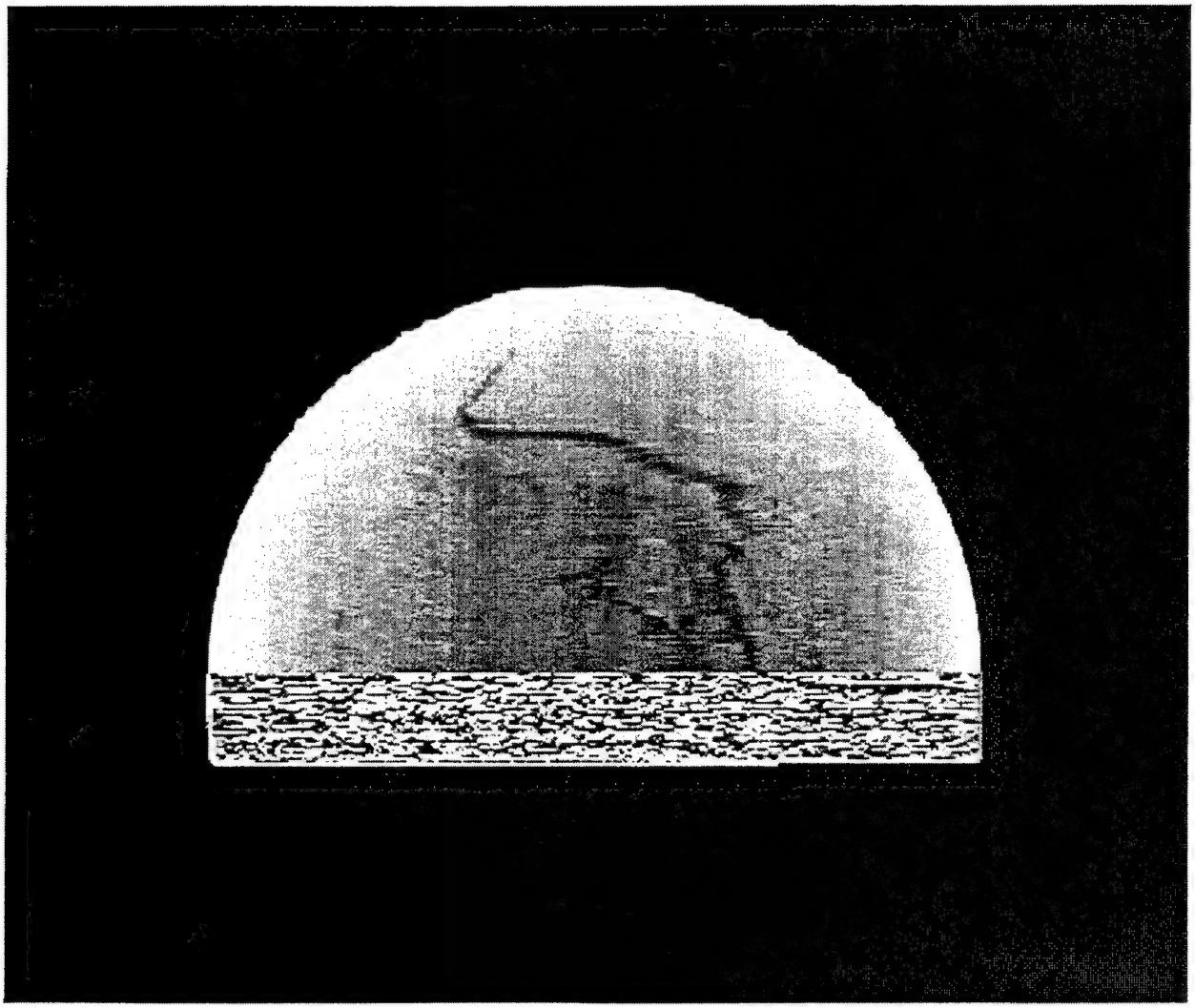

Figure A-31. 18.47 mm from bottom of disk with 65° rotation about X-axis.

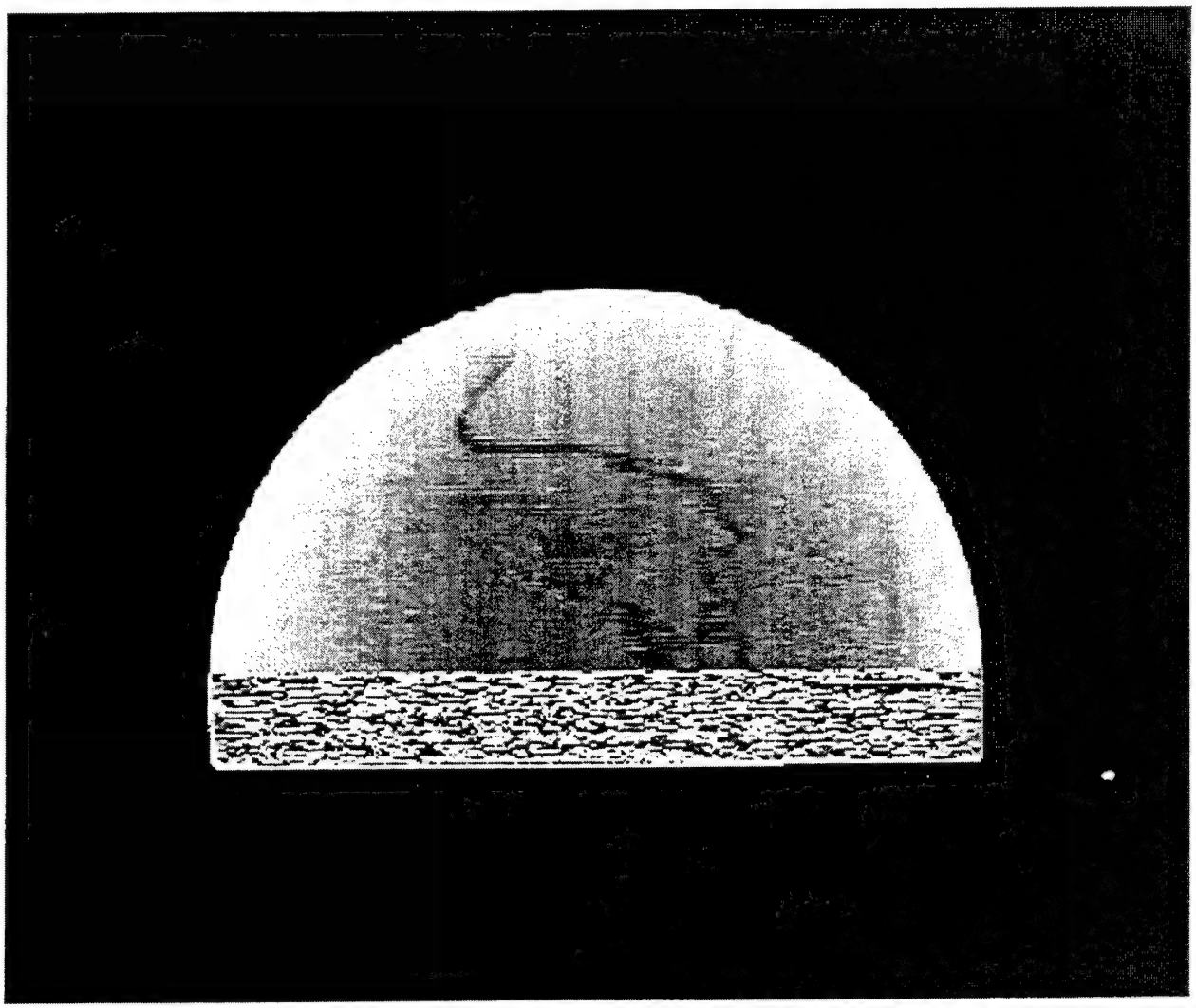

Figure A-32. 19.20 mm from bottom of disk with 65° rotation about X-axis.

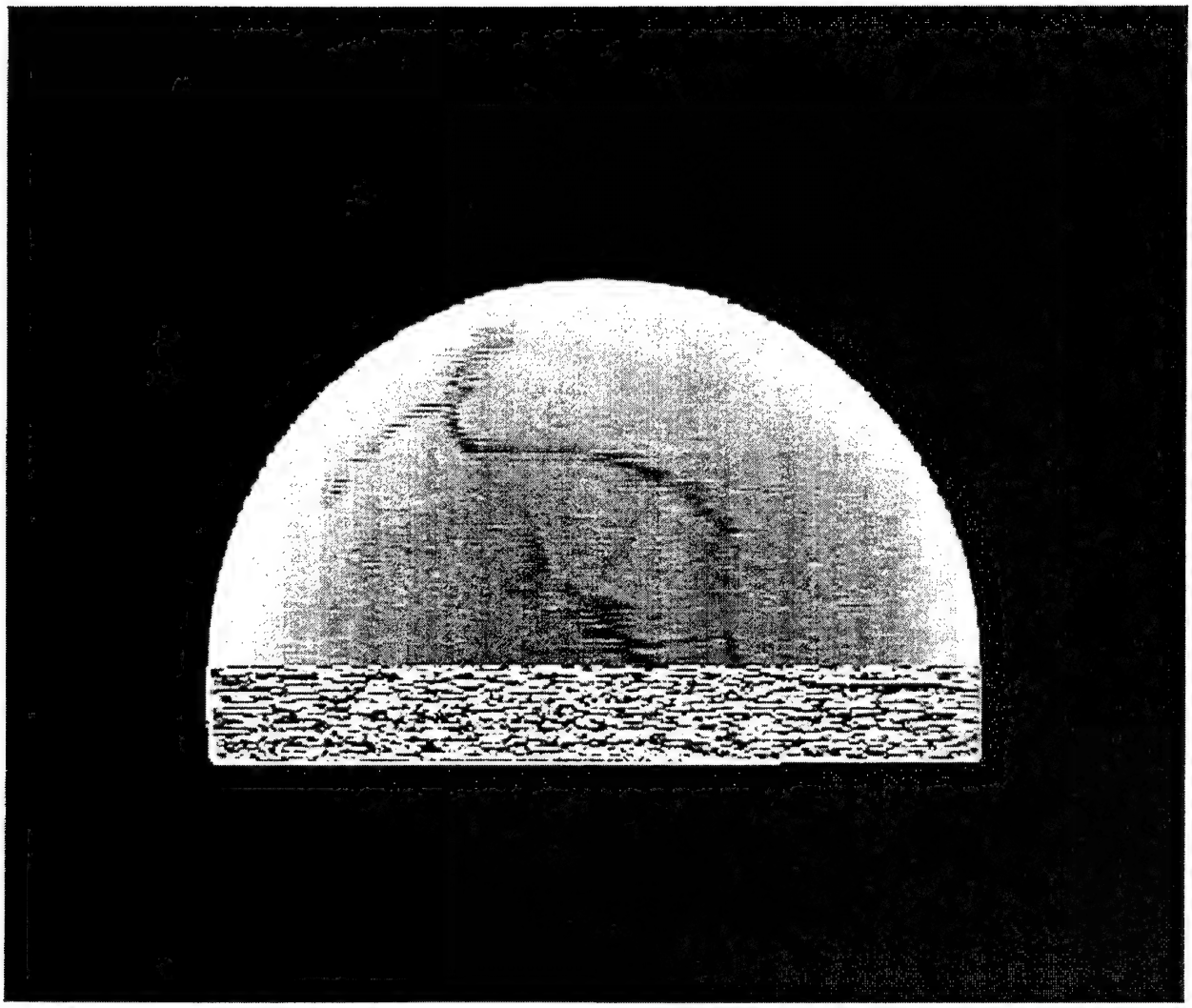

Figure A-33. 19.69 mm from bottom of disk with 65° rotation about X-axis.

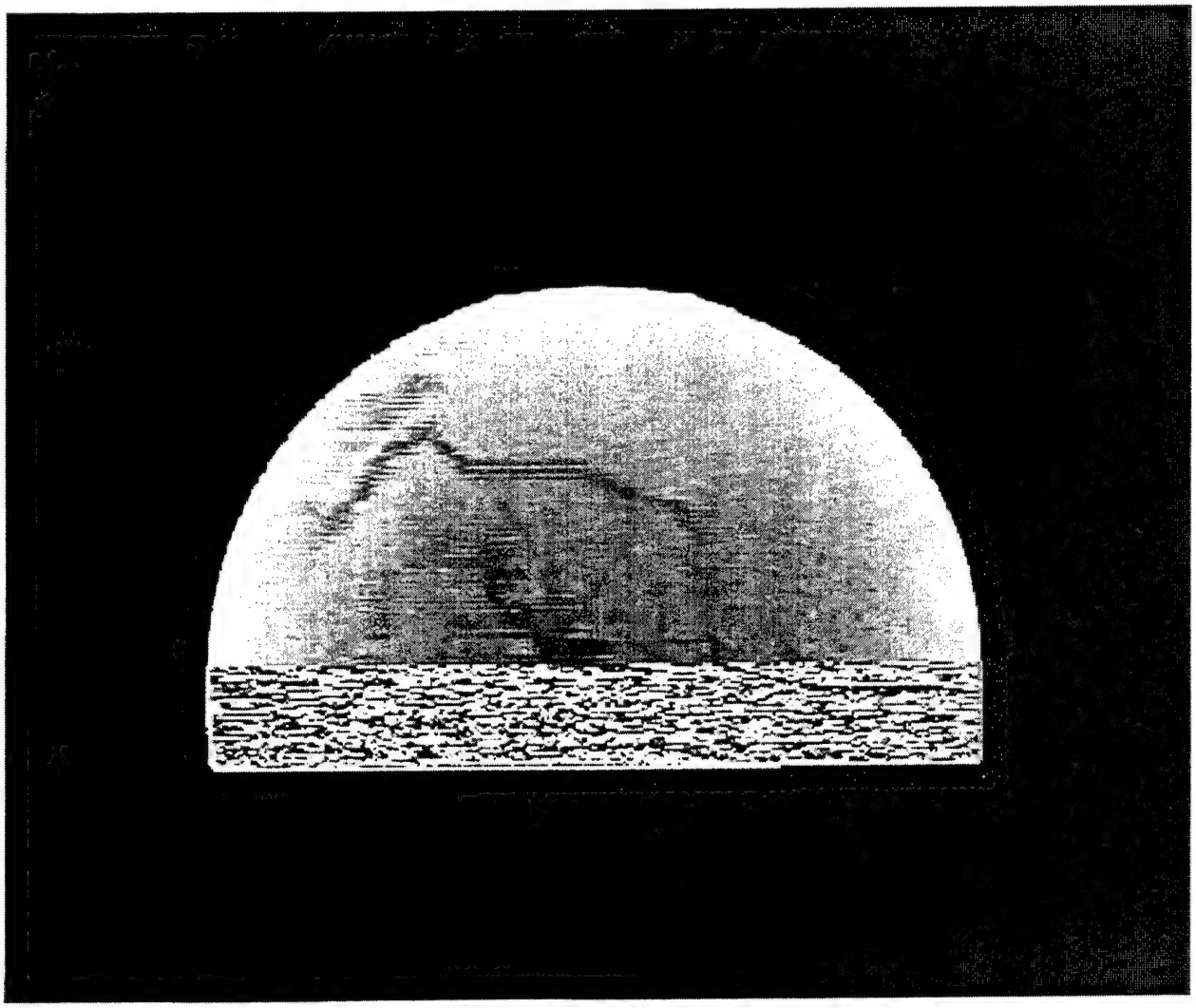

Figure A-34. 20.18 mm from bottom of disk with 65° rotation about X-axis.

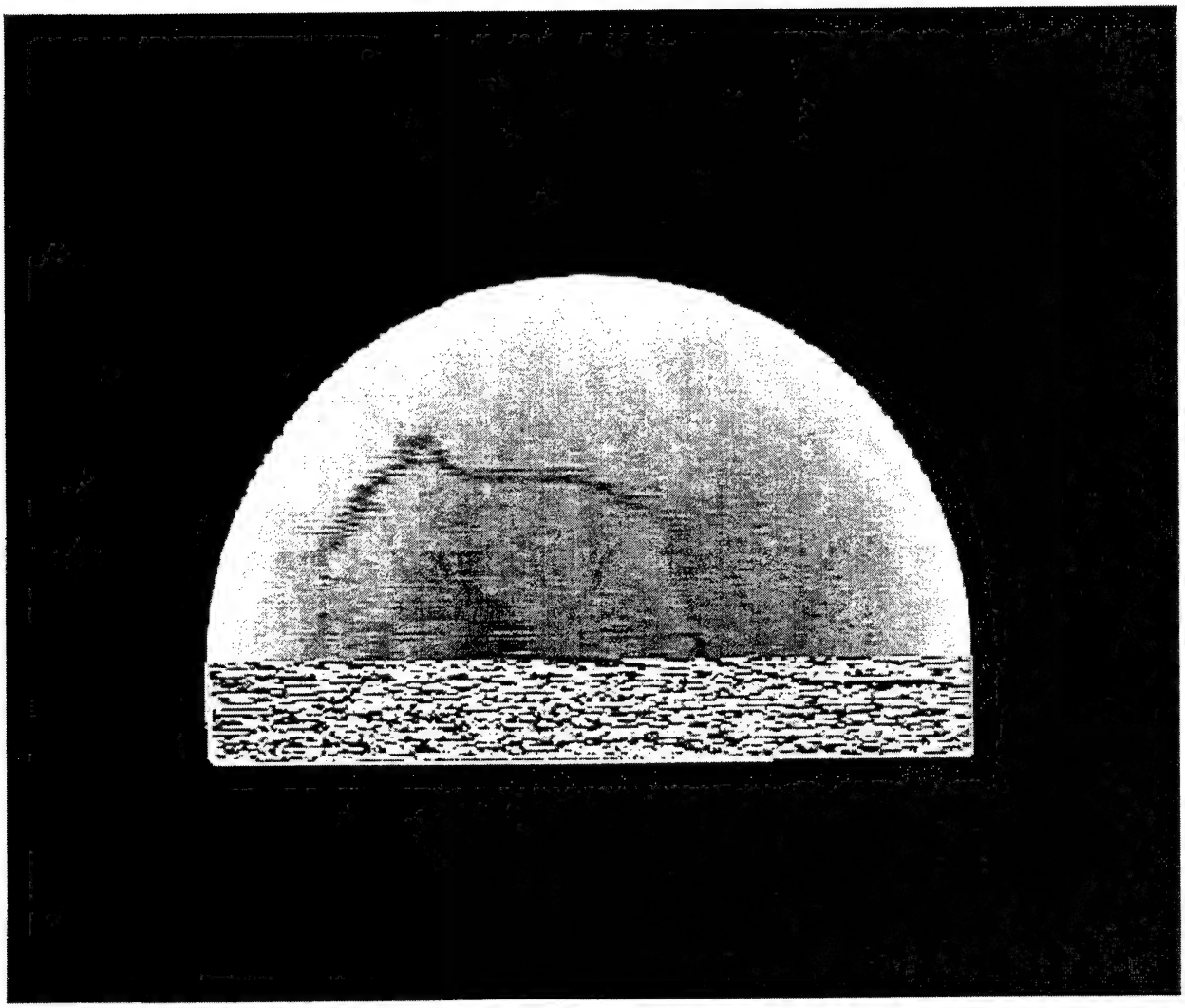

Figure A-35. 20.91 mm from bottom of disk with 65° rotation about X-axis.

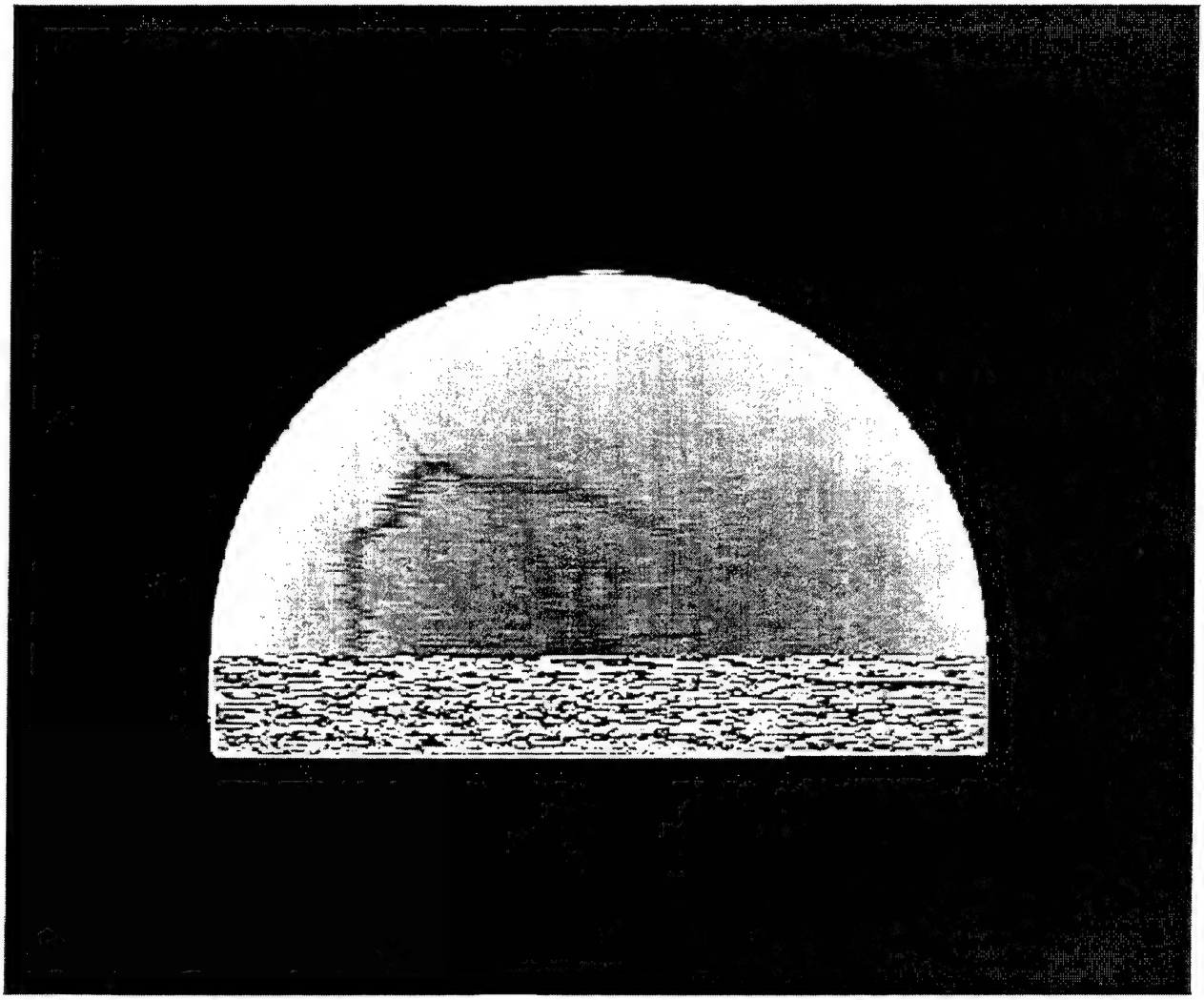

Figure A-36. 21.40 mm from bottom of disk with 65° rotation about X-axis.

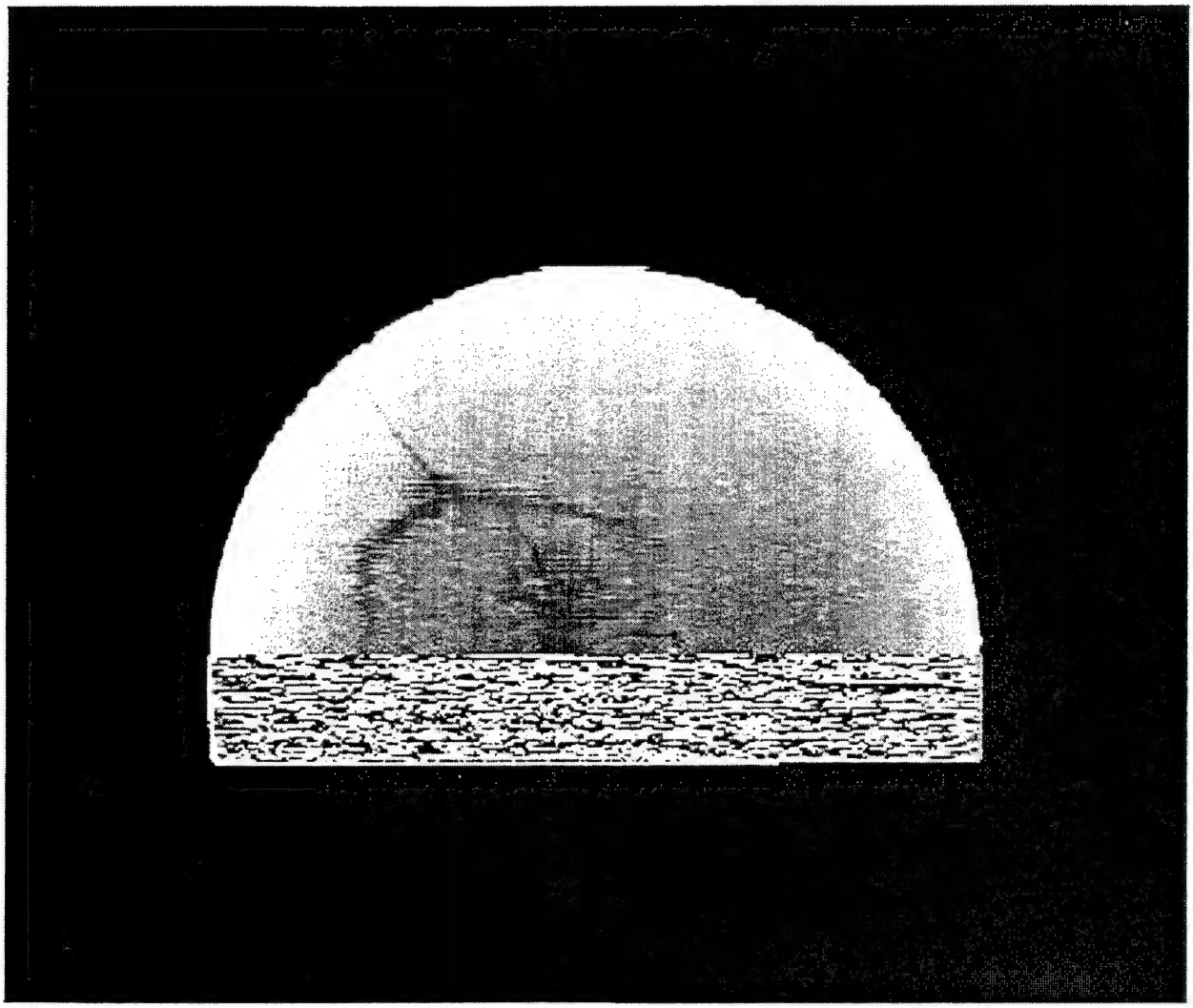

Figure A-37. 22.13 mm from bottom of disk with 65° rotation about X-axis.

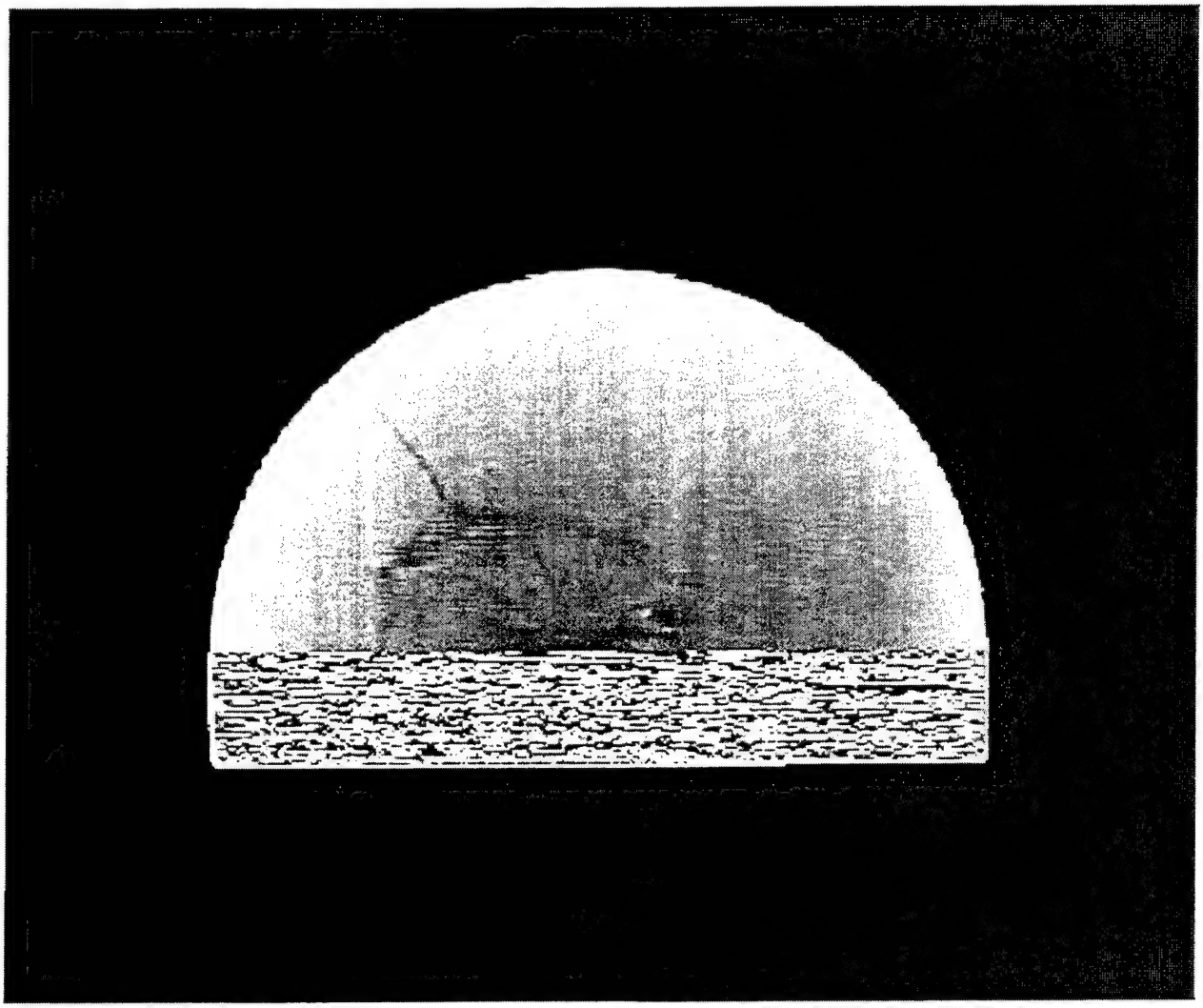

Figure A-38. 22.62 mm from bottom of disk with 65° rotation about X-axis.

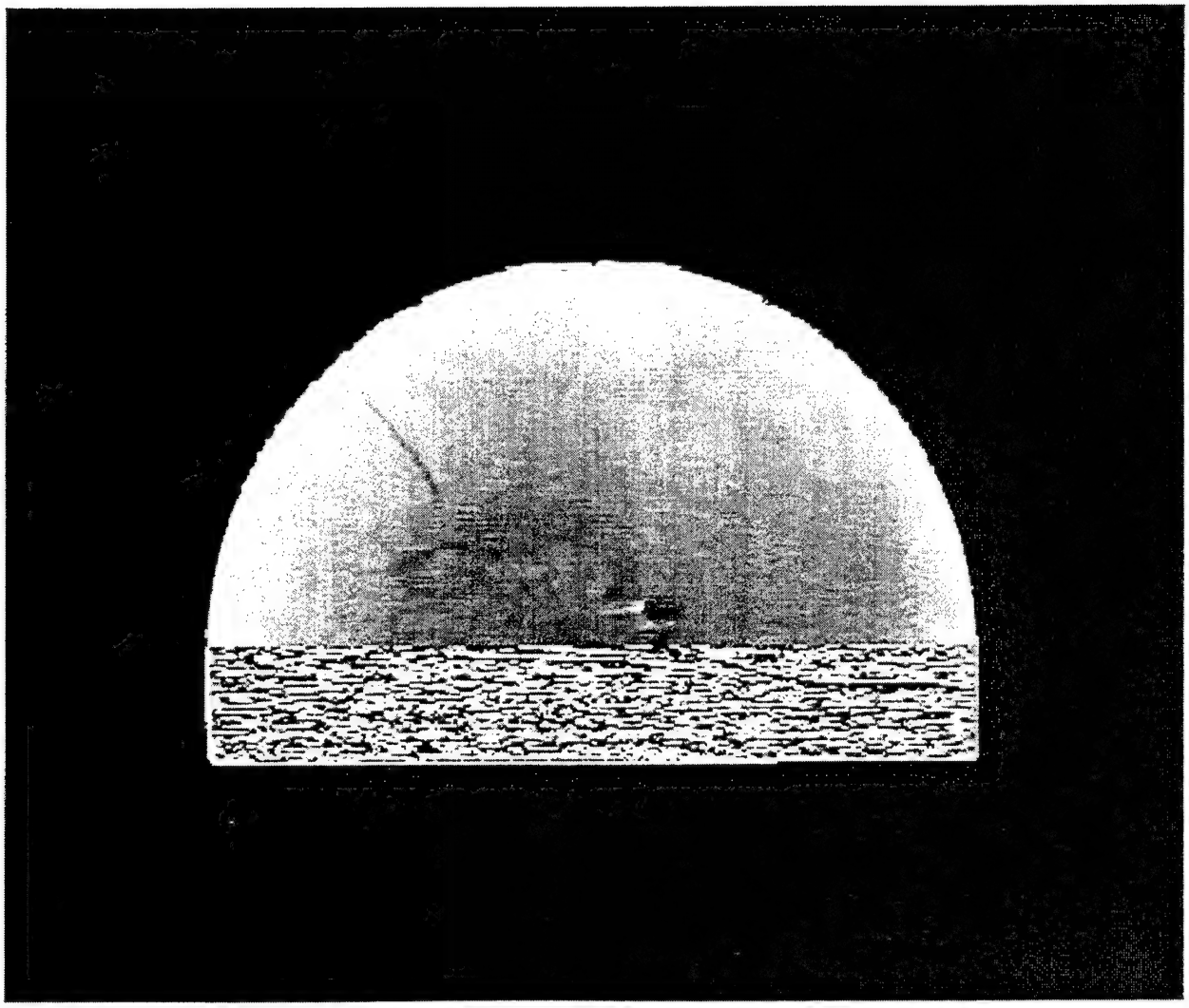

Figure A-39. 23.35 mm from bottom of disk with 65° rotation about X-axis.

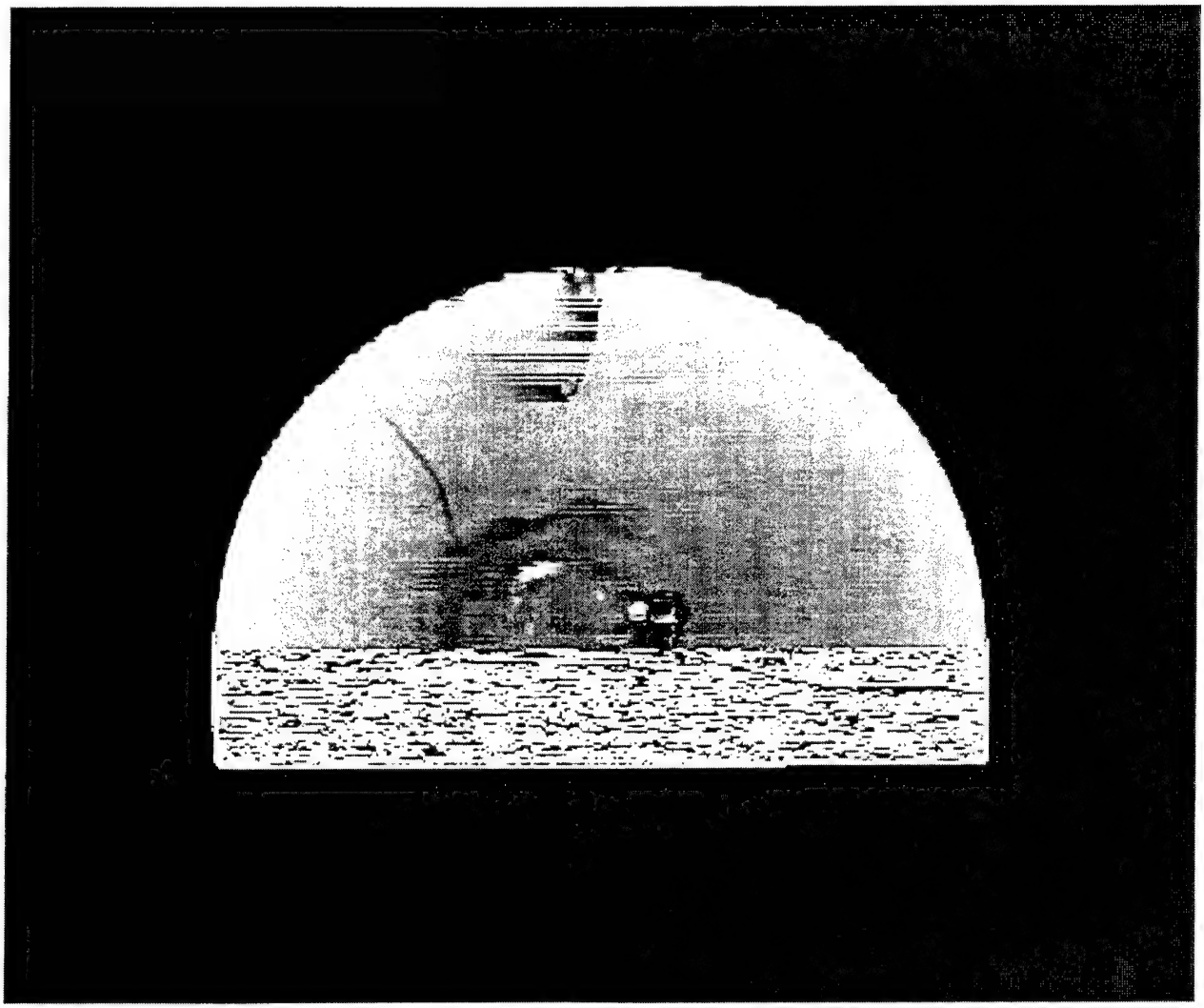

Figure A-40. 23.84 mm from bottom of disk with 65° rotation about X-axis.

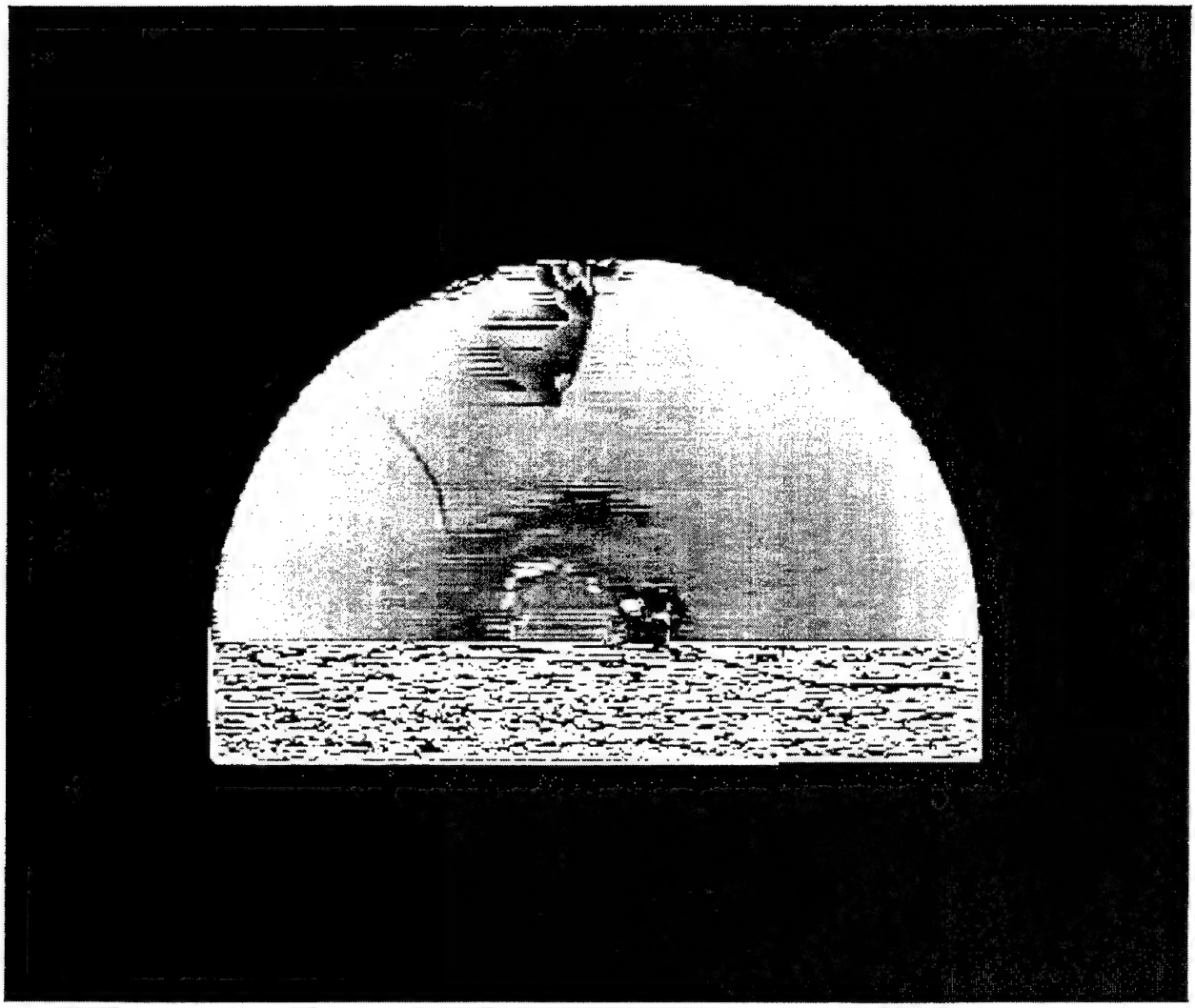

Figure A-41. 24.33 mm from bottom of disk with 65° rotation about X-axis.

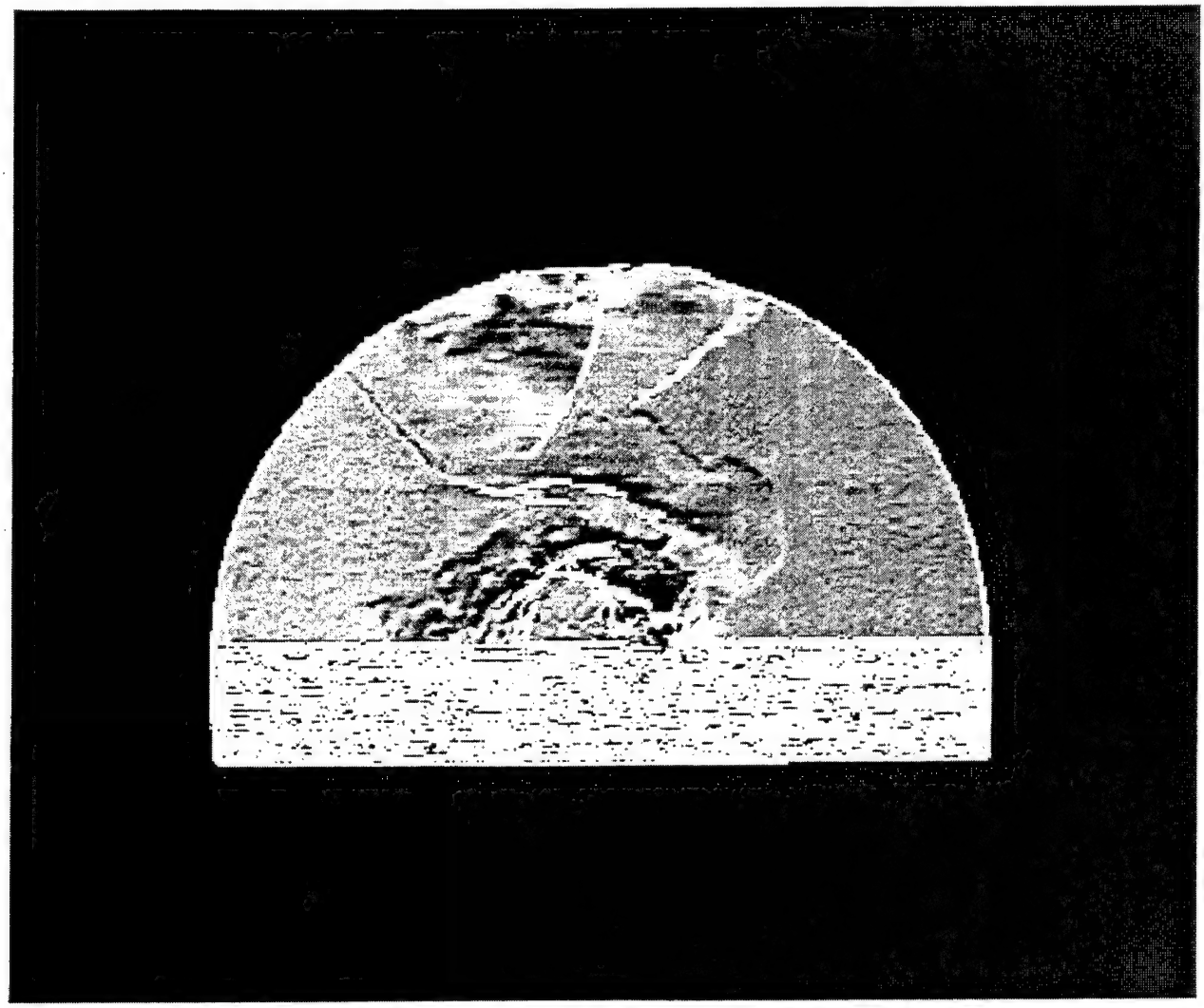

Figure A-42. 24.57 mm from bottom of disk with 65° rotation about X-axis.

Appendix B. Point Clouds of Titanium Carbide (TiC) Sample

INTENTIONALLY LEFT BLANK.

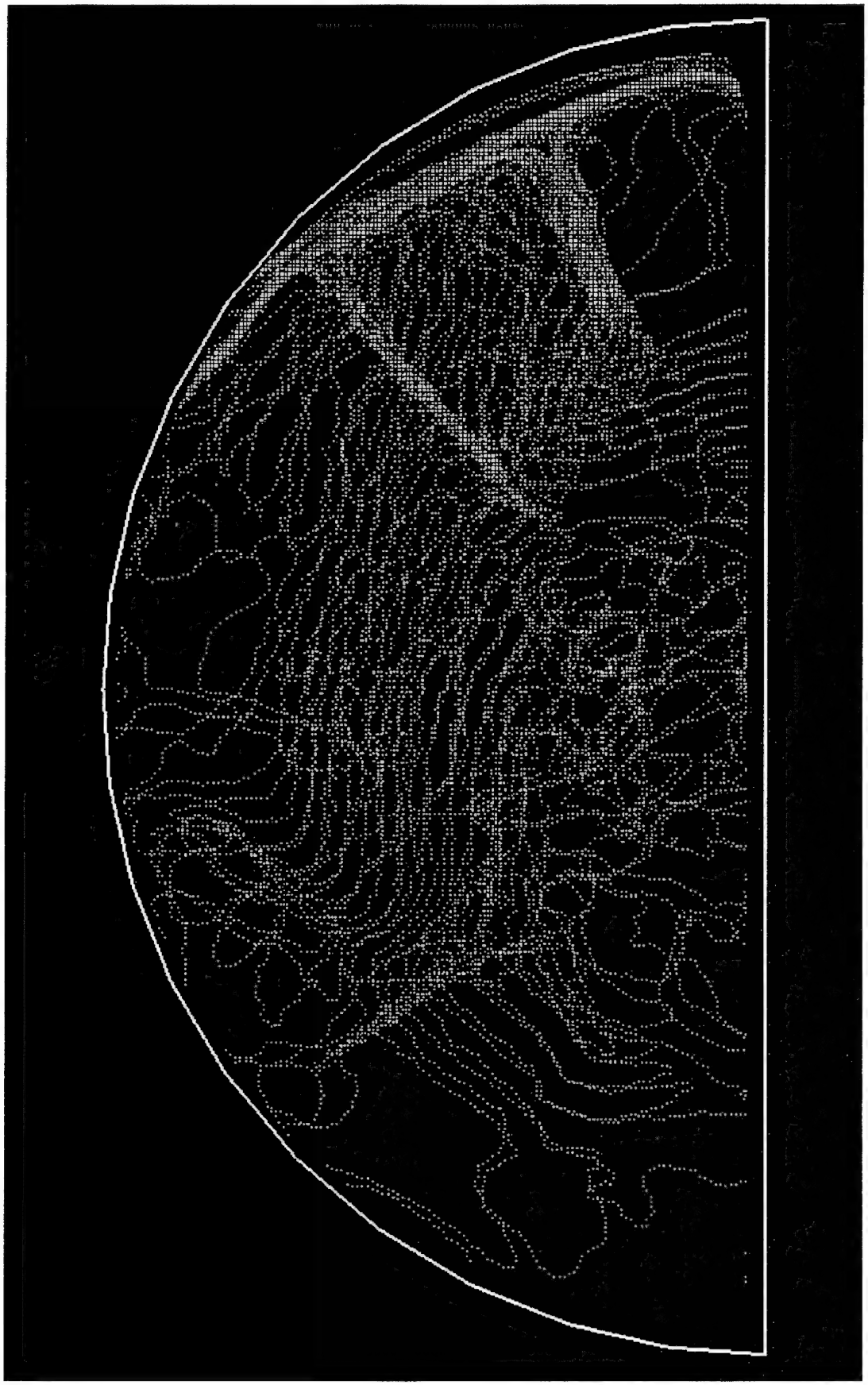

Figure B-1. 0° rotation about X-axis.

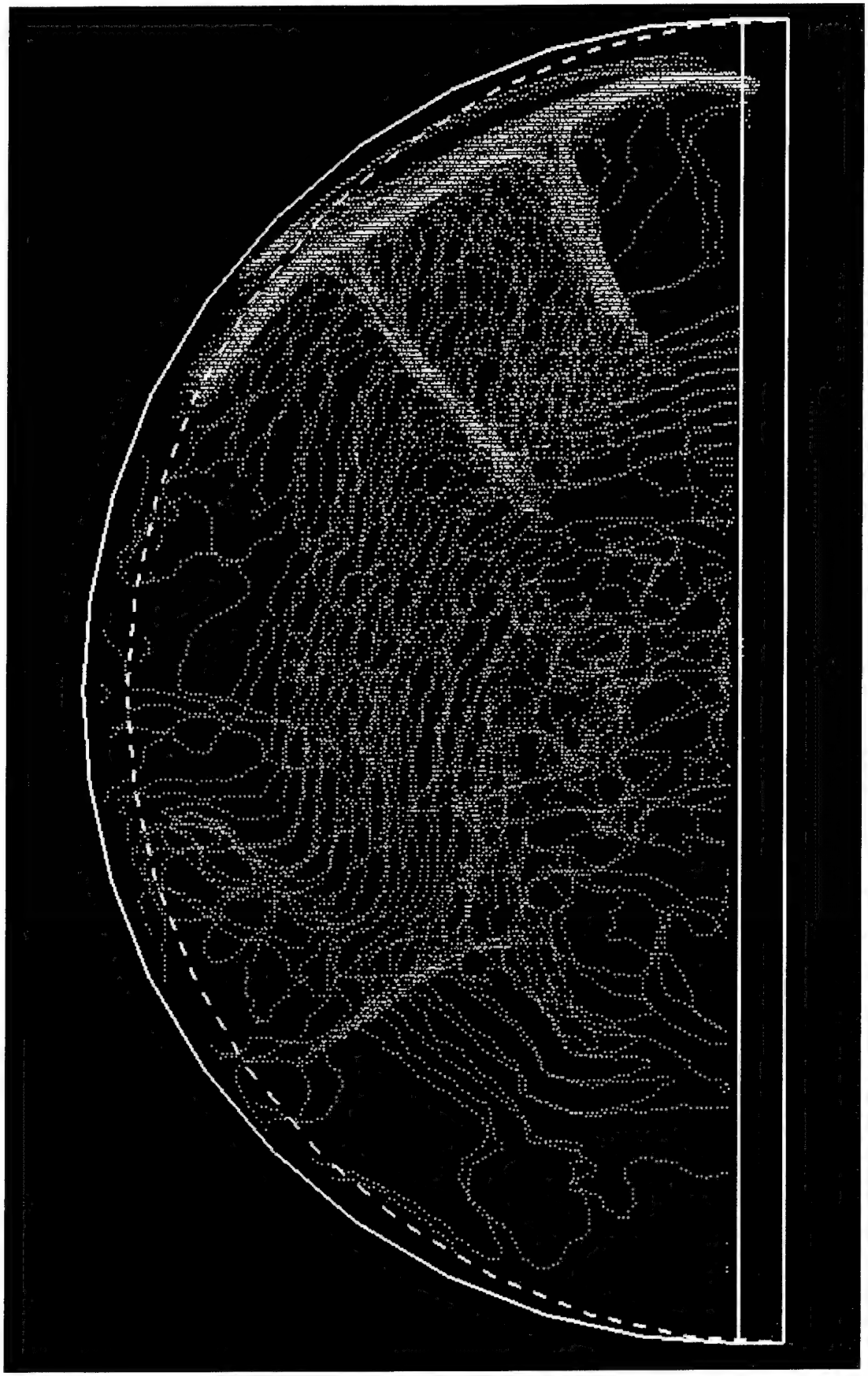

Figure B-2. 5° rotation about X-axis.

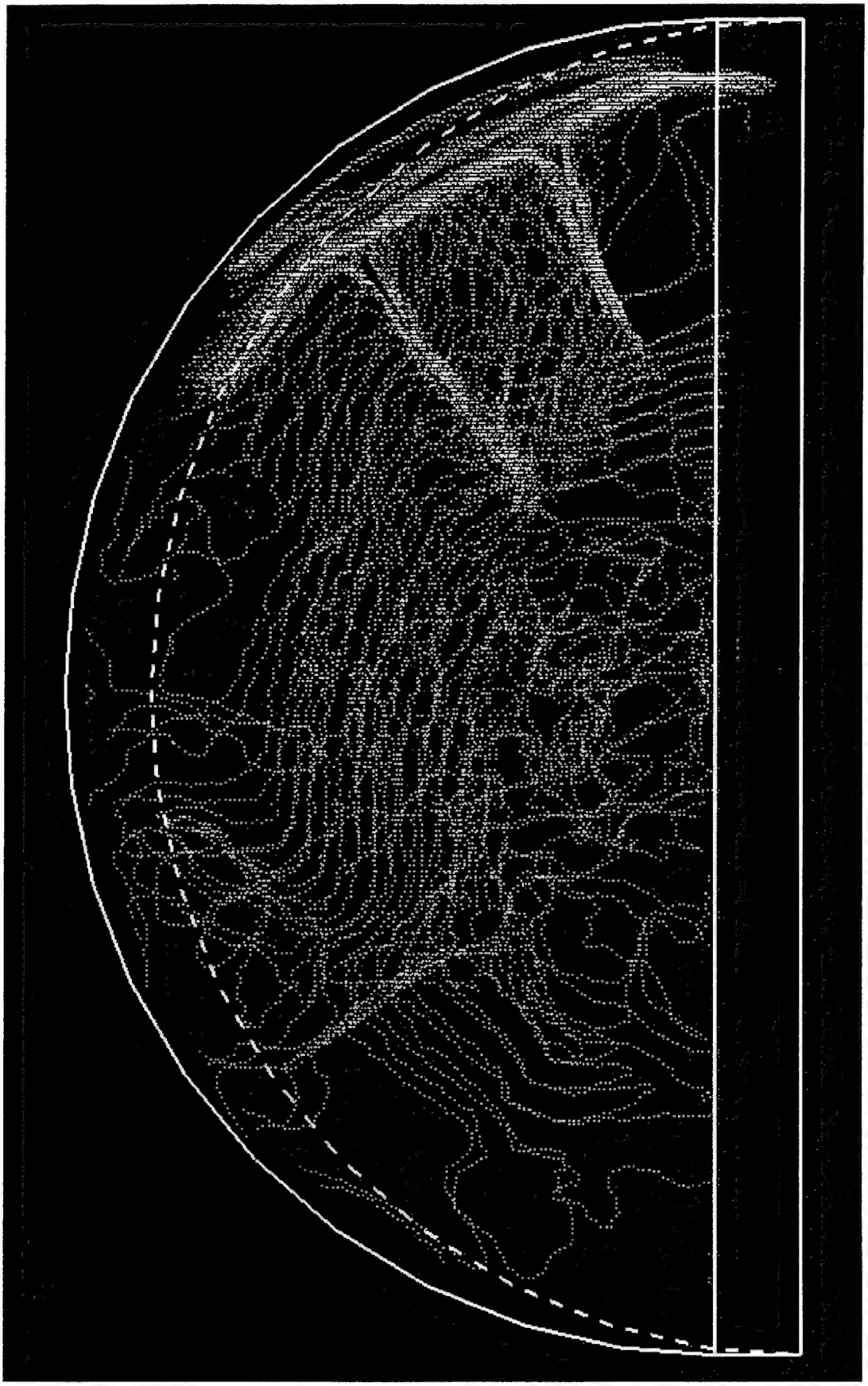

Figure B-3. 10° rotation about X-axis.

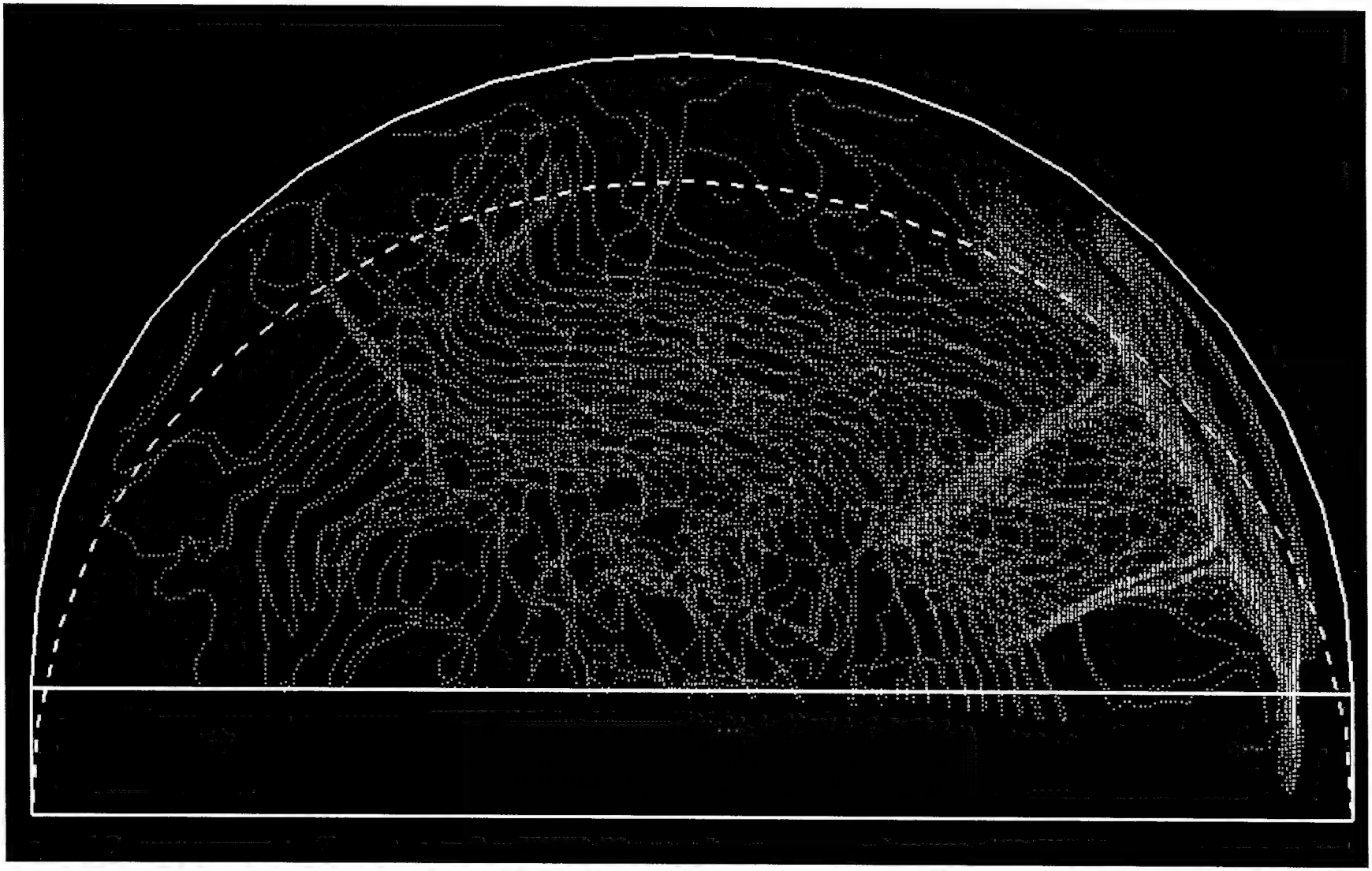

Figure B-4. 15° rotation about X-axis.

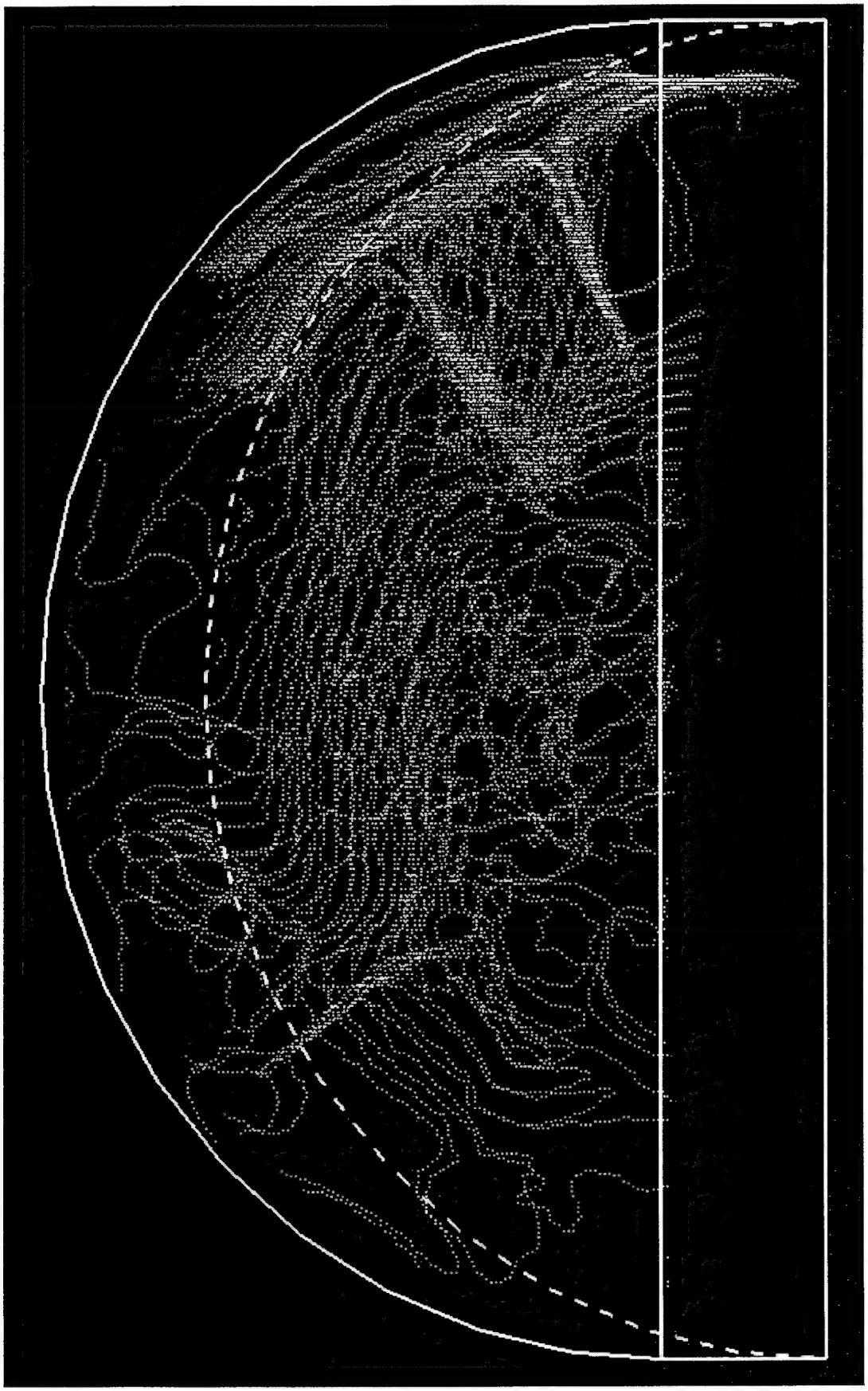

Figure B-5. 20° rotation about X-axis.

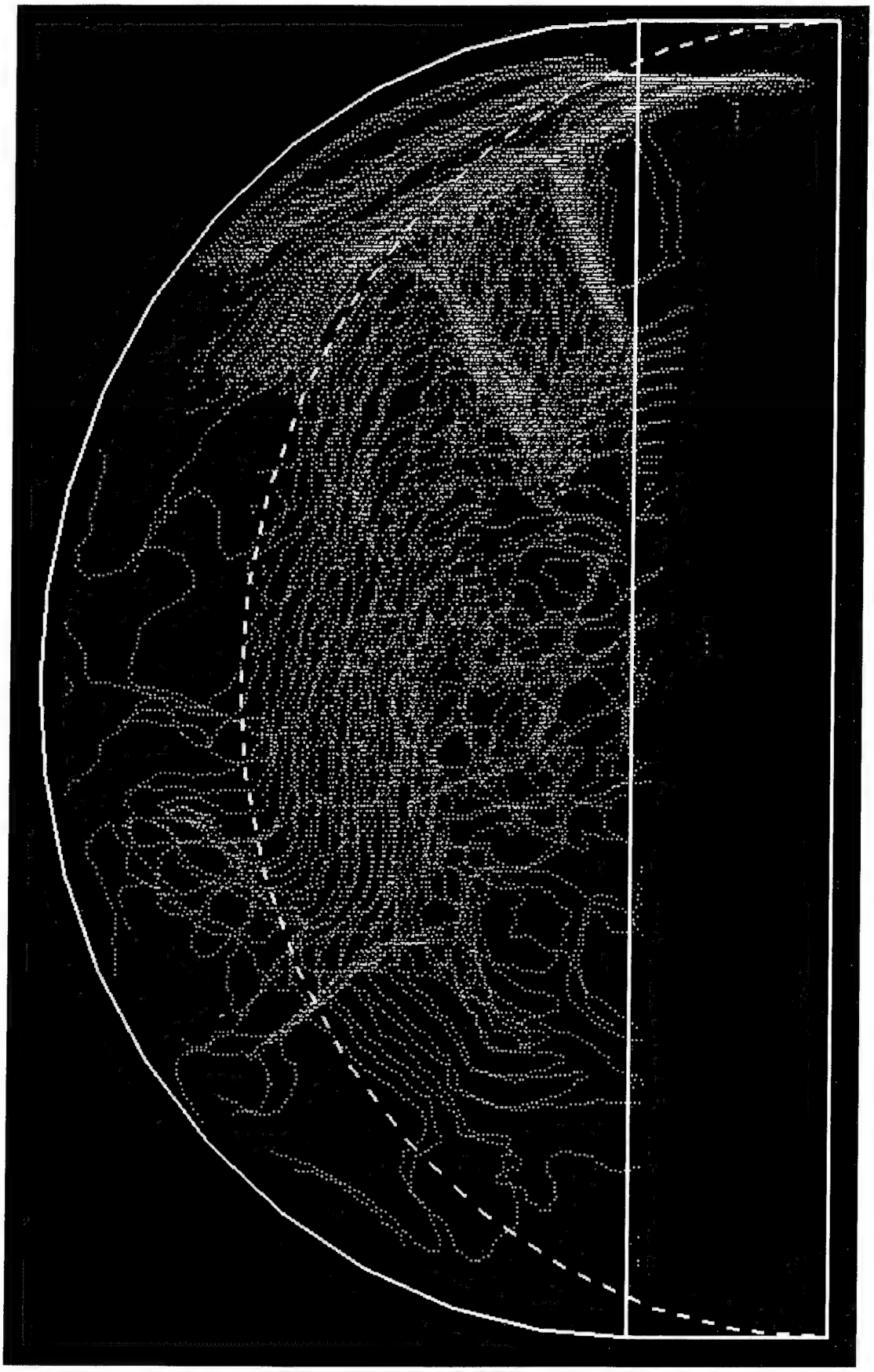

Figure B-6. 25° rotation about X-axis.

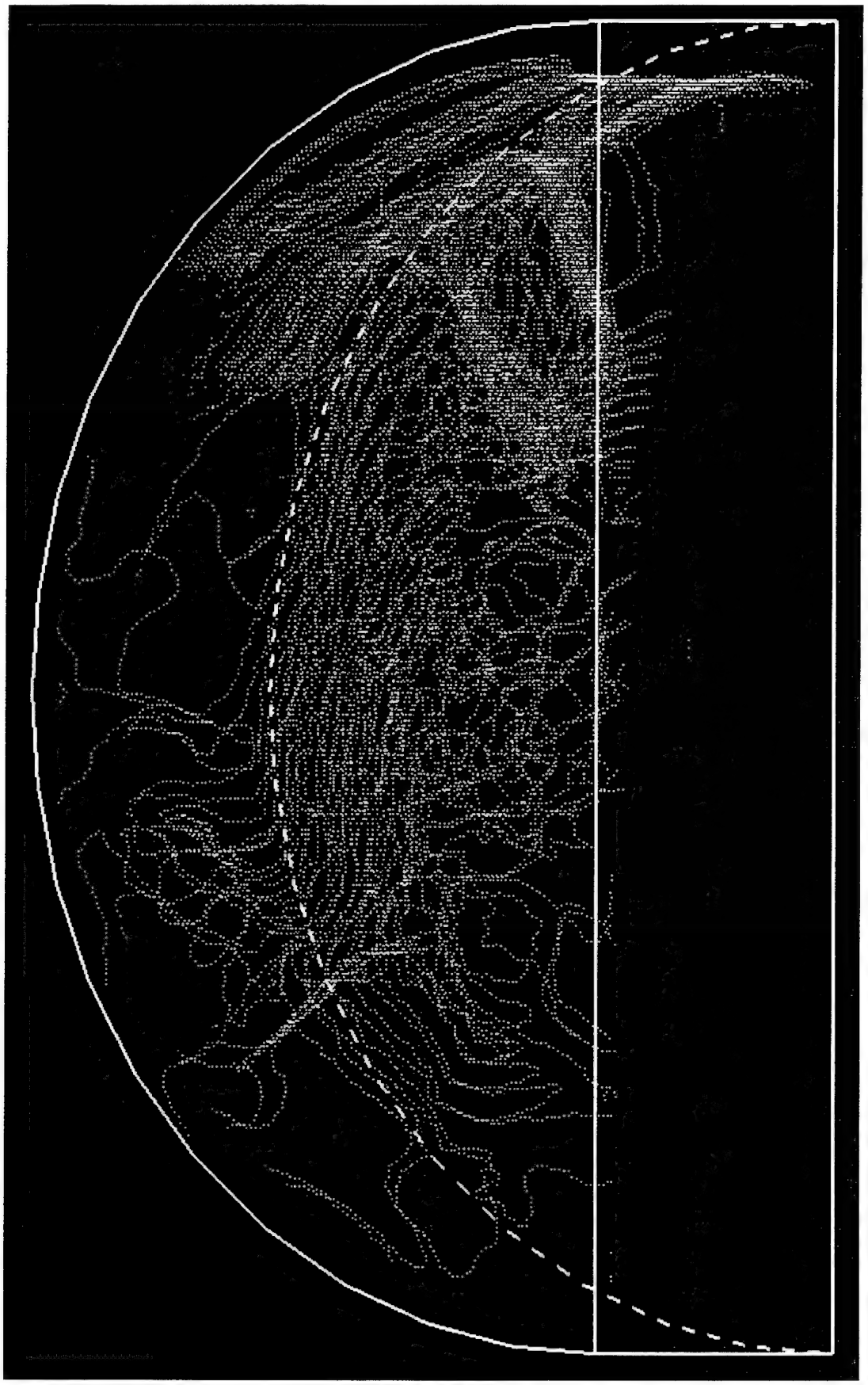

Figure B-7. 30° rotation about X-axis.

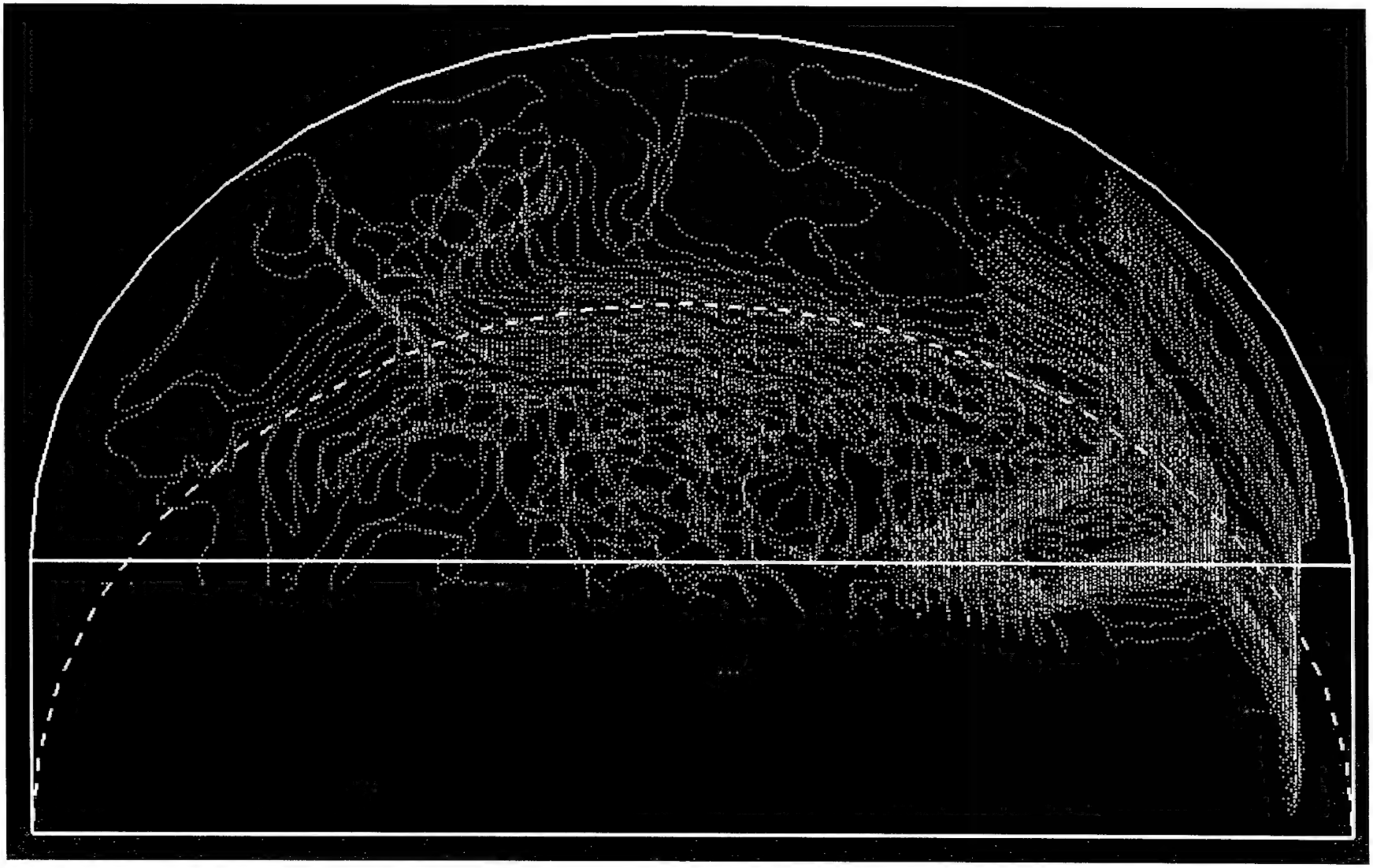

Figure B-8. 35° rotation about X-axis.

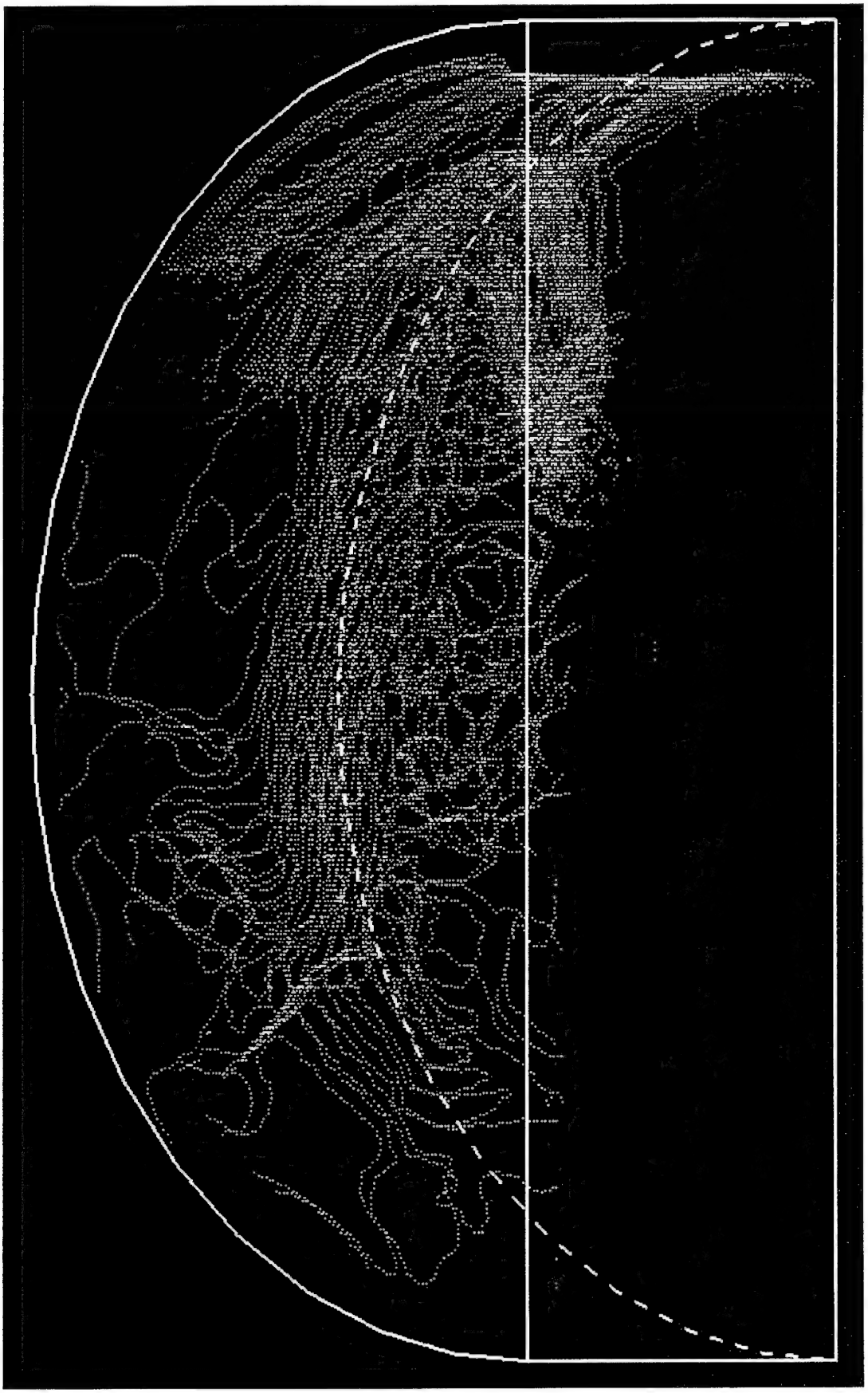

Figure B-9. 40° rotation about X-axis.

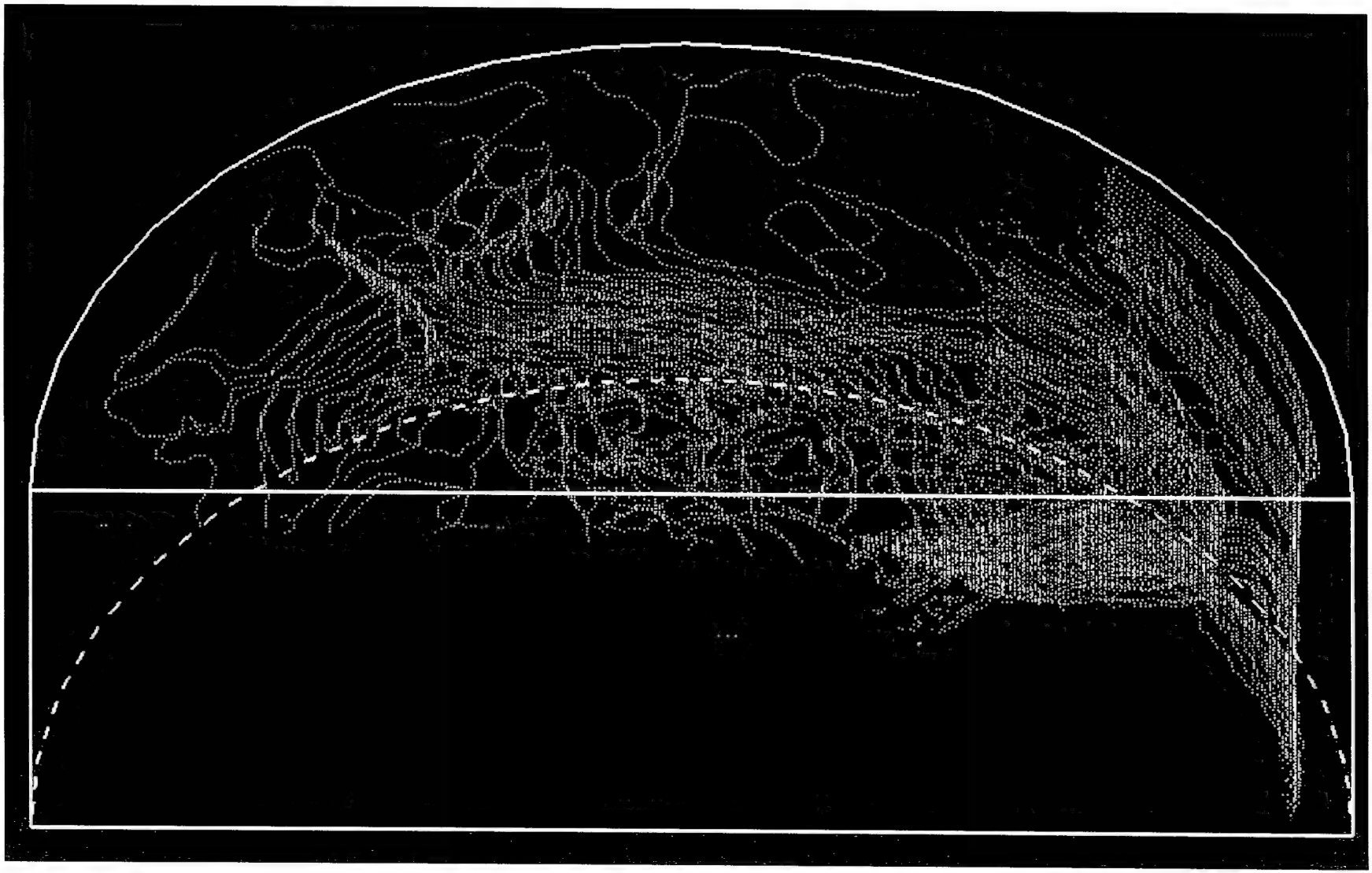

Figure B-10. 45° rotation about X-axis.

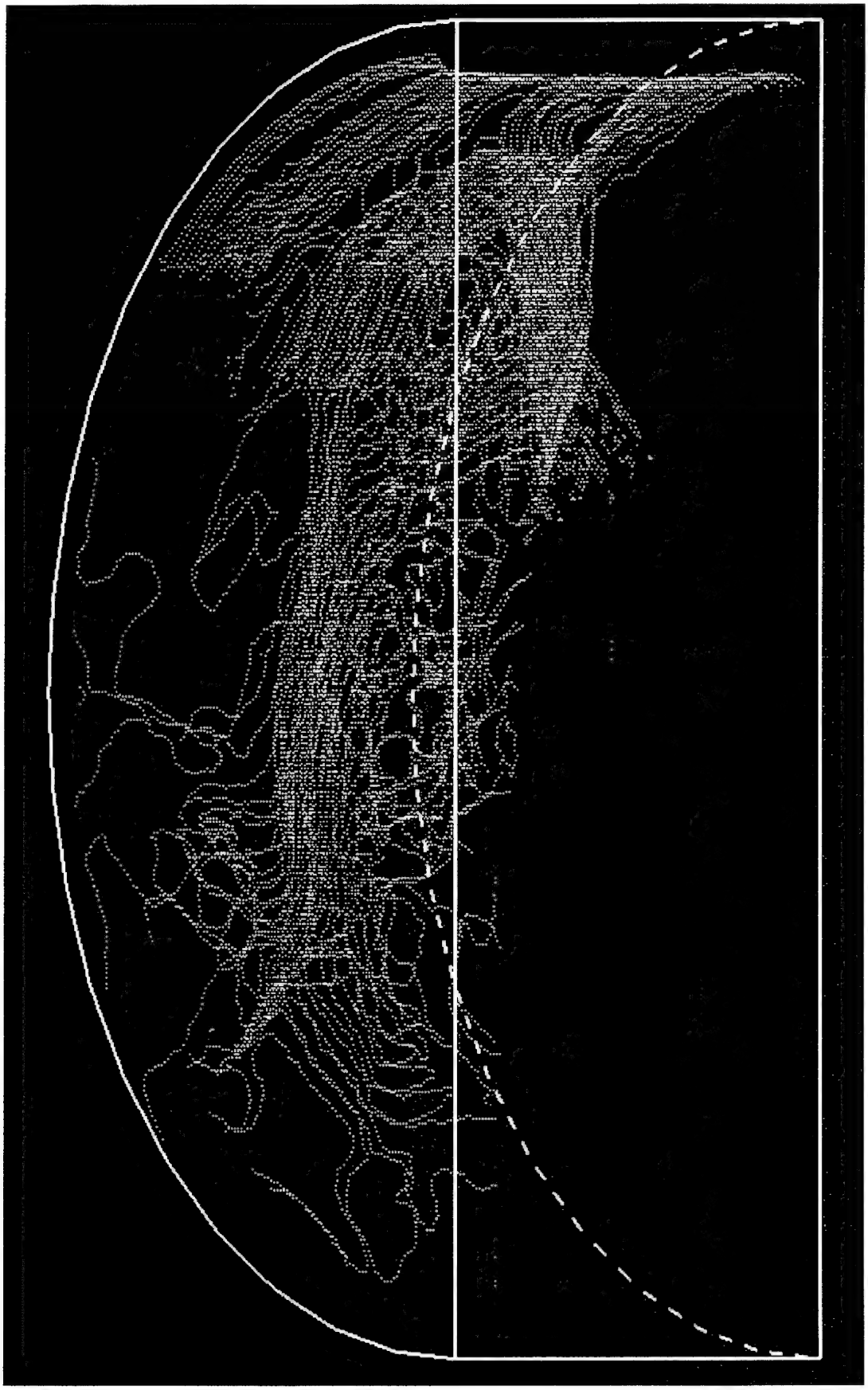

Figure B-11. 50° rotation about X-axis.

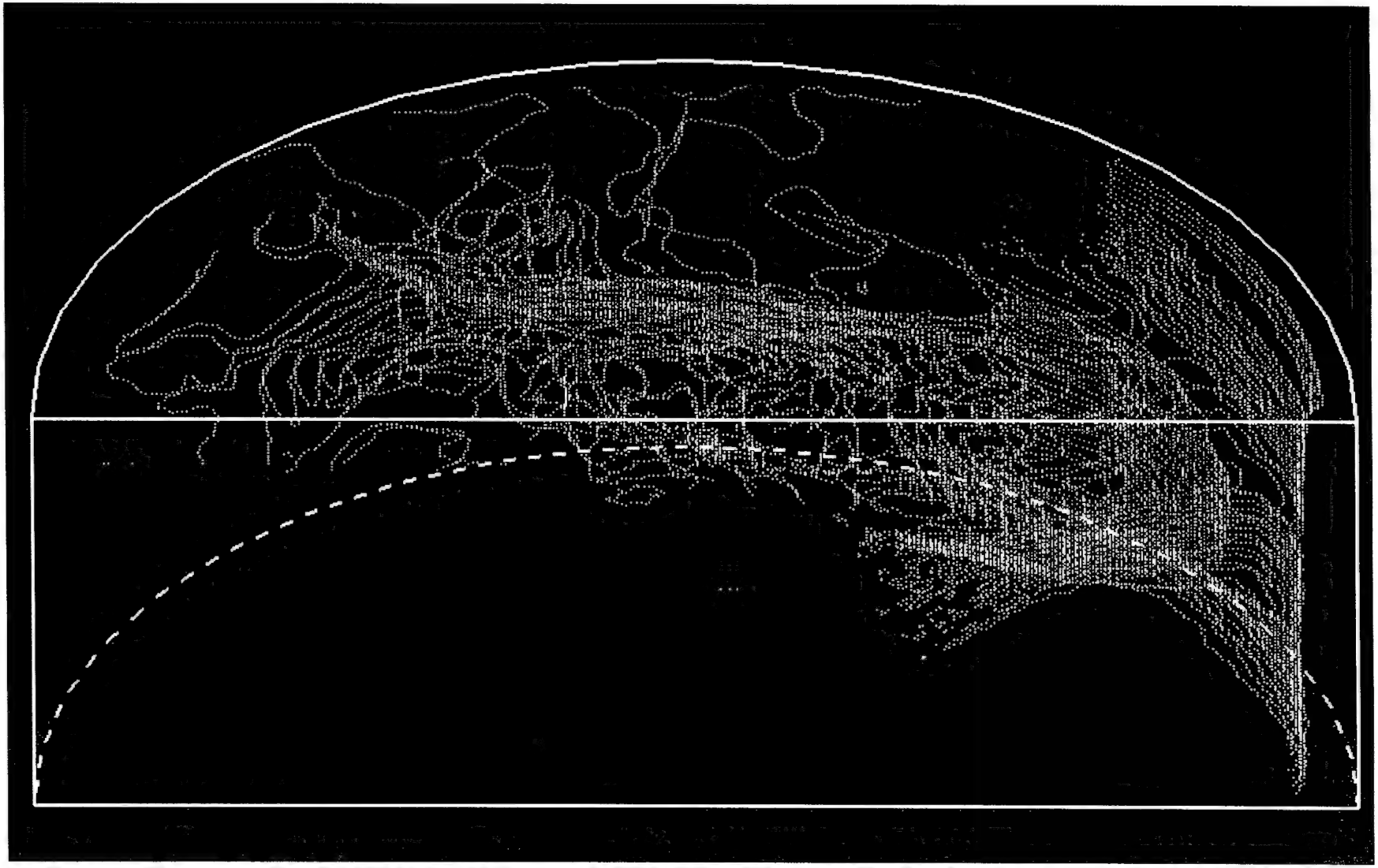

Figure B-12. 55° rotation about X-axis.

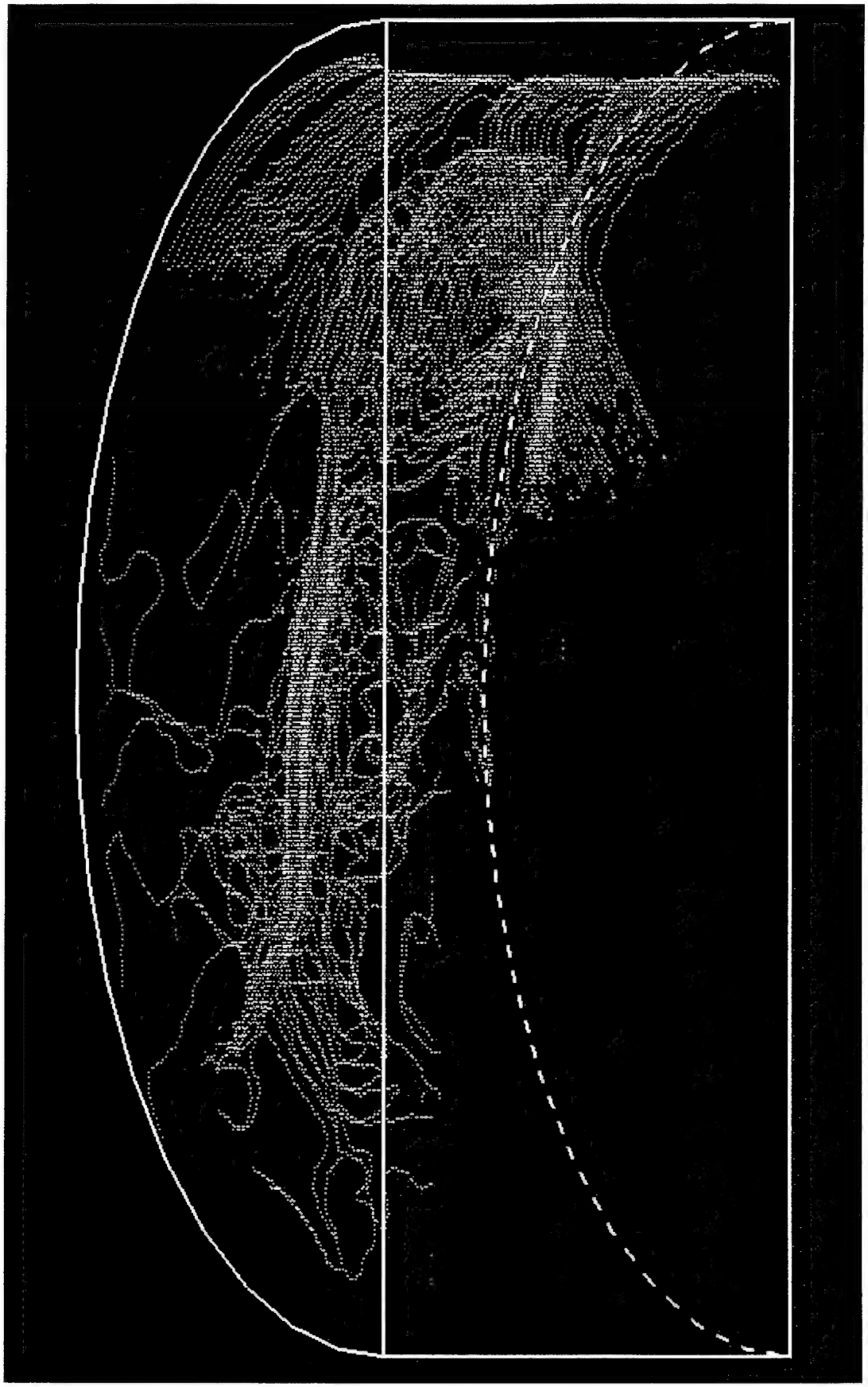

Figure B-13. 60° rotation about X-axis.

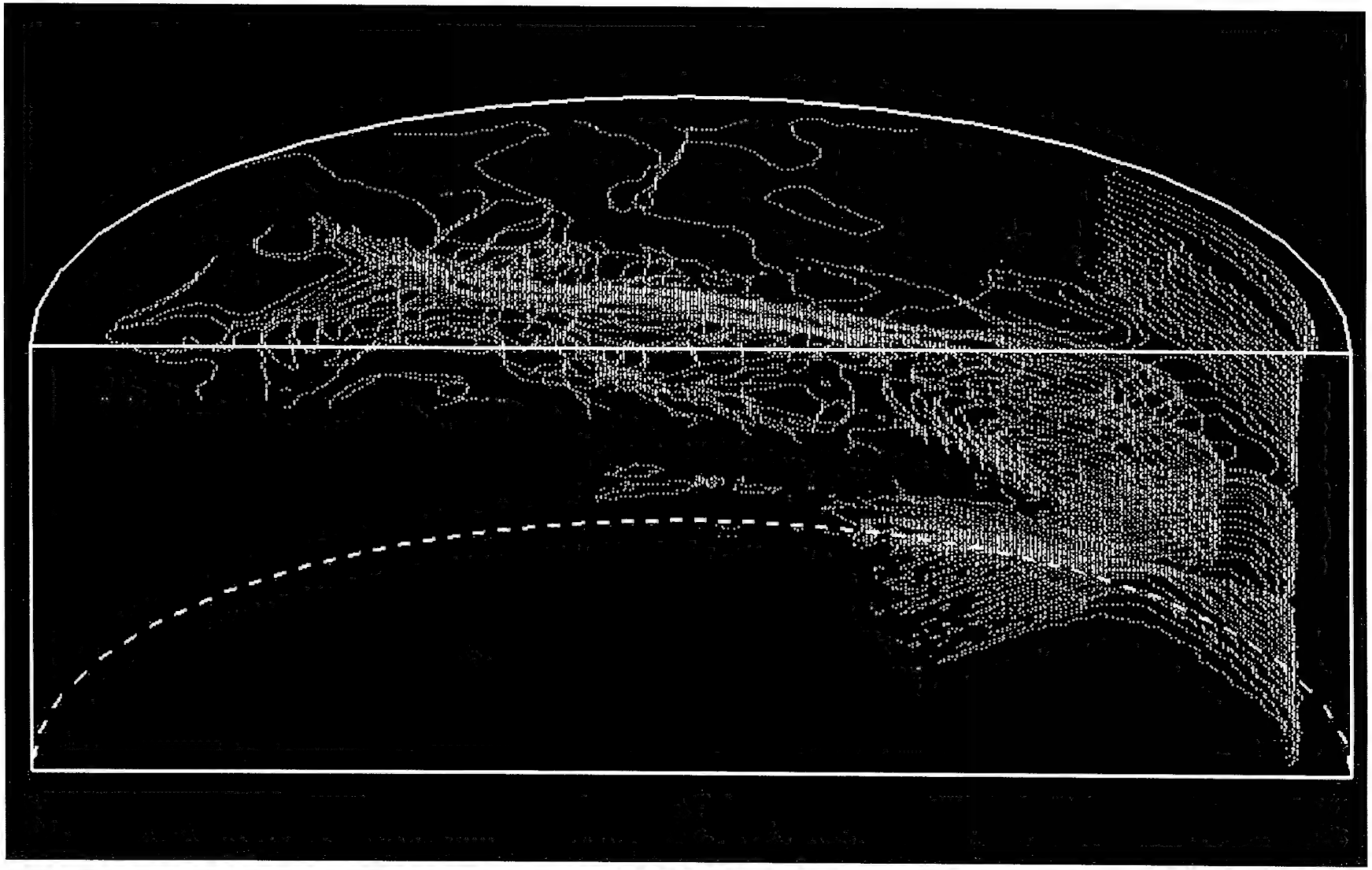

Figure B-14. 65° rotation about X-axis.

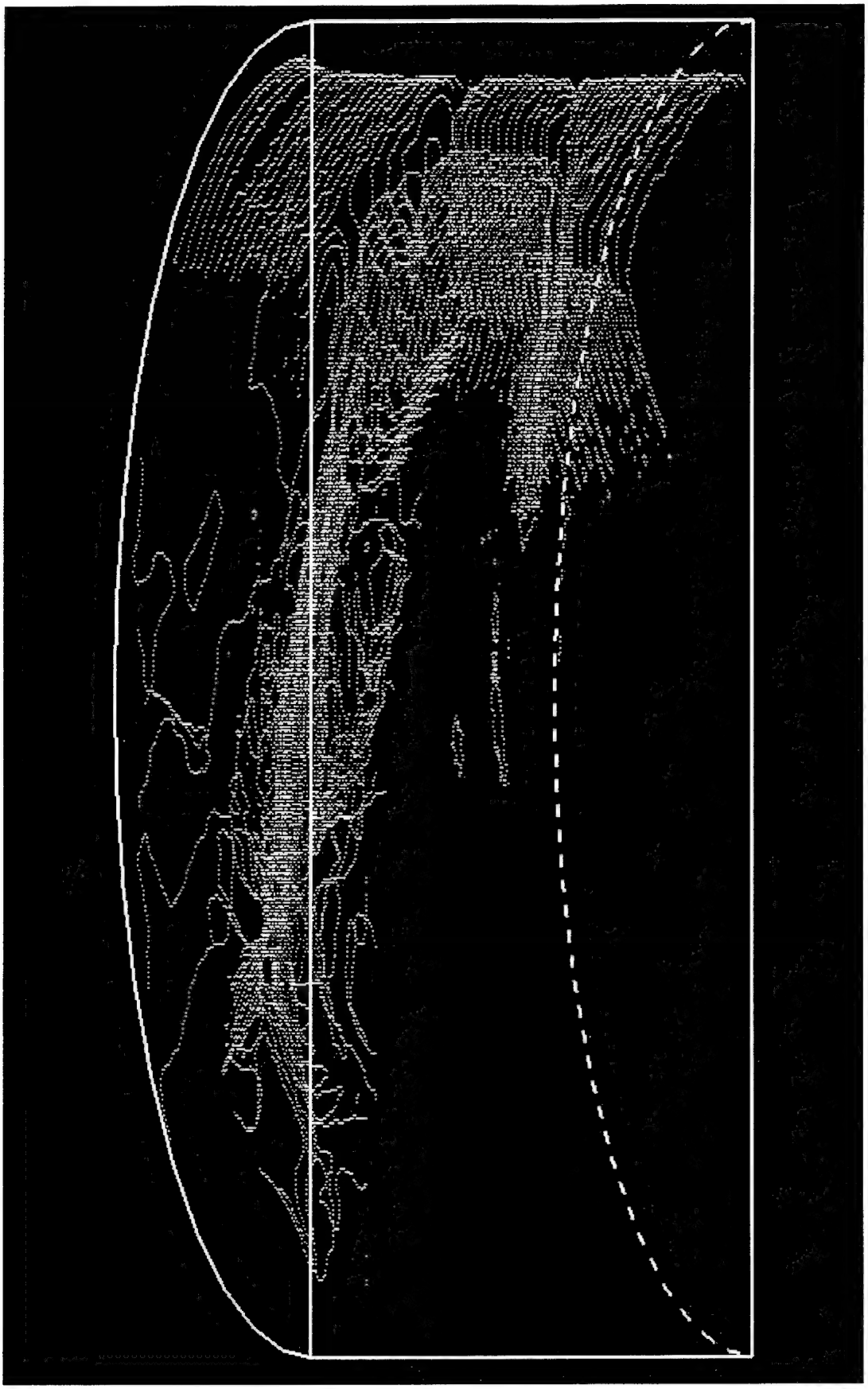

Figure B-15. 70° rotation about X-axis.

Figure B-16. 75° rotation about X-axis.

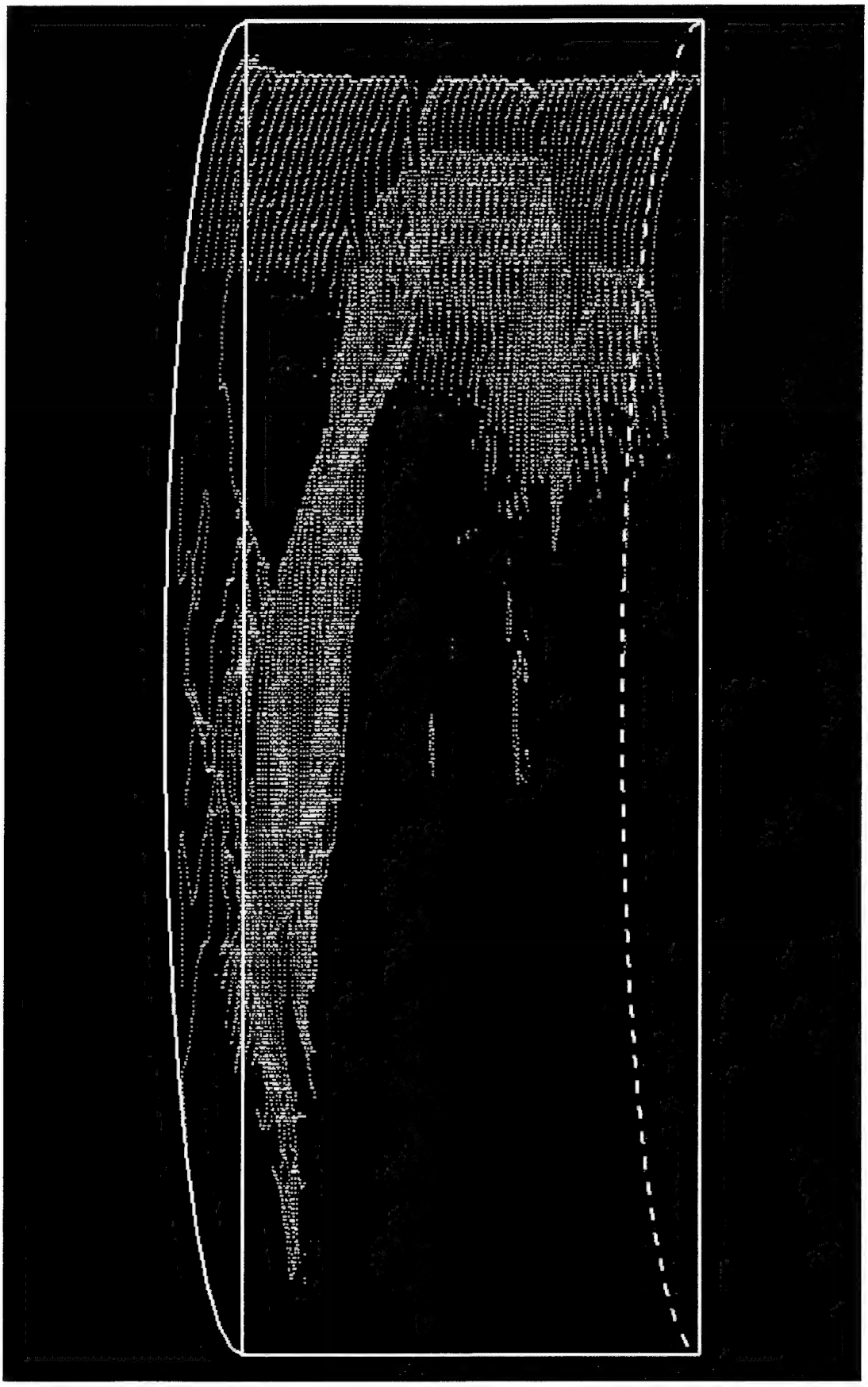

Figure B-17. 80° rotation about *X*-axis.

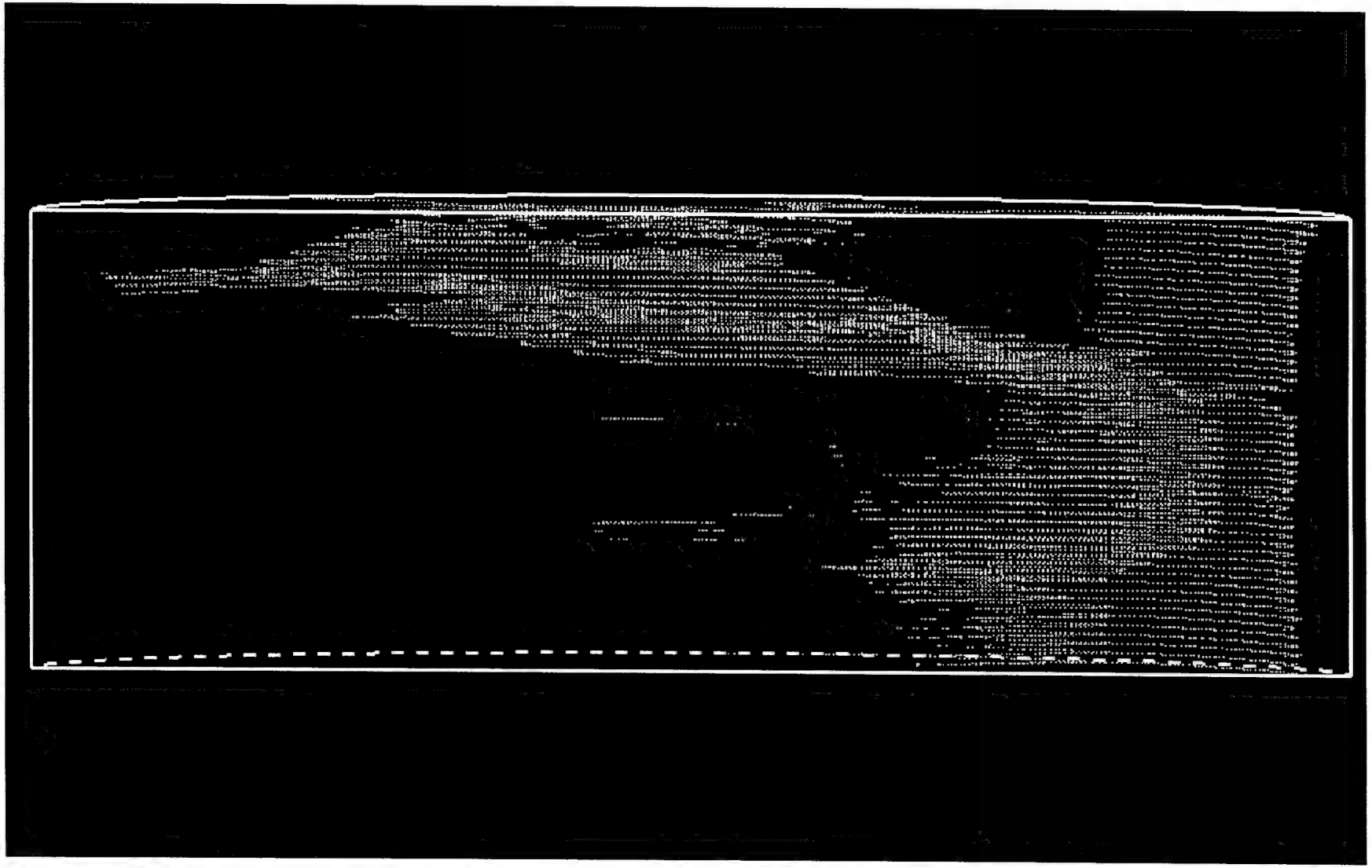

Figure B-18. 85° rotation about X-axis.

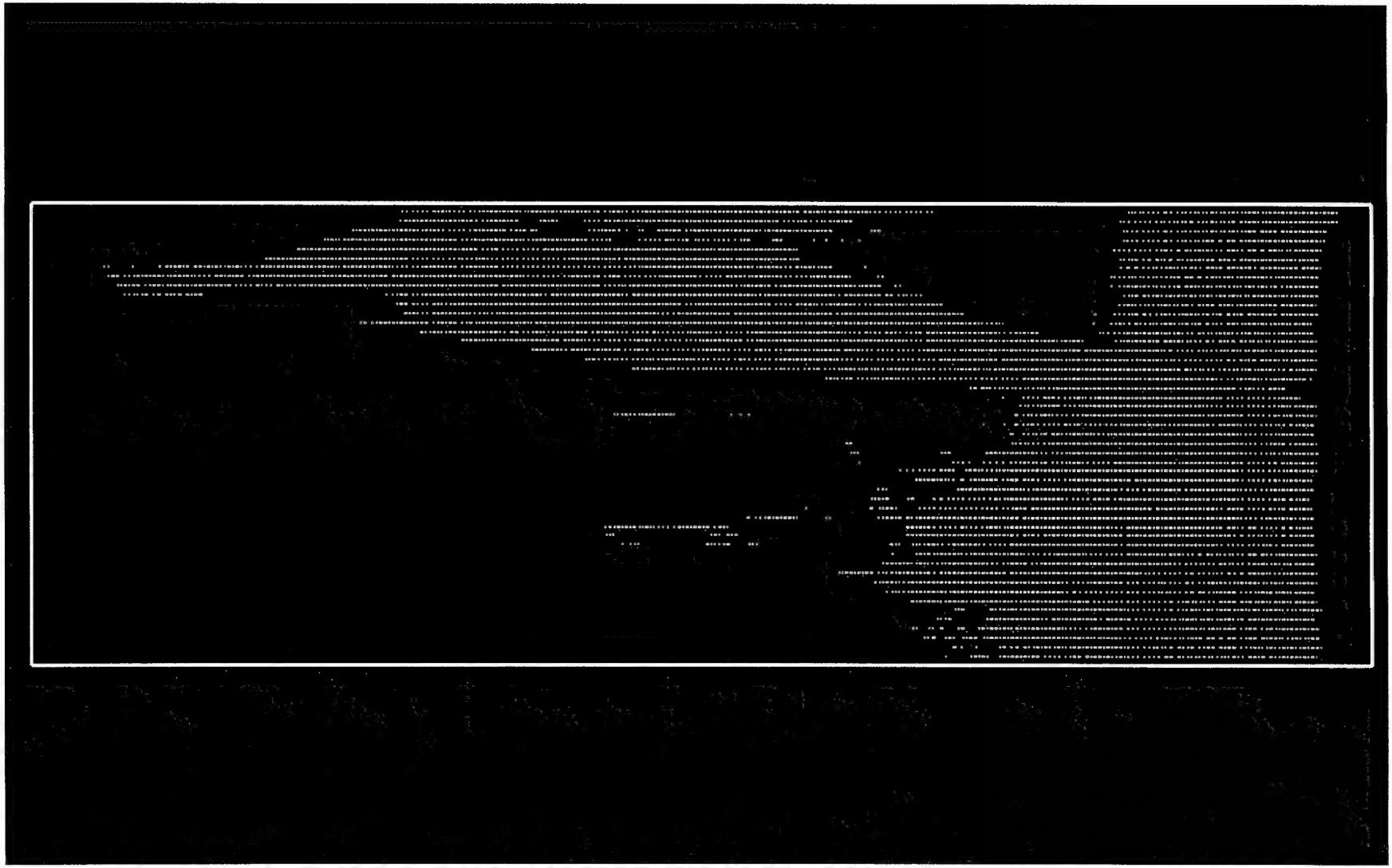

Figure B-19. 90° rotation about X-axis.

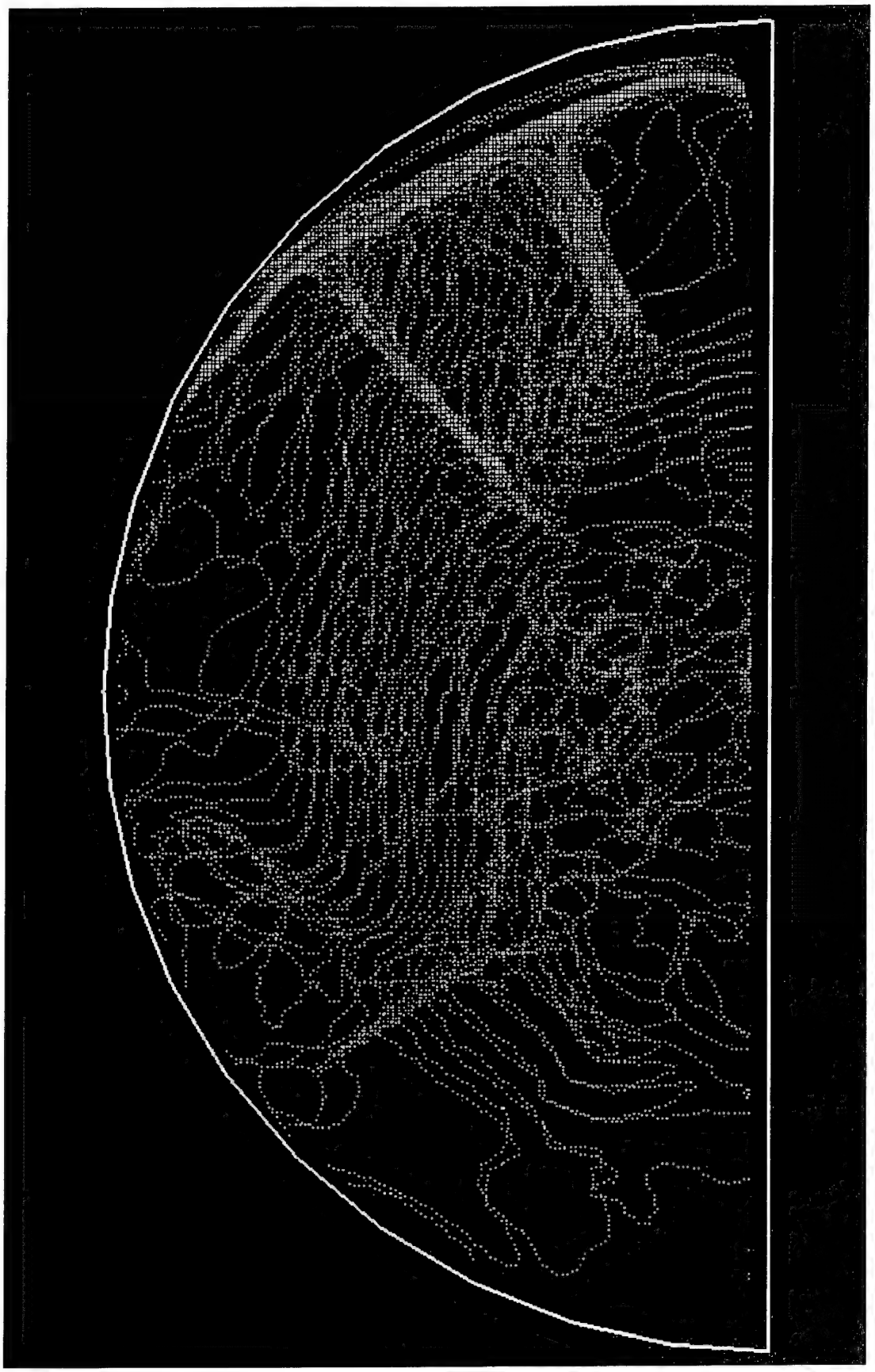

Figure B-20. 0° rotation about Y-axis.

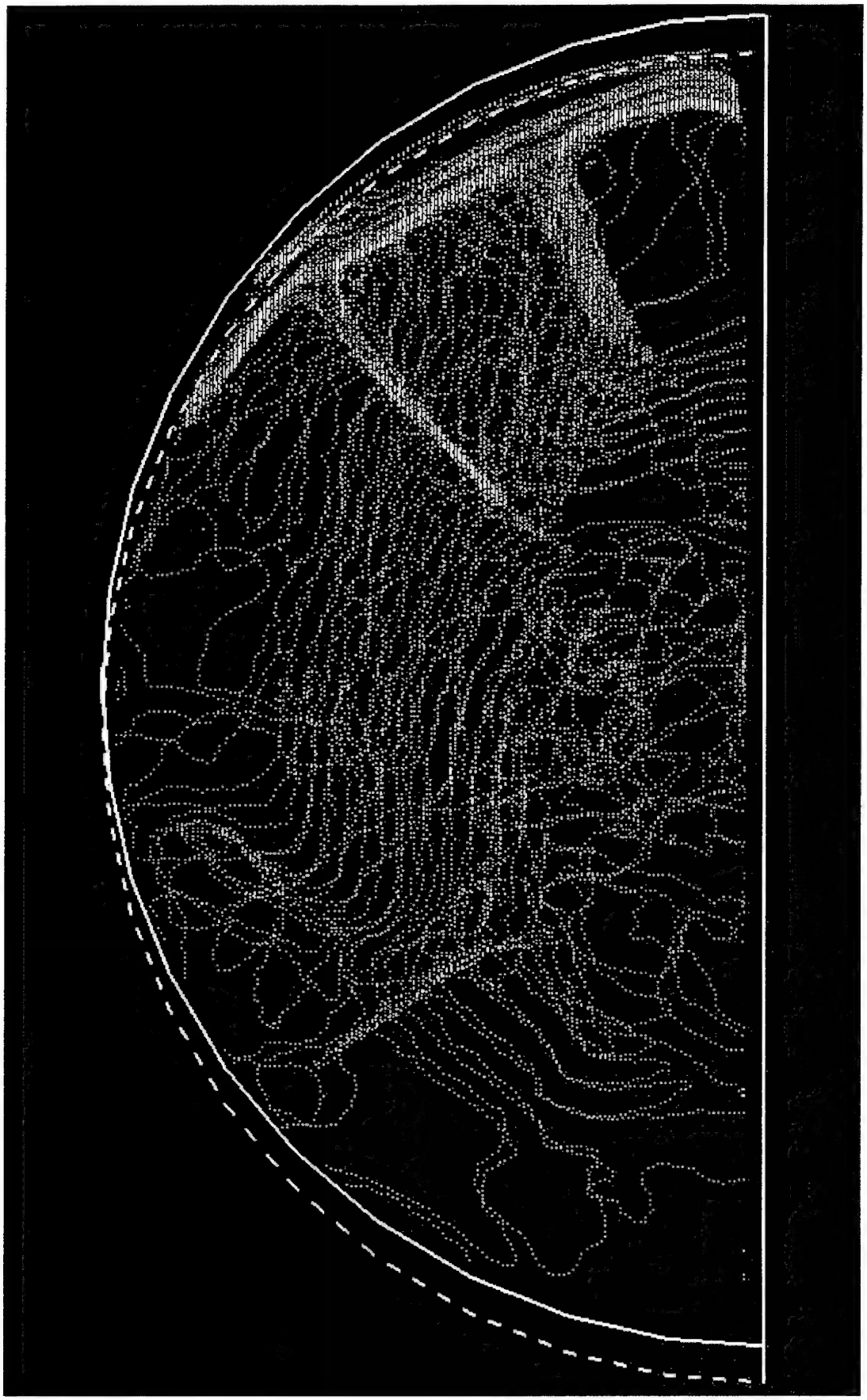

Figure B-21. 4.5° rotation about Y-axis.

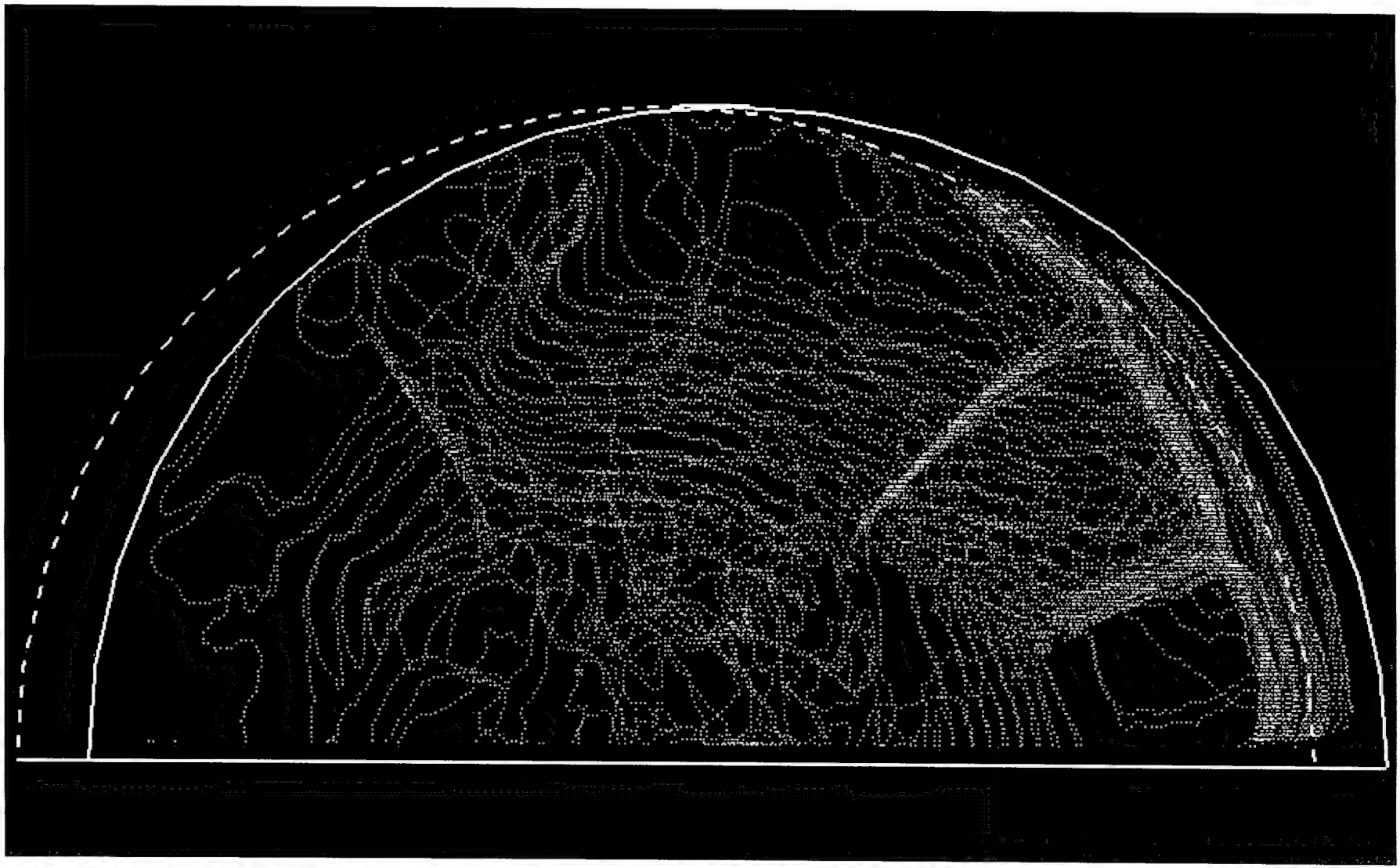

Figure B-22. 9° rotation about Y-axis.

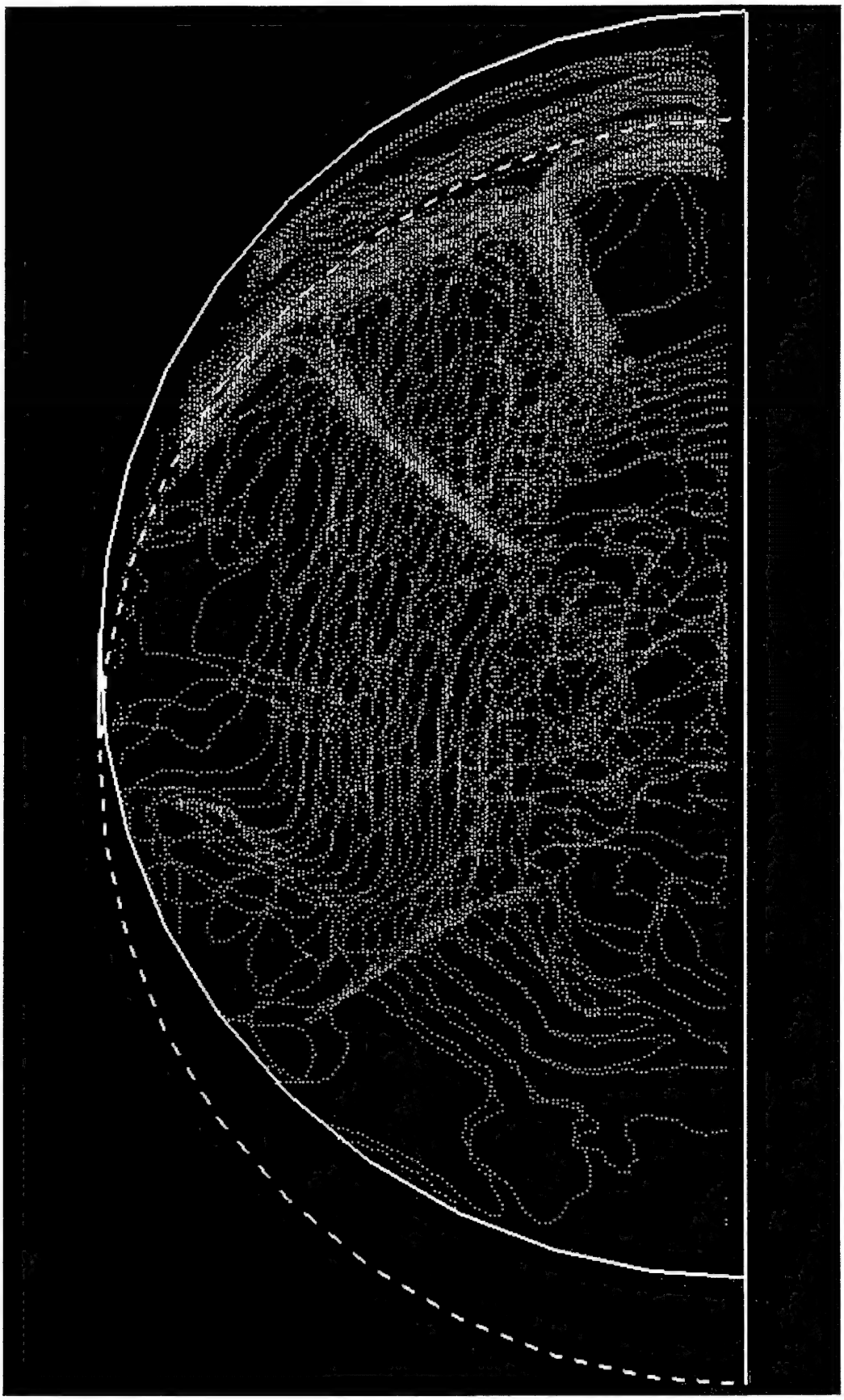

Figure B-23. 13.5° rotation about Y-axis.

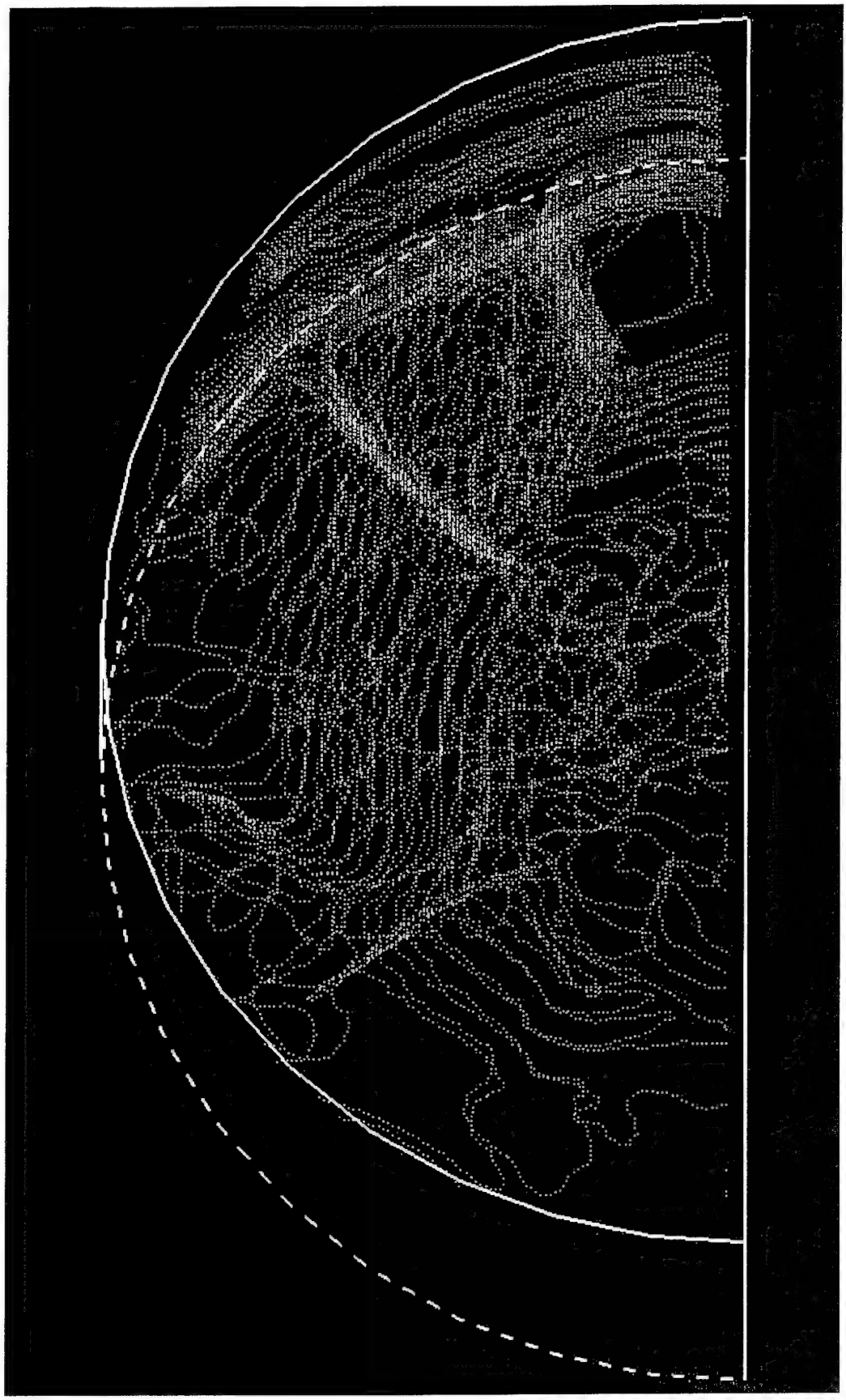

Figure B-24. 18° rotation about Y-axis.

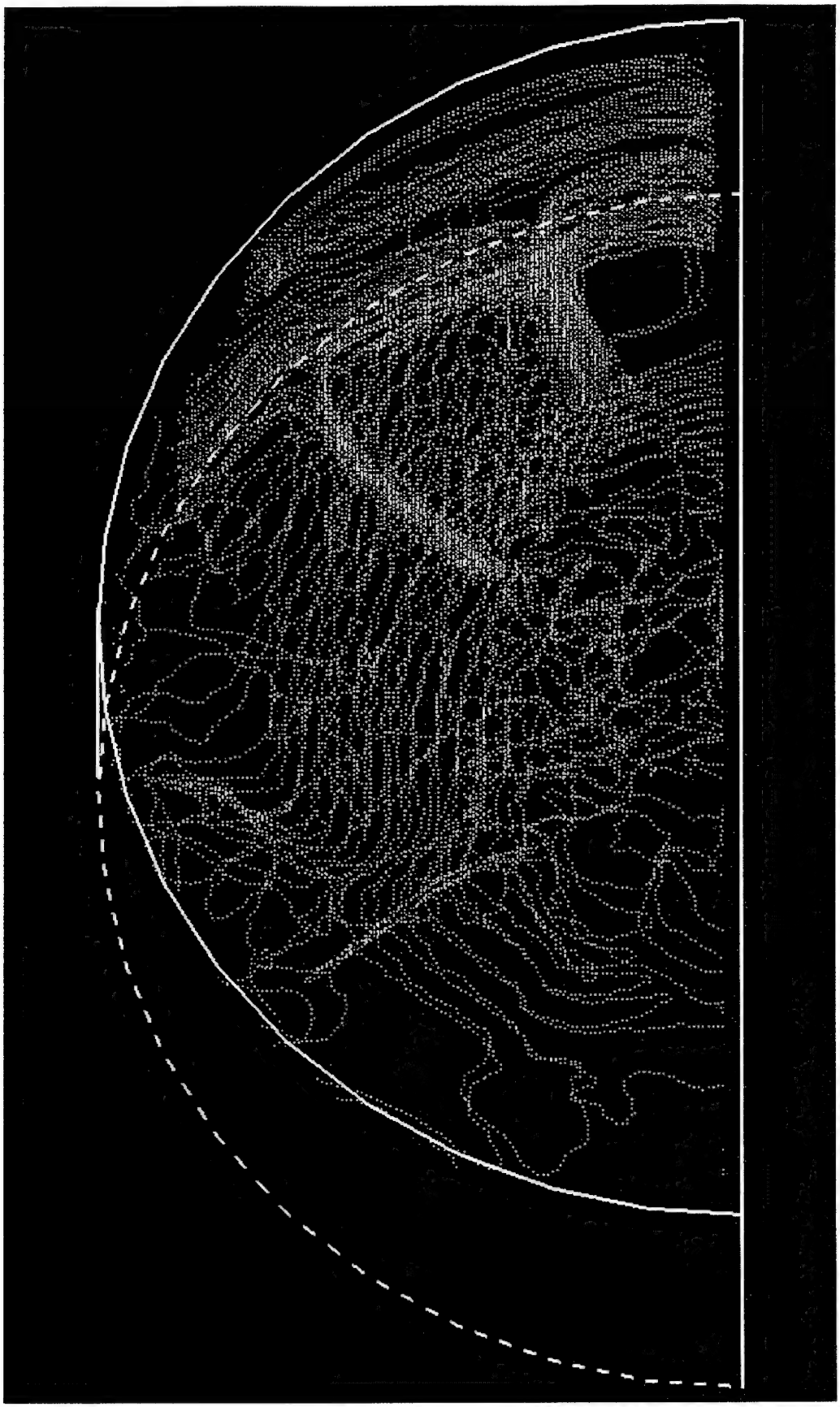

Figure B-25. 22.5° rotation about Y-axis.

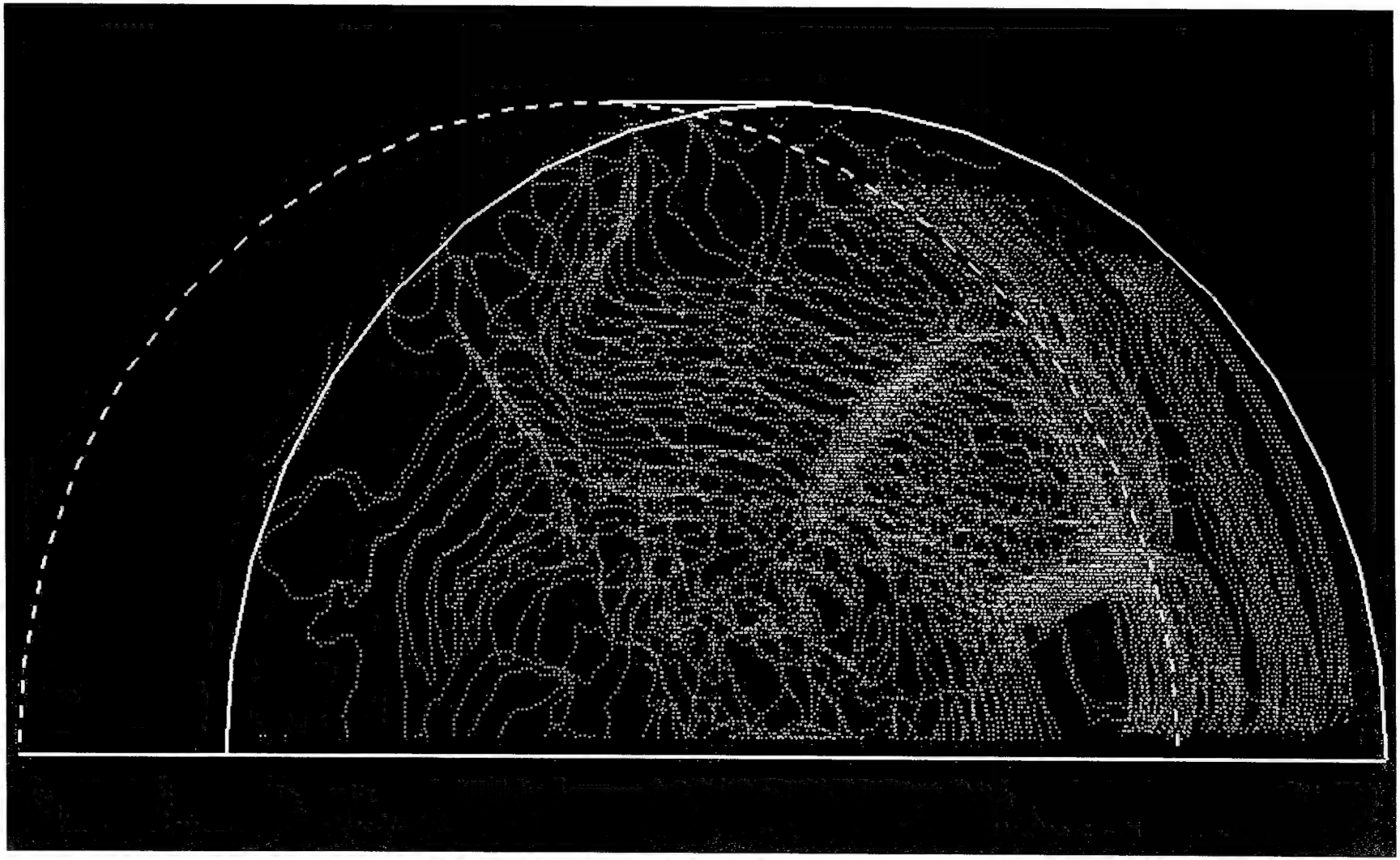

Figure B-26. 27° rotation about Y-axis.

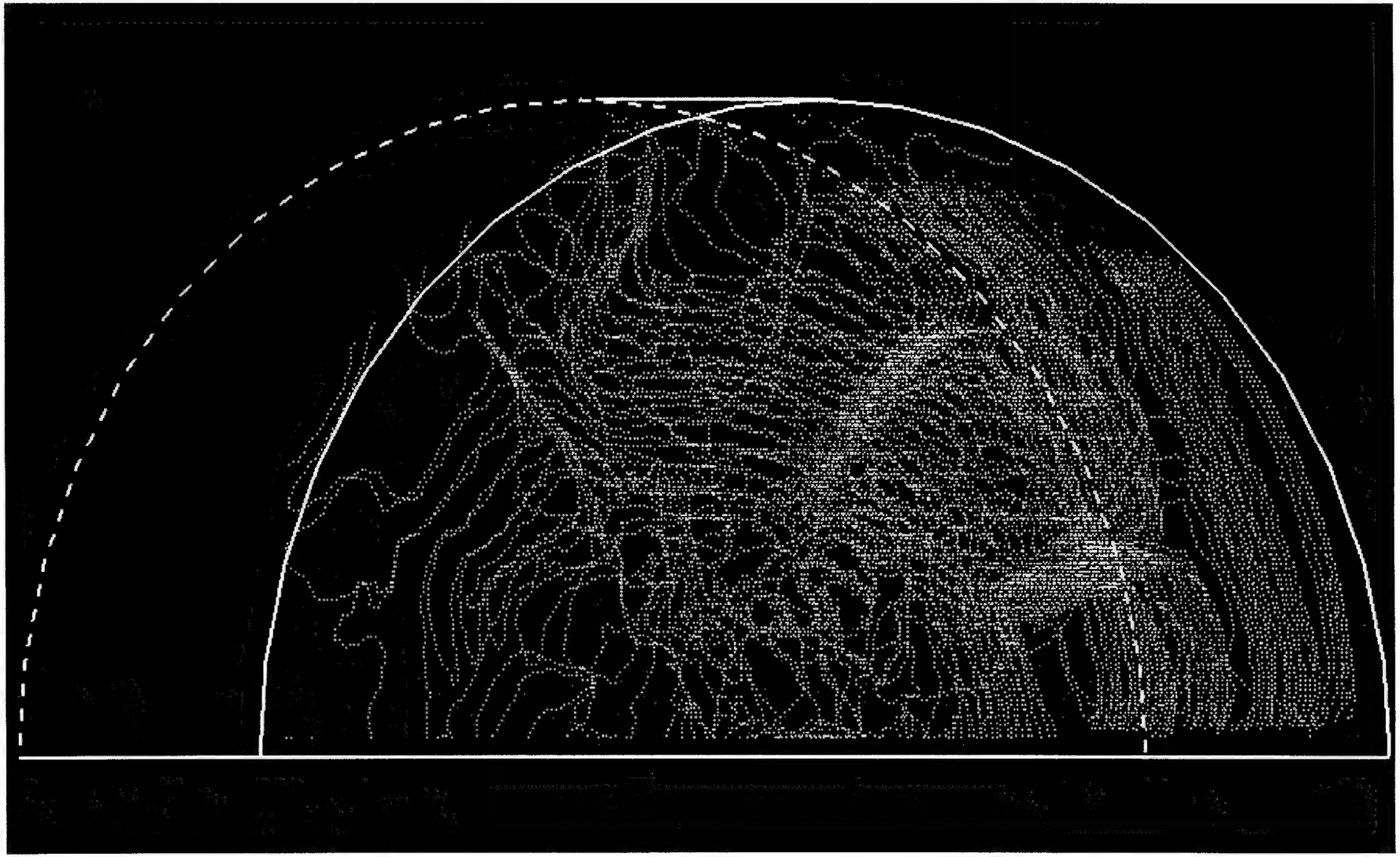

Figure B-27. 31.5° rotation about Y-axis .

Figure B-28. 36° rotation about Y-axis.

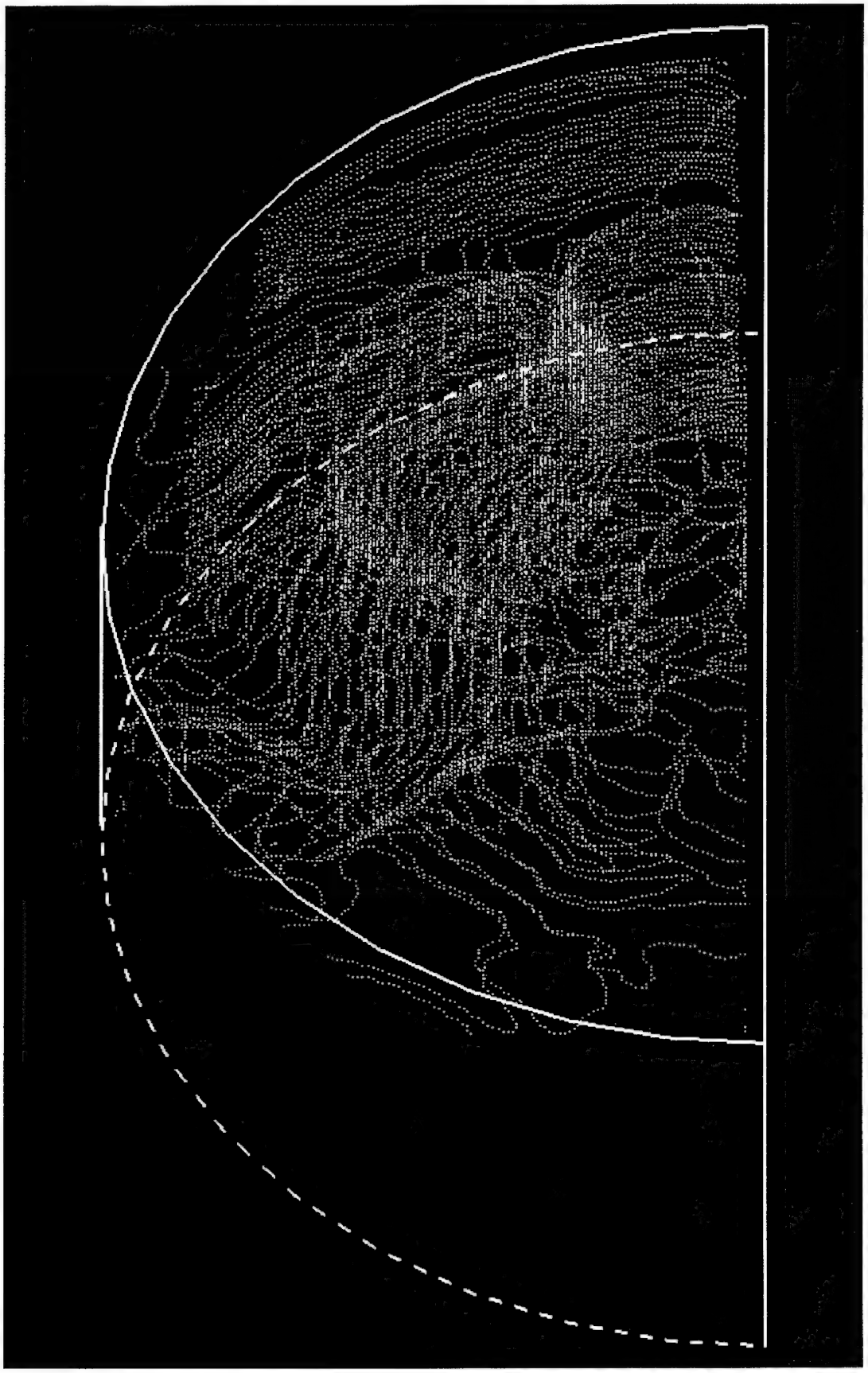

Figure B-29. 40.5° rotation about Y-axis.

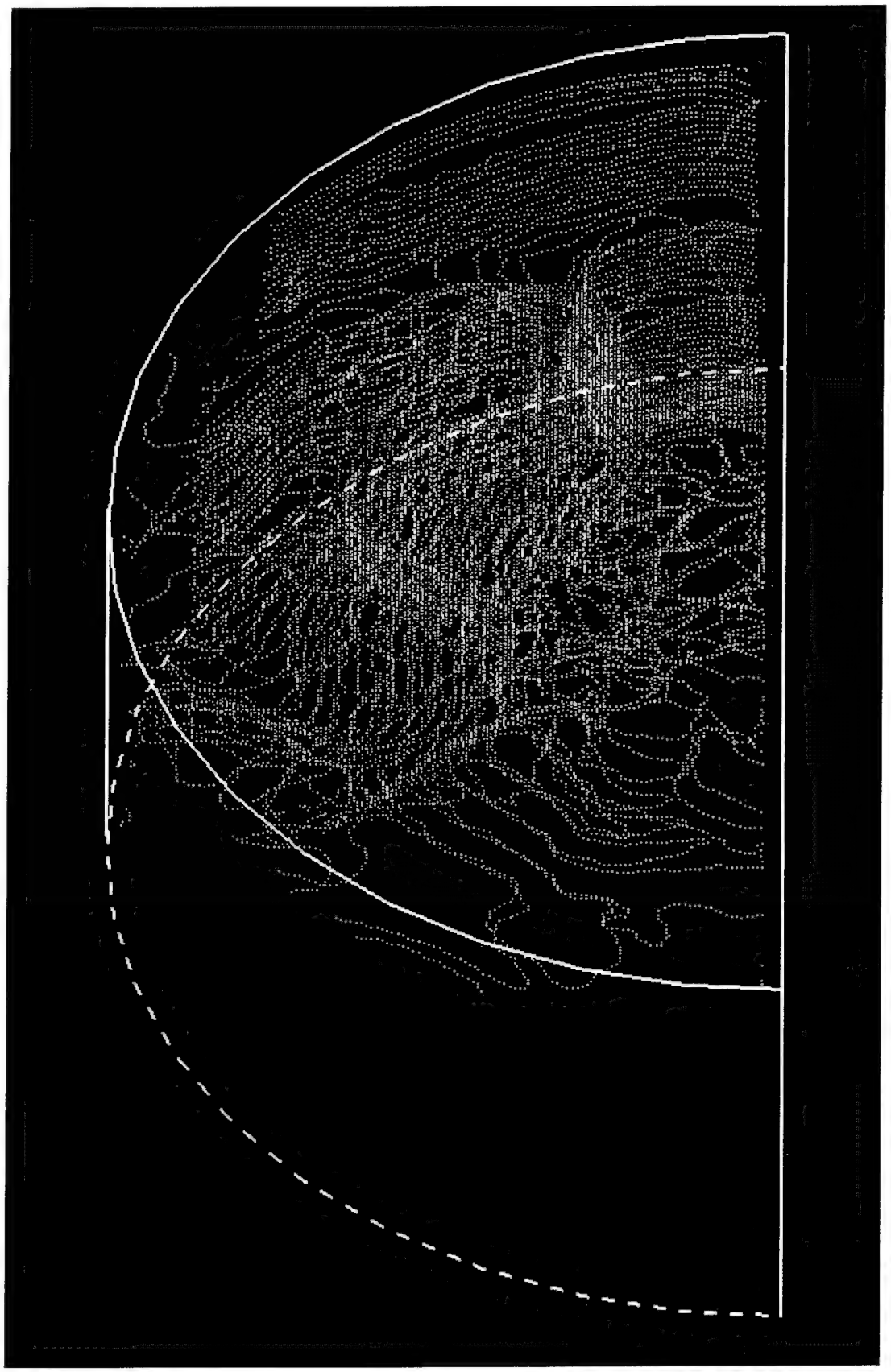

Figure B-30. 45° rotation about Y-axis.

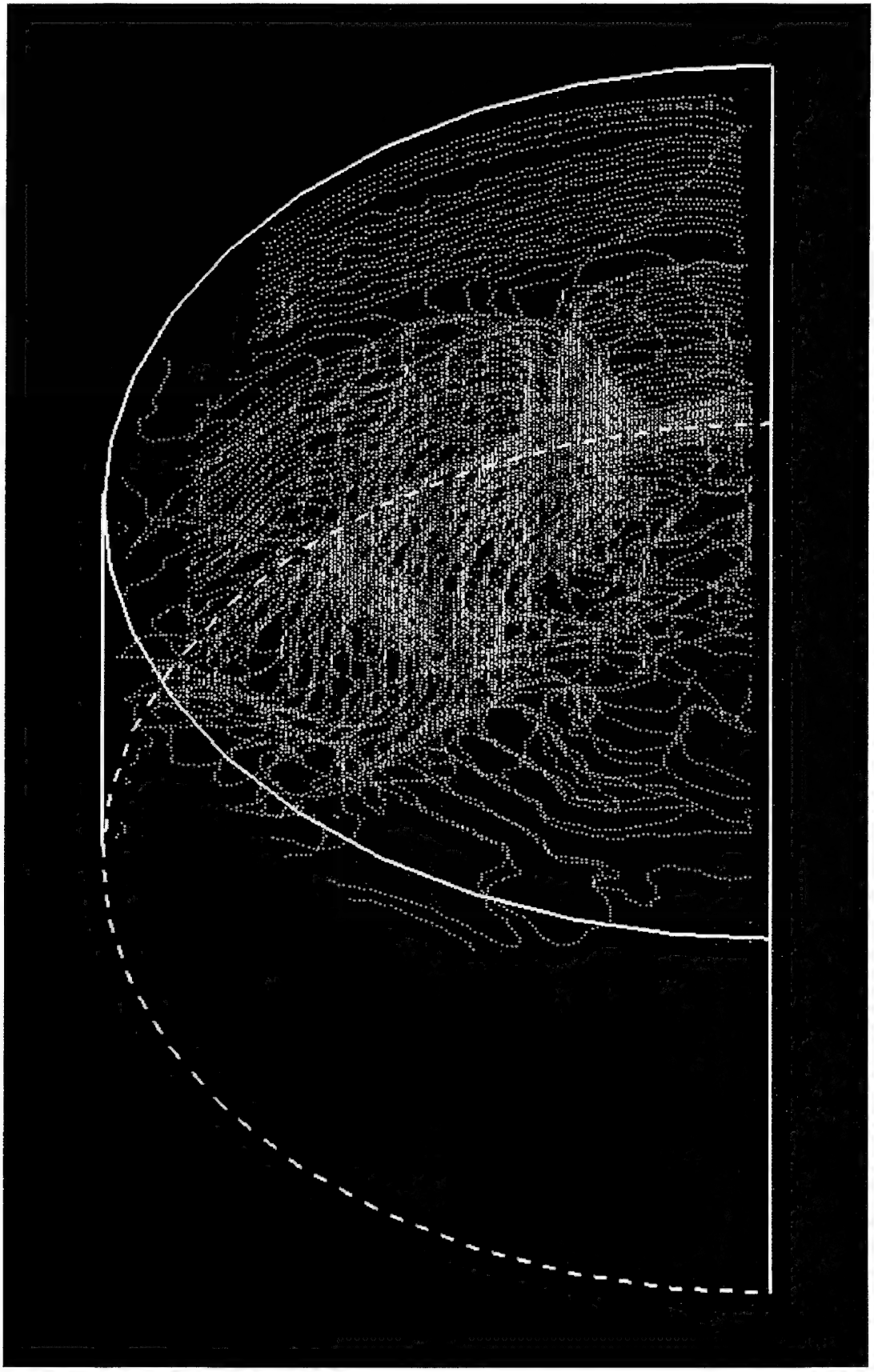

Figure B-31. 49.5° rotation about Y-axis.

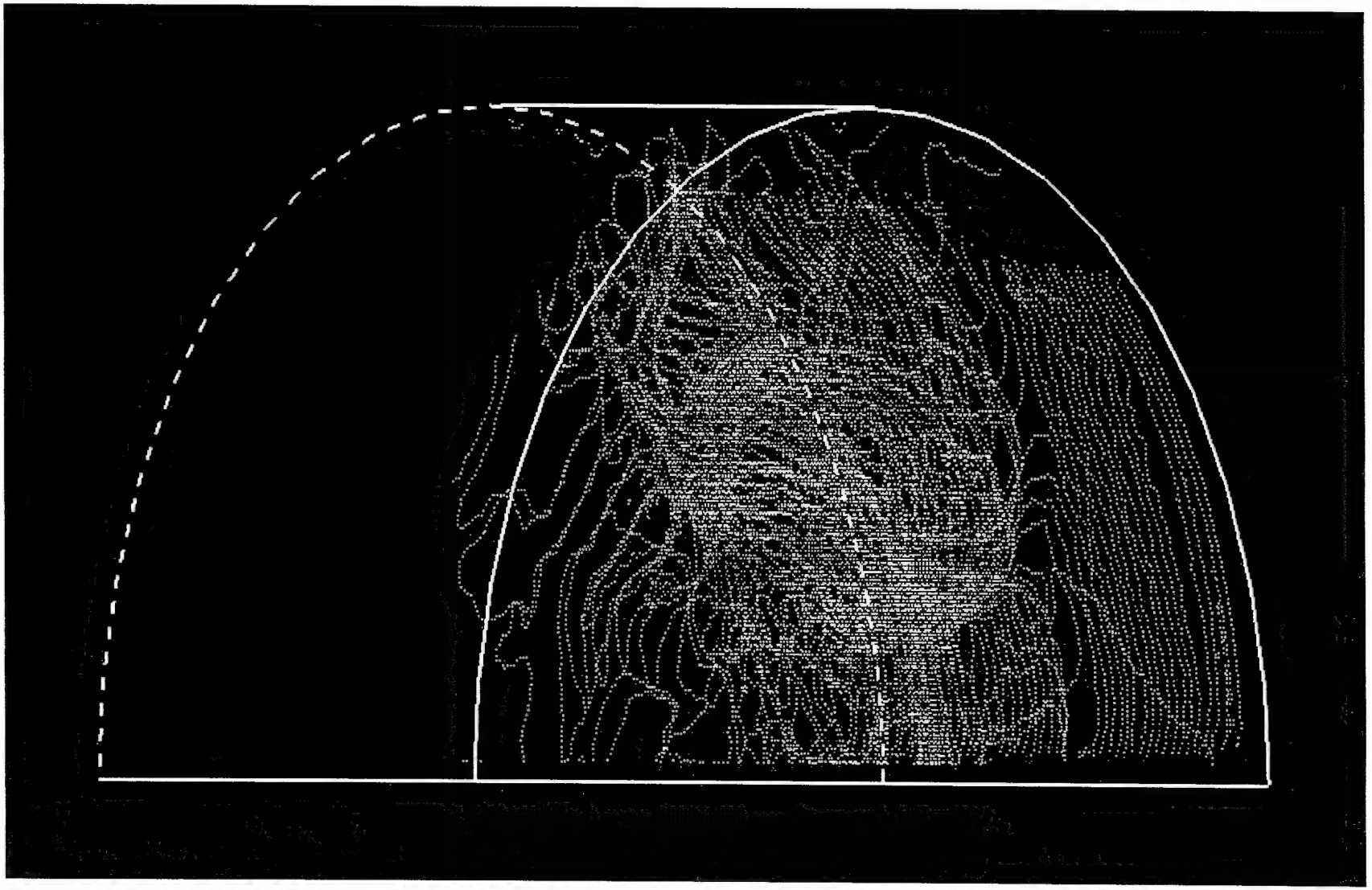

Figure B-32. 54° rotation about Y-axis.

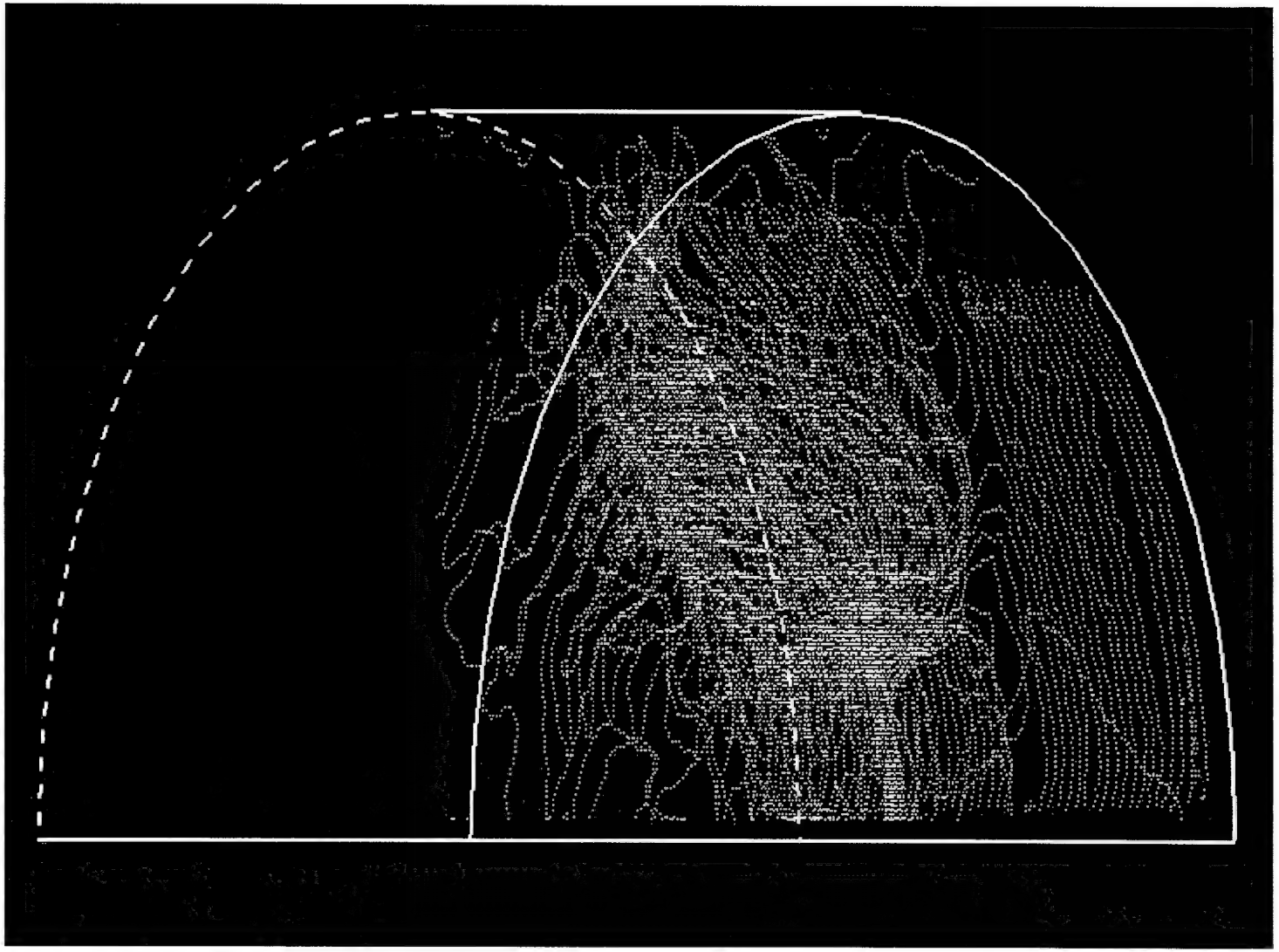

Figure B-33. 58.5° rotation about Y-axis.

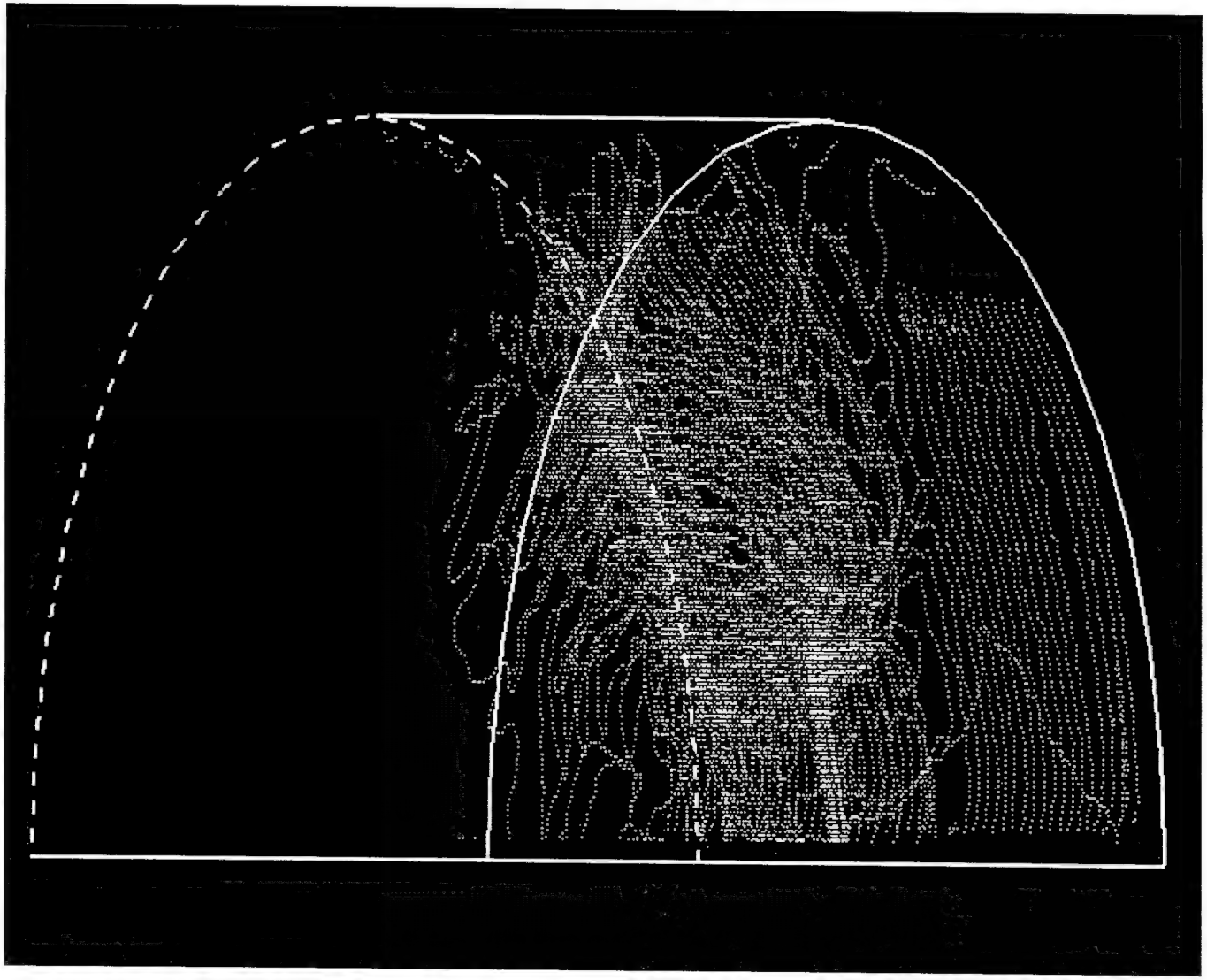

Figure B-34. 63° rotation about Y-axis.

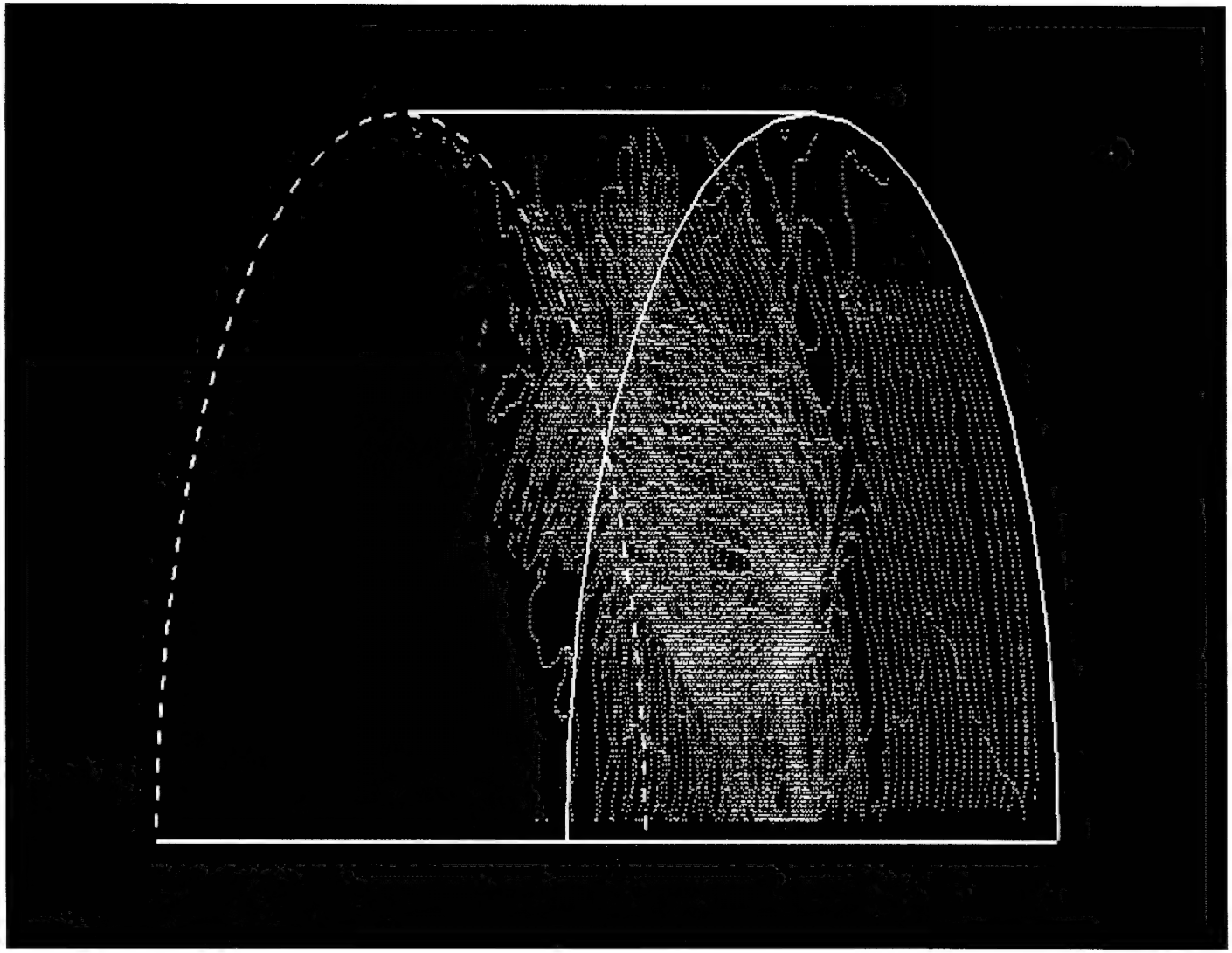

Figure B-35. 67.5° rotation about Y-axis.

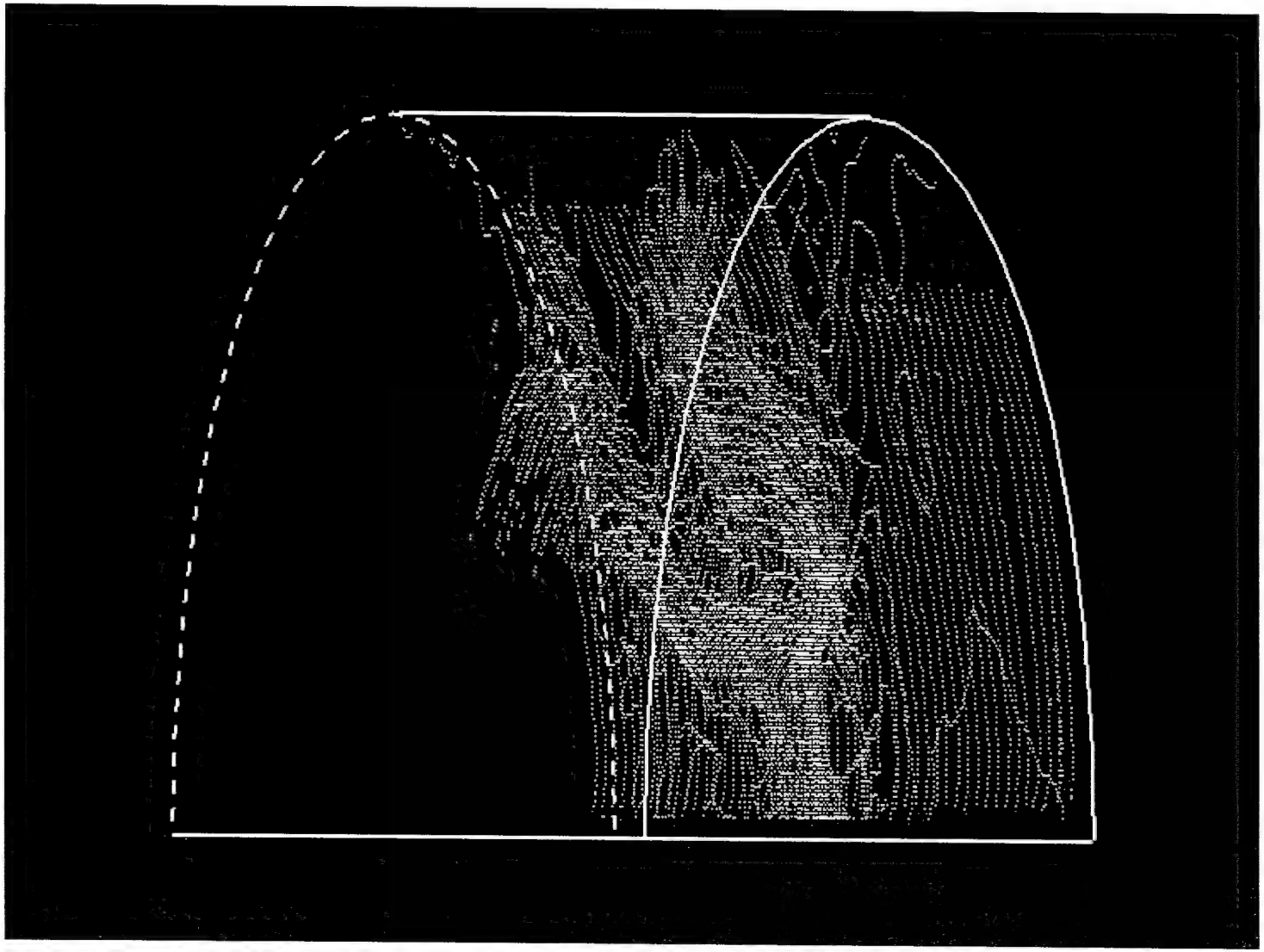

Figure B-36. 72° rotation about Y-axis.

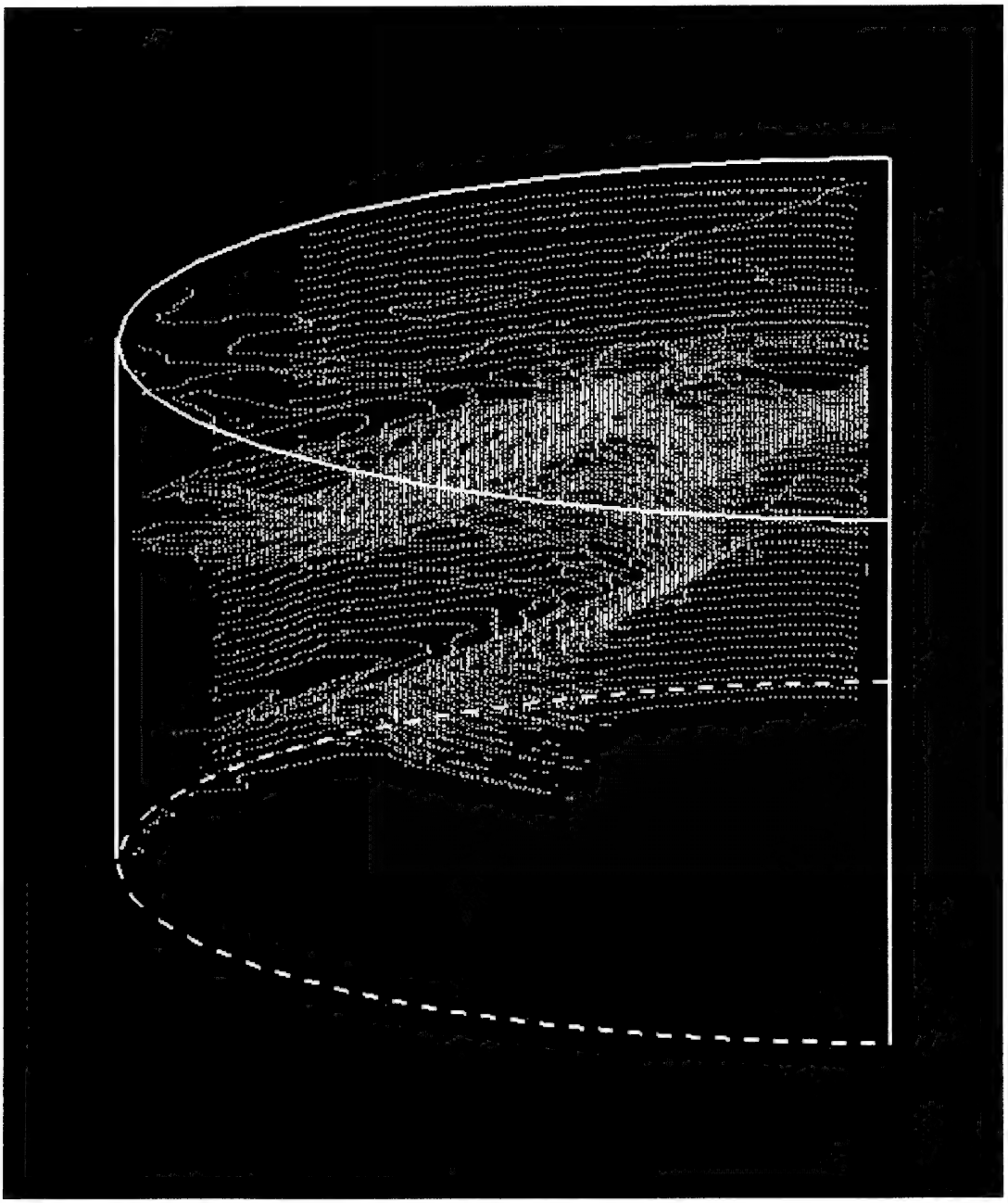

Figure B-37. 76.5° rotation about Y-axis.

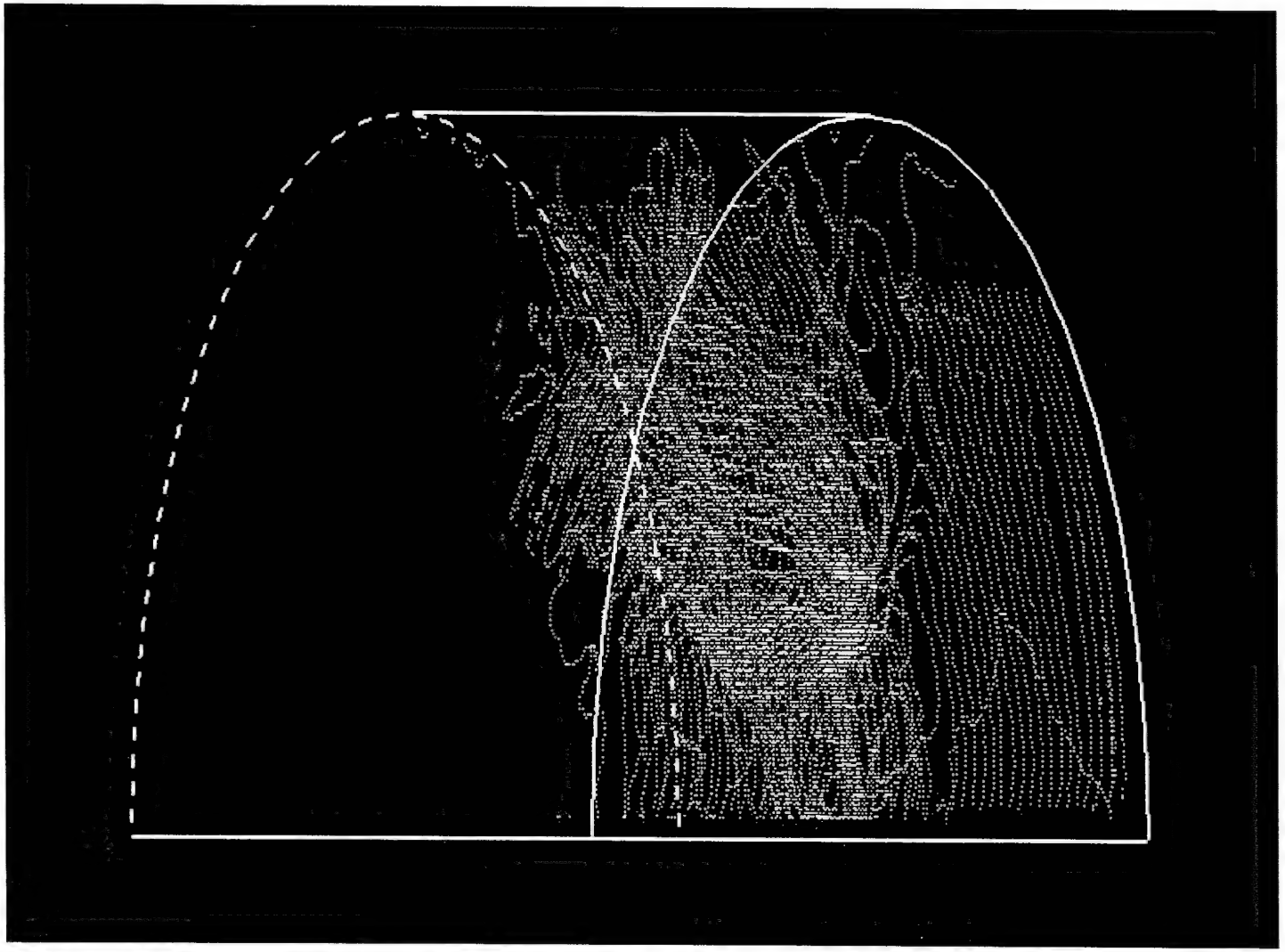

Figure B-38. 81° rotation about Y-axis.

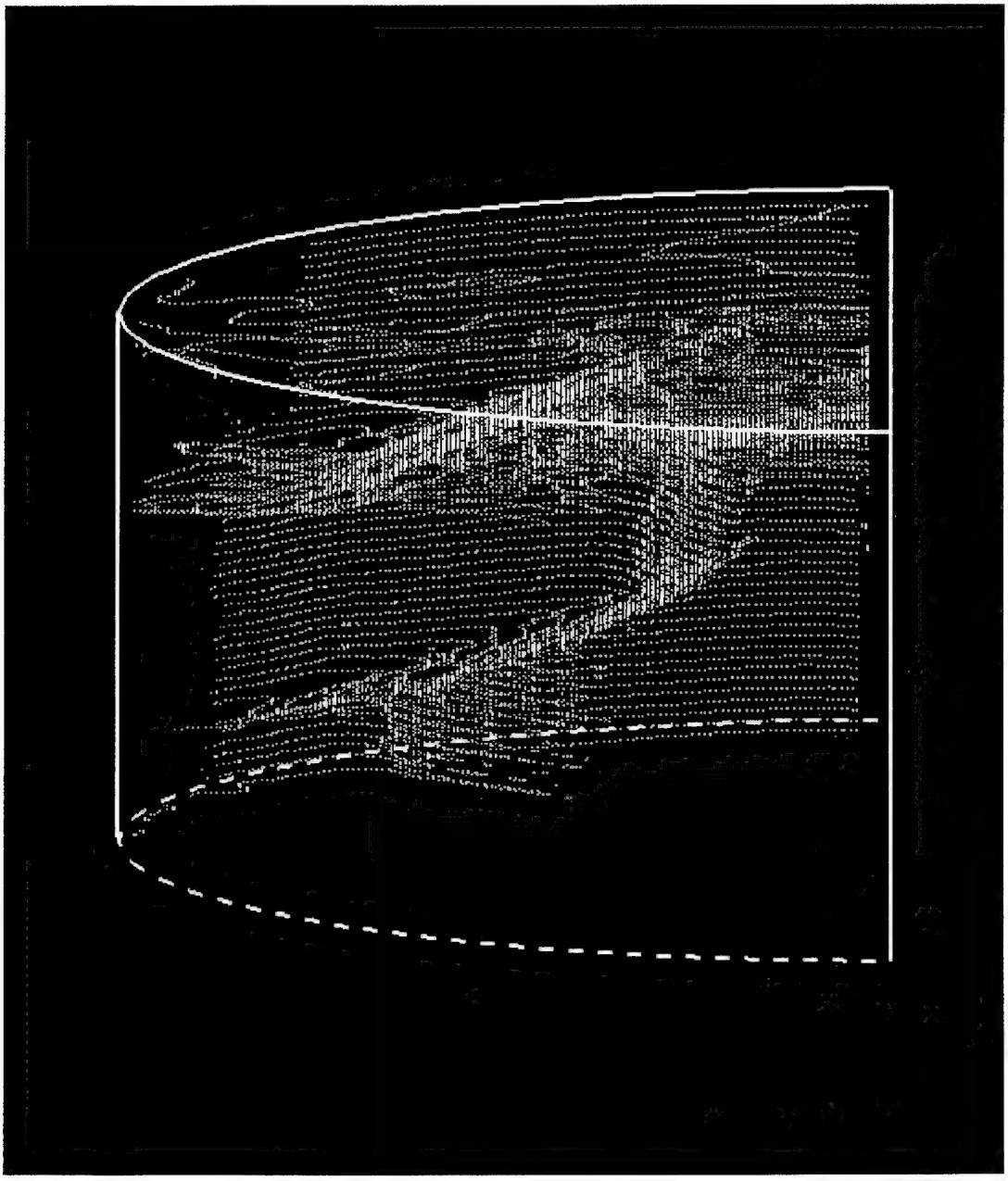

Figure B-39. 85.5° rotation about Y-axis.

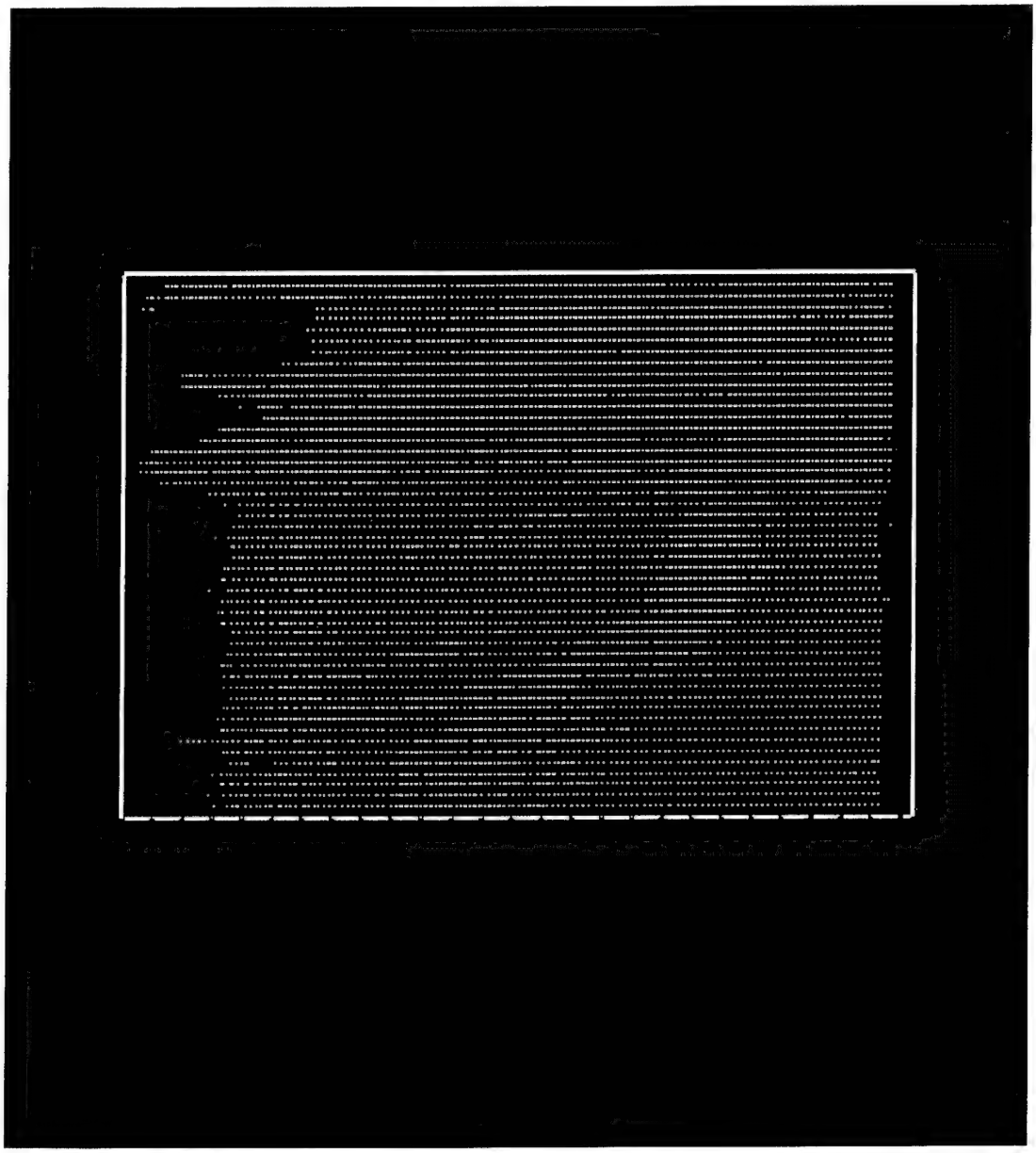

Figure B-40. 90° rotation about Y-axis.

NO. OF COPIES	ORGANIZATION
2	DEFENSE TECHNICAL INFORMATION CENTER DTIC OCA 8725 JOHN J KINGMAN RD STE 0944 FT BELVOIR VA 22060-6218
1	HQDA DAMO FDT 400 ARMY PENTAGON WASHINGTON DC 20310-0460
1	OSD OUSD(A&T)/ODDR&E(R) DR R J TREW 3800 DEFENSE PENTAGON WASHINGTON DC 20301-3800
1	COMMANDING GENERAL US ARMY MATERIEL CMD AMCRDA TF 5001 EISENHOWER AVE ALEXANDRIA VA 22333-0001
1	INST FOR ADVNCD TCHNLGY THE UNIV OF TEXAS AT AUSTIN 3925 W BRAKER LN STE 400 AUSTIN TX 78759-5316
1	US MILITARY ACADEMY MATH SCI CTR EXCELLENCE MADN MATH MAJ HUBER THAYER HALL WEST POINT NY 10996-1786
1	DIRECTOR US ARMY RESEARCH LAB AMSRL D DR D SMITH 2800 POWDER MILL RD ADELPHI MD 20783-1197
1	DIRECTOR US ARMY RESEARCH LAB AMSRL CI AI R 2800 POWDER MILL RD ADELPHI MD 20783-1197

NO. OF COPIES	ORGANIZATION
3	DIRECTOR US ARMY RESEARCH LAB AMSRL CI LL 2800 POWDER MILL RD ADELPHI MD 20783-1197
3	DIRECTOR US ARMY RESEARCH LAB AMSRL CI IS T 2800 POWDER MILL RD ADELPHI MD 20783-1197
	ABERDEEN PROVING GROUND
2	DIR USARL AMSRL CI LP (BLDG 305)

NO. OF COPIES	ORGANIZATION
7	CDR US ARMY TACOM AMSTA TR S T FURMANIAK S GOODMAN D HANSEN L P FRANKS D THOMAS AMSTA TR E MATL B ROOPCHAND AMSTA TR STI J CARIE WARREN MI 48397-5000
2	PROJECT MANAGER GROUND SYSTEM INTEGRATION SFAE GCSS W GSI T DEAN J ROWE WARREN MI 48397-5000
13	CDR US ARMY RSCH OFC A CROWSON D SKATRUD J PRATER D STEPP J BAILEY D MANN G ANDERSON R HARMON A RAJENDRA M DUTTA J KRUGER E SEGAN W MULLINS PO BOX 12211 RSCH TRIANGLE PARK NC 27709-2211
1	USA AMCOM AATD J C SHUCK LEE BLVD BLDG 401 FORT EUSTIS VA 23604
2	CDR NGIC J CRIDER W GSTATTENBAUER 220 SEVENTH AVE CHARLOTTESVILLE VA 22901-5391

NO. OF COPIES	ORGANIZATION
1	CIA OSWR DSD W WALTMAN ROOM 5P0110 NHB WASHINGTON DC 20505
1	PM BFVS SFAE GCSS W BV S DAVIS WARREN MI 48397-5000
3	CDR CARDEROCK DIV NSWC R PETERSON CODE 28 K G LIPETZKY CODE 615 W T MESSICK CODE 0115 9500 MACARTHUR BLVD W BETHESDA MD 20817-5700
1	DEPT OF THE NAVY OFC DIR REPORTING PROG MGR ADVNCD AMPHIBIOUS ASSAULT D ERDLEY WASHINGTON DC 20380-0001
13	DIR LLNL J REAUGH L290 M FINGER MS 35 D BAUM L170 D STEINBERG M WILKINS M J MURPHY L282 R WHIRLEY L122 H E MARTZ A WALTERS E N C DALDER H MARTZ J HALL TECH LIBRARY PO BOX 808 LIVERMORE CA 94550-9234
3	NAVAL RSCH LABORATORY B METZBOWER D MICHEL R KERANS 4555 OVERLOOK AVE SW WASHINGTON DC 20375

NO. OF COPIES	ORGANIZATION
13	DIR LOS ALAMOS NATL LAB G E CORT F663 R KARPP MS 1960 F GAC B HOGAN W GASKILL J CHAPYAK MS G787 S MARSH MS 970 M 6 T N CLAYTON M H JONES R M BONITA D M WRIGHT K E SIMMONDS MS 6352 TECH LIBRARY PO BOX 1663 LOS ALAMOS NM 87545
2	AIR FORCE ARMAMENT LAB AFATL DLJW W COOK TECH LIBRARY EGLIN AFB FL 32542
1	NAVAL POST GRAD SCHOOL J STERNBERG CODE EW MONTEREY CA 93943
2	MSD ENL W DYESS J FOSTER EGLIN AFB FL 32542-5000
1	NEW MEXICO TECH D EMARY TERA GROUP SOCORRO NM 87801
1	DEFENSE NUCLEAR AGENCY TECH LIBRARY 6801 TELEGRAPH RD ALEXANDRIA VA 22192
6	SANDIA NATL LAB R GRAHAM DIV 1551 P YARRINGTON D GRADY MS 0821 L CHHABILDAS MS 0821 TECH LIBRARY PO BOX 5800 ALBUQUERQUE NM 87185-0307

NO. OF COPIES	ORGANIZATION
1	CIA OSWR DSD W WALTMAN RM 5P0110 NHB WASHINGTON DC 20505
1	FEDERAL HIGHWAY ADMINSTR G WASHER NONDEST VALIDATION CTR TURNER FAIRBANK HWY RES CTR 6300 GEORGETOWN PIKE MCLEAN VA 22101
7	INST FOR ADVNCD TECH W REINECKE S BLESS H FAIR P SULLIVAN T KIEHNE D LITTLEFIELD R SUBRAMANIAN PO BOX 202797 AUSTIN TX 78720-2797
2	UNIV OF DAYTON RSCH INST KLA14 N BRAR A PIEKUTOWSKI 300 COLLEGE PARK DAYTON OH 45469-0182
3	SOUTHWEST RSCH INST C ANDERSON J RIEGEL J WALKER 6220 CULEBRA RD SAN ANTONIO TX 78238
2	BROWN UNIV DIV OF ENGINEERING R CLIFTON S SUNDARAM PROVIDENCE RI 02912
2	UNIV OF CA SAN DIEGO DEPT OF APPL MECH & ENGR SVCS R011 S N NASSER M MEYERS LA JOLLA CA 92093-0411

NO. OF COPIES	ORGANIZATION
2	AERONAUTICAL RSCH ASSOC R CONTILIANO J WALKER PO BOX 2229 50 WASHINGTON RD PRINCETON NJ 08540
2	ALLIANT TECHSYSTEMS INC T HOLMQUIST G JOHNSON 600 SECOND STREET NE HOPKINS MN 55343
1	ALME AND ASSOC M ALME PO BOX 1388 LOS ALAMOS NM 87544-1388
1	APPLIED RSRCH ASSOC INC J YATTEAU 5941 S MIDDLEFIELD RD STE 100 LITTLETON CO 80123
1	APPLIED RSCH ASSOC INC D GRADY 4300 SAN MATEO BLVD NE STE A 220 ALBUQUERQUE NM 87110
1	BRIGGS COMPANY J BACKOFEN 2668 PETERSBOROUGH ST HERNDON VA 20171-2443
1	CENTURY DYNAMICS INC N BIRNBAUM 2333 SAN RAMON VALLEY BLVD SAN RAMON CA 94583-1613
3	CERCOM INC R PALICKA G NELSON B CHEN 1960 WATSON WAY VISTA CA 92083
1	CYPRESS INTERNATIONAL A CAPONECCHI 1201 E ABINGDON DR ALEXANDRIA VA 22314
1	R J EICHELBERGER 409 W CATHERINE ST BEL AIR MD 21014-3613
1	EPSTEIN AND ASSOC K EPSTEIN 2716 WEMBERLY DRIVE BELMONT CA 94002
2	GALT ALLOYS INC S FELLOWS S GIANGIORDANO 122 CENTRAL PLAZA N CANTON OH 44702
6	GDLS W BURKE MZ436 21 24 G CAMPBELL MZ436 30 44 D DEBUSSCHER MZ436 20 29 J ERIDON MZ436 21 24 W HERMAN MZ435 01 24 S PENTESCU MZ436 21 24 38500 MOUND RD STERLING HTS MI 48310-3200
2	GENERAL RSCH CORP PO BOX 6770 SANTA BARBARA CA 93160-6770
1	INTERNATL RSCH ASSOC D ORPHAL 4450 BLACK AVE PLEASANTON CA 94566
1	JET PROPULSION LABORATORY IMPACT PHYSICS GROUP M ADAMS 4800 OAK GROVE DRIVE PASADENA CA 91109-8099
1	KAMAN SCIENCES CORP 1500 GARDEN OF THE GODS RD COLORADO SPRINGS CO 80907

NO. OF COPIES	ORGANIZATION
3	O GARA HESS AND EISENHARDT G ALLEN D MALONE T RUSSELL 9113 LE SAINT DR FAIRFIELD OH 45014
1	OREMET WAH CHANG Y KOSAKA PO BOX 580 ALBANY OR 97321
4	POULTER LABORATORY SRI INTERNATIONAL D CURRAN R KLOOP L SEAMAN D SHOCKEY 333 RAVENSWOOD AVE MENLO PARK CA 94025
1	SAIC J FURLONG MS 264 1710 GOODRIDGE DR MCLEAN VA 22102
1	BOB SKAGGS RT 11 BOX 81E SANTA FE NM 87501
4	SIMULA INC R WOLFFE R HUYETT G GRACE G YANIU 10016 SOUTH 51ST ST PHOENIX AZ 85044
8	UNITED DEFENSE LP J DORSCH V HORVATICH B KARIYA M MIDDIONE J MORROW R MUSANTE R RAJAGOPAL D SCHADE PO BOX 367 SANTA CLARA CA 95103

NO. OF COPIES	ORGANIZATION
3	UNITED DEFENSE LP E BRADY R JENKINS J JOHNSON PO BOX 15512 YORK PA 17405-1512
1	ZERNOW TECH SVCS INC L ZERNOW 425 W BONITA AVE SUITE 208 SAN DIMAS CA 91773
1	PNIN DPTY FOR TCHNLGY HQ US ARMY MATCOM AMCDCG T 5001 EISENHOWER AVE ALEXANDRIA VA 22333-0001
1	PNIN DPTY FOR ACQUSTN HQ US ARMY MATCOM AMCDCG A 5001 EISENHOWER AVE ALEXANDRIA VA 22333-0001
1	DPTY CG FOR RDE HQS US ARMY MATCOM AMCRD 5001 EISENHOWER AVE ALEXANDRIA VA 22333-0001
1	DPTY ASSIST SCY FOR R&T SARD TT THE PENTAGON WASHINGTON DC 20301-7100
1	OSD OUSD(A&T)/ODDR&E (W) L SLOTER 1777 N KENT ST SUITE 9030 ARLINGTON VA 22209
1	US MILITARY ACADEMY DEPARTMENT OF MATH SCI WEST POINT NY 10996-1786
2	DIR DARPA S WAX L CHRISTODOULOU 3701 NORTH FAIRFAX DR ARLINGTON VA 22203-1714

NO. OF COPIES	ORGANIZATION
2	CDR USAF RSCH LAB W GRIFFITH J MALAS WPAFB OH 45433-7131
2	UNIV OF CA SAN DIEGO DEPT OF EXPERIMENTAL MECH AND STRUCTURAL ENGR V M KARBHARI F L DISCALEA LA JOLLA CA 92093-0085
2	THE JOHNS HOPKINS UNIV R E GREEN J B SPICER 102 MARYLAND HALL 3400 N CHARLES ST BALTIMORE MD 21218
5	PENN STATE UNIV DEPT SCI & MECH R MCNITT B TITTMANN C LIFFENDEN DEPT CIVIL ENG R QUEENEY T KRAUTHAMMER ENRGY & GEO ENVIR ENG A S GRADER UNIVERSITY PARK PA 16802
2	NSWC INDIAN HD DIV CONCORD DETACHMENT CODE 722 M SKIPALIS W BROWN 10 DELTA ST CONCORD CA 94520-5100
1	NASA LANGLEY RSCH CNTR NDE SCI BRANCH J N ZALAMEDA BLDG 1230 RM 154 HAMPTON VA 23681-0001
1	DIRECTOR AMPTIAC D ROSE 201 MILL ST ROME NY 13440-6916

NO. OF COPIES	ORGANIZATION
1	DIRECTOR NTIAC G A MATZKANIN 415 CRYSTAL CREEK DR AUSTIN TX 78746
2	MATERIEL TEST DIR CSTE DTC WS MT H W BENNETT R GRAJEDA WSMR NM 88002
2	CDR US ARMY MRDEC AMSMI RD ST WF D LOVELACE M SCHEXNAYER REDSTONE ARSENAL AL 34898-5250
1	CDR US BLVR RD&E CTR STRBE NAN TECH LIBRARY FORT BELVOIR VA 22060-5166
2	CDR US ARMY ARDEC SMCAR AAE W J PEARSON TECH LIBRARY PICATINNY ARSENAL NJ 07806-5000
1	PM TANK MAIN ARMNT SYS SSAE AR TMA MT PICATINNY ARSENAL NJ 07806-5000
2	CDR ERO USARDSG (UK) S SAMPATH J ILLINGER PSC 802 BOX 15 FPO AE 09499-1500
1	USMC MCRDAC PM GRNDS WPNS BR D HAYWOOD FIREPOWER DIV QUANTICO VA 22134
1	CHIEF OF NAVAL RSCH OFC OF NAVAL TECH A J FAULSDITCH ONT 23 BALLSTON TOWERS ARLINGTON VA 22217

NO. OF COPIES	ORGANIZATION
1	NAVAL WPNS CTR TECH LIBRARY CHINA LAKE CA 93555
1	NUSC NEWPORT S DICKINSON CODE 8214 NEWPORT RI 02841
1	NAWC J J LUNDEEN CODE 4342 BLDG 2188 PATUXENT RIVER MD 20670-1908
14	NSWC DAHLGREN DIV V GEHMAN B20 E E ROWE G22 (5 CPS) B D SMITH G22 (5 CPS) J MCCONKIE G32 TECH LIBRARY B60 MISSILE SYS DATA CTR G205B 17320 DAHLGREN RD DAHLGREN VA 22448
3	DYNA EAST CORP P C CHOU R CICCARELLI W FLIS 3201 ARCH ST PHILADELPHIA PA 19104
2	S CUBED R SEDGWICK PO BOX 1620 LA JOLLA CA 92038-1620
2	ORLANDO TECH INC D MATUSKA J OSBORN PO BOX 855 SHALIMAR FL 32579
1	LIVERMORE SOFTWARE TECH CORP J O HALLQUIST 1876 WAVERLY WAY LIVERMORE CA 94550
2	MARTIN MARIETTA MISSILE SYSTEMS C E HAMMOND MP 004 L WILLIAMS MP 126 PO BOX 555837 ORLANDO FL 32855-5837

NO. OF COPIES	ORGANIZATION
1	SCHWARZKOPFF TECH CORP E KOSINISKI 35 JEFFREY AVE HOLLISTON MA 01746
1	PRIMEX CORP D EDMONDS 10101 9TH ST N ST PETERSBURG FL 33716
1	BATTELLE D TROTT 505 KING AVE COLUMBUS OH 43201
1	RAYTHEON CO R LLOYD PO BOX 1201 TEWKSBURY MA 01876
1	THE CARBORUNDUM CO R PALIA PO BOX 1054 NIAGARA FALLS NY 19302
1	ADELMAN ASSOC C CLINE 3301 EL CAMINO REAL SUITE 280 ATHERTON CA 94027
1	DOW CHEMICAL INC K EPSTEIN ORDNANCE SYS 800 BUILDING MIDLAND MI 48667
1	CALKINS R&D INC N CALKINS 515 SEWARD PK AVE ALBUQUERQUE NM 87123
1	KERAMONT CORPORATION E SAVRUN 4231 S FREEMONT AVE TUCSON AZ 85714
1	CORNING INC S HAGG SP DV 22 CORNING NY 14831

NO. OF COPIES	ORGANIZATION
1	UNIV OF DAYTON R HOFFMAN 300 COLLEGE PARK DAYTON OH 45469
1	ROCKWELL INTL ROCKETDYNE DIV J MOLDENHAUER 6633 CANOGA AVE HB 23 CANOGA PK CA 91303
2	ALLIED SIGNAL L LIN PO BOX 31 PETERSBURG VA 23804
1	MCDONNELL DOUGLAS HELICOPTER L R BIRD MS 543 D216 5000 E MCDOWELL RD MESA AZ 85205
1	BOEING CORP T M MURRAY MS 84 84 PO BOX 3999 SEATTLE WA 98124
1	EMBASSY OF AUSTRALIA COUNSELLOR DEFENCE SCIENCE 1601 MASSACHUSETTS AVE NW WASHINGTON DC 20036-2273
1	MILITARY VEHICLES AND ORDNANCE REPORT L S NESS 20 EAST DEL RAY AVE ALEXANDRIA VA 22301
1	TRACOR AEROSPACE R E BROWN PO BOX 196 SAN RAMON CA 94583
1	AEROJET J CARLEONE PO BOX 13222 SACRAMENTO CA 95813-6000

NO. OF COPIES	ORGANIZATION
1	NDIA L F SKIBBIE 2101 WILSON BLVD STE 400 ARLINGTON VA 22201-3061
2	UNIV OF TEXAS AT EL PASO MATERIALS ENGINEERING L E MURR MAIL CODE 00520 EL PASO TX 79968
1	F I GRACE 90 CHURCHILL DR YORK PA 17403
5	J J FROST S REYNOLDS ST APT 1001 ALEXANDRIA VA 22304
1	H T YOLKEN TRI AUSTIN 15400 EDWARDS FERRY RD POOLESVILLE MD 20837
1	GENERAL ELECTRIC COMPANY CORPORATE R & D C BUENO BLDG KW RM D246 PO BOX 8 SCHENECTADY NY 12301-0008
1	INDUSTRIAL QUALITY INC T S JONES VP 640 EAST DIAMOND AVE SUITE C GAITHERSBURG MD 20877-5323
2	WISS JANNEY ELSTNER ASSOC H H SALEH R LIVINGSTON NONDEST VALIDATION CTR TURNER FAIRBANK HWY RES CTR 6300 GEORGETOWN PIKE MCLEAN VA 22101
2	MSE INC HIGH PERFORMANCE MAT GRP K LEIGHTON 1300 MARROWS ROAD NEWARK DE 19711

NO. OF COPIES ORGANIZATION

ABERDEEN PROVING GROUND

1 DIR USA EBCC
SCBRD RT
5183 BLACKHAWK RD
APG MD 21010-5424

1 CDR USA SBCCOM
AMSCB CII
5183 BLACKHAWK RD
APG MD 21010-5424

2 DIR USAMSAA
AMXSY D
AMXSY MP
H COHEN
BLDG 392
APG MD 21005

1 CDR USATEC
AMSTE TC
RYAN BLDG
APG MD 21005

3 CDR USAATC
STEAC LI LV
E SANDERSON
M SIMON (2 CPS)
BLDG 400
APG MD 21005

97 DIR USARL
AMSRL SL I
AMSRL WM
J SMITH
M PETERSON
E SCHMIDT
AMSRL WM M
D VIECHNICKI
G HAGNAUER
J MCCAULEY
AMSRL WM MA
R SHUFORD
AMSRL WM MB
B FINK
T BOGETTI
D GRANVILLE
C HOPPEL
P DEHMER
AMSRL WM MC
J BEATTY
J WELLS (5 CPS)

NO. OF COPIES ORGANIZATION

ABERDEEN PROVING GROUND (CONT'D)

J ADAMS
E CHIN
G GILDE
L LASALVIA
J MONTGOMERY
P PATEL
A WERESZCZAK
AMSRL WM MD
W ROY
W GREEN (5 CPS)
P SINCEBAUGH
S WALSH
W DEROSSET
R DOWDING
V CHAMPAGNE
F STENTON
L KECSKES
D SNOHA
M PEPI
S GRENDAHL
D HELFRITCH
K CHO
D STRAND
AMSRL WM T
T B BURNS
T WRIGHT
AMSRL WM TA
W BRUCHEY
M BURKINS
W GILLICH
W GOOCH
T HAVEL
D HACKBARTH
E HORWATH
Y HUANG
D KLEPONIS
H MEYER
M NORMANDIA
J RUNYEON
M ZOLTOSKI
AMSRL WM TB
R FREY
AMSRL WM TC
R COATES
K KIMSEY
M LAMPSON
L MAGNESS
D SCHEFFLER
G SILSBY
R SUMMERS

NO. OF
COPIES ORGANIZATION

ABERDEEN PROVING GROUND (CONT'D)

W WALTERS
AMSRL WM TD
J BARB
D DANDEKAR
A DIETRICH
T FARRAND
K FRANK
N GNIAZDOWSKI
F GREGORY
A GUPTA
T HADUCH
T MOYNIHAN
D PRITCHARD
M RAFTENBERG
E RAPACKI
N RUPERT (10 CPS)
M SCHEIDLER
S SCHOENFELD
S SEGLETES
T WEERASOORIYA
AMSRL WM TE
A NIILER

NO. OF COPIES	ORGANIZATION
2	ARO FAR EAST G DANDREA S HYU ARO FE AKASAKA PRESS CENTER 7 23 17 ROPPONGI MINATO KÚ TOKYO 106-0032 JAPAN
8	DSTO AERONAUTICAL & MARITIME RSCH LABORATORY E GELLERT H BILLON G EGGLESTONE S ALKEMADE S PATTIE J DIMAS S CIMPOERU D PAUL PO BOX 4331 MELBOURNE VIC 3001 AUSTRALIA
1	BATTELLE INGENIEURTECHNIK GMBH W FUCKE DUESSELDORFFER STR 9 D 65760 ESCHBORN GERMANY
1	CARLOS III UNIV OF MADRID C NAVARRO ESCUELA POLITÉENICA SUPERIOR C BUTARQUE 15 28911 LEGANÉS MADRID SPAIN
1	CELSIUS MATERIALTEKNIK KARLSKOGA AB L HELLNER S 691 80 KARLSKOGA SWEDEN
3	CENTRE D'ETUDES GRAMAT J CAGNOUX C GALLIC J TRANCHET GRAMAT 46500 FRANCE

NO. OF COPIES	ORGANIZATION
1	MINISTRY OF DEFENCE DGA DSP STTC G BRAULT 4 RUE DE LA PORTE D ISSY 00460 ARMÉES F 75015 PARIS FRANCE
1	CONDAT J KIERMEIR MAXILLANSTR 28 8069 SCHEYERN FERNHAG GERMANY
2	DEFENCE PROCUREMENT AGCY G LAUBE W ODERMATT BALLISTICS WPNS & COMBAT VEHICLE TEST CTR CH 3602 THUN SWITZERLAND
1	TDW M HELD POSTFACH 1340 D 86523 SCHROBENHAUSEN GERMANY
6	DEFENCE RSCH AGENCY W CARSON I CROUCH C FREW T HAWKINS B JAMES B SHRUBSALL CHOBHAM LANE CHERTEY SURREY KT16 OEE UNITED KINGDOM
1	DEFENCE RSCH ESTAB SUFFIELD C WEICKERT BOX 4000 MEDICINE HAT ALBERTA TIA 8K6 CANADA

NO. OF COPIES	ORGANIZATION
1	DEFENCE RSH ESTAB VALCARTIER ARMAMENTS DIVISION R DELAGRAVE 2459 PIE X1 BLVD N PO BOX 8800 CORCELETTE QUEBEC GOA 1RO CANADA
5	DEUTSCH FRANZÖSISCHES FORSCHUNGSINSTITUT ST LOUIS H ERNST K HOOG H LERR T WOLF R NUSING CÉDEX 5 RUE DU GÉNÉRAL CASSAGNOU F 68301 SAINT LOUIS FRANCE
1	DIEHL GMBH AND CO M SCHILDKNECHT FISCHBACHSTRASSE 16 D 90552 RÖTBENBACH AD PEGNITZ GERMANY
1	DYNAMEC RSCH AB Å PERSSON PO BOX 201 S 151 23 SÖDERTÄLJE SWEDEN
3	ETBS DSTI P BARNIER M SALLES B GAILLY ROUTE DE GUERAY BOITE POSTALE 712 18015 BOURGES CEDEX FRANCE
2	FEDERAL MINISTRY OF DEFENCE DIR OF EQPT & TECH LAND RÜV 2 D HAUG L REPPER POSTFACH 1328 53003 BONN GERMANY
4	FRANHOFER INSTITUT FÜR KURZZEITDYNAMIK ERNST MACH INSTITUT V HOHLER E STRASSBURGER R THAM K THOMA ECKERSTRASSE 4 D 79 104 FREIBURG GERMANY
3	FRANHOFER INSTITUT FÜR KURZZEITDYNAMIK ERNST MACH INSTITUT K WINEMAN H SENF E STRASSBURGER HAUPTSTRASSE 18 D79 576 WEIL AM RHEIN GERMANY
1	MINISTRY OF DEFENCE DGA SPART C CANNAVO 10 PLACE GEORGES CLEMENCEAU BP19 F 92211 SAINT CLOUD CÉDEX FRANCE
2	HIGH ENERGY DENSITY RSCH CTR V FORTOV G KANEL IZHORSKAYA STR 13 19 MOSCOW 127412 RUSSIAN REPUBLIC
1	INGENIEURBÜRO DEISENROTH F DEISENROTH AUF DE HARDT 33 35 D 5204 LOHMAR 1 GERMANY
1	INST OF CHEMICAL PHYSICS S RAZORENOV 142432 CHERNOGOLOVKA MOSCOW REGION RUSSIAN REPUBLIC

NO. OF COPIES	ORGANIZATION
7	INST FOR PROBLEMS IN MATERIALS SCIENCE S FIRSTOV B GALANOV O GRIGORIEV V KARTUZOV V KOVTUN Y MILMAN V TREFILOV 3 KRHYZHANOVSKY STR 252142 KIEV 142 UKRAINE
1	INST FOR PROBLEMS OF STRESS G STEPANOV TIMIRYAZEVSKAYA STR 2 252014 KIEV UKRAINE
3	INST OF MECH ENGINEERING PROBLEMS V BULATOV D INDEITSEV Y MESCHERYAKOV BOLSHOY 61 VO ST PETERSBURG 199178 RUSSIAN REPUBLIC
2	IOFFE PHYSICO TECH INST E DROBYSHEVSKI A KOZHUSHKO ST PETERSBURG 194021 RUSSIAN REPUBLIC
1	K&W THUN W LANZ ALLMENDSSTRASSE 86 CH 3602 THUN SWITZERLAND
1	R OGORKIEWICZ 18 TEMPLE SHEEN LONDON SW 14 7RP UNITED KINGDOM
1	MAX PLANCK INSTITUT FUR EISENFORSCHUNG GMBH C DERDER MAX PLANCK STRASSE 1 40237 DUSSELDORF GERMANY

NO. OF COPIES	ORGANIZATION
2	NATL DEFENCE HEADQUARTERS M PACEY PMO MRCV A HODAK PMO LAV OTTAWA ONTARIO KIA OK2 CANADA
1	OTO BREDA M GUALCO VIA VALDIOCCHI 15 I 19136 LA SPEZIA ITALY
5	RAPHAEL BALLISTICS CENTER M MAYSELESS Y PARTOM G ROSENBERG Z ROSENBERG Y YESHURUN BOX 2250 HAIFA 31021 ISRAEL
1	RSCH INST OF MECHANICS NIZHNIY NOVGOROD STATE UNIV A SADYRIN PR GAYARINA 23 KORP6 NIZHNIY NOVGOROD 603600 RUSSIAN REPUBLIC
1	ROYAL NETHERLANDS ARMY J HOENEVELD V D BURCHLAAN 31 PO BOX 90822 2509 LS THE HAGUE NETHERLANDS
1	DEFENCE MATERIEL ADMIN WEAPONS DIRECTORATE A BERG S 11588 STOCKHOLM SWEDEN
2	SWEDISH DEFENCE RSCH ESTAB DIVISION OF MATERIALS S J SAVAGE J ERIKSON S 172 90 STOCKHOLM SWEDEN

NO. OF COPIES	ORGANIZATION
3	SWEDISH DEFENCE RSCH ESTAB L HOLMBERG B JANZON I MELLGARD BOX 551 S 147 25 TUMBA SWEDEN
1	TECHNION INST OF TECH FACULTY OF MECH ENGR S BODNER TECHNION CITY HAIFA 32000 ISRAEL
3	TECHNISCHE UNIVERSITÄT CHEMNITZ ZWICKAU A SCHROEDTER L KRUEGER L MEYER POSTFACH D 09107 CHEMNITZ GERMANY
2	TNO PRINS MAURITS LAB H PESKES R IJSSELSTEIN LANGE KLEIWEG 137 PO BOX 45 2280 AA RIJSWIJK THE NETHERLANDS
1	MONASH UNIVERSITY DEPT OF CIVIL ENG R GRZEBIETA CLAYTON VICTORIA 3168 AUSTRALIA
6	CENTRE DE RECHERCHES ET D'ETUDES D'ARCUEIL D BOUVART C COTTENNOT S JONNEAUX H ORSINI S SERROR F TARDIVAL 16 BIS AVENUE PRIEUR DE LA CÔTE D'OR F 94114 ARCUEIL CÉDEX FRANCE

NO. OF COPIES	ORGANIZATION
2	DERA FT HALSTEAD I CULLIS D SCOTT SEVENOAKS KENT TN14 7BP UNITED KINGDOM
1	ERNST MACH INSTITUT R HEISER AM KLINGELBERG 1 D 79588 EFRINGEN KIRCHEN GERMANY
1	TACHKEMONY ST 6 E HIRSCH NETANYA 42611 ISRAEL
1	DEFENCE PROCUREMENT AGENCY (GR) I CREWTHER WEAPONS AND AMMO DIV FEUERWERKERSTRASSE 39 CH 3602 THUN SWITZERLAND
1	DEFENCE RESEARCH ESTAB VALCARTIER A DUPUIS 2459 BLVD PIE XI NORTH VAL BELAIR QUEBEC GEJ 1X5 CANADA
1	CRANFIELD UNIVERSITY HEAD BALLISTICS GROUP A B CROWLEY RMCS SHRIVENHAM SWINDON SN6 8LA UNITED KINGDOM
3	FRENCH GERMAN RSCH INST D HENSEL M GIRAUD G KRAUTH 5 RUE DU GENERAL CASSAGNOU BOITE POSTALE 34 F 68301 SAINT LOUIS CEDEX FRANCE

NO. OF COPIES	ORGANIZATION
2	SABO ARMSCOR COMBAT SPT P NEL L DU PLESSIS G KRAUTH PRIVATE BAG X337 0001 PRETORIA REPUBLIC OF SOUTH AFRICA
1	RIMAT ADVANCED TECHNOLOGIES LTD M RAVID 8 B SIMATAT HAYEREK HOD HASHARON 45264 ISRAEL
1	TNO DEFENCE RESEARCH H PASMAN POSTBUS 6006 2600 JA DELFT THE NETHERLANDS
2	DSTO WEAPONS SYS DIV A WILDEGGER-GAISSN N BURMAN PO BOX 1500 SALISBURY SA 5108 AUSTRALIA
1	ECOLE ROYAL MILITAIRE E CELENS AVENUE DE LA RENAISSANCE 30 1000 BRUXELLE BELGIQUE
1	A STILP BUSSARDWEG 7 79110 FREIBURG GERMANY
1	G A SCHROEDER IN DEN GATTERN 3 79594 INZLINGEN GERMANY
1	DEFENCE RES & DEV ORG P U DESHPANDE MINISTRY OF DEFENCE 316 B WING SENA BHAVAN NEW DELHI 110 011 INDIA

NO. OF COPIES	ORGANIZATION
1	DIRECTOR UNIVERSIDAD POLITECNICA V SANCHEZ-GALVEZ ETSI CAMINOS UPM CIUDAD UNIVERSITARIA MADRID 28040 SPAIN
1	RUSS ACADEMY OF ROCKET AND ARTILLERY SCIENCE V SOLOVIEV GOSPITALITY LANE 10 107564 MOSCOW RUSSIA
2	CSIRO MANUFACTURING SCI AND TECH R G ODONNELL A STEVENSON PRIVATE BAG 33 CLAYTON SOUTH VICTORIA 3169 AUSTRALIA
1	DERA STRUCTURAL MATERIALS CTR GRIFFITH BLDG A 7 R A SMITH FARNBOROUGH HAMPSHIRE GU14 OLX UNITED KINGDOM

INTENTIONALLY LEFT BLANK.

REPORT DOCUMENTATION PAGE

Form Approved
OMB No. 0704-0188

1. AGENCY USE ONLY *(Leave blank)*	2. REPORT DATE	3. REPORT TYPE AND DATES COVERED
	September 2001	Final, January 1999–January 2000

4. TITLE AND SUBTITLE
Comprehensive Visualization of Interface Defeat-Based Ballistic Impact Damage in a Titanium Carbide (TiC) Ceramic Target Disk

5. FUNDING NUMBERS
98M434

6. AUTHOR(S)
William H. Green, Joseph M. Wells, and Nevin L. Rupert

7. PERFORMING ORGANIZATION NAME(S) AND ADDRESS(ES)
U.S. Army Research Laboratory
ATTN: AMSRL-WM-MD
Aberdeen Proving Ground, MD 21005-5069

8. PERFORMING ORGANIZATION REPORT NUMBER
ARL-TR-2565

9. SPONSORING/MONITORING AGENCY NAMES(S) AND ADDRESS(ES)

10.SPONSORING/MONITORING AGENCY REPORT NUMBER

11. SUPPLEMENTARY NOTES

12a. DISTRIBUTION/AVAILABILITY STATEMENT
Approved for public release; distribution is unlimited.

12b. DISTRIBUTION CODE

13. ABSTRACT*(Maximum 200 words)*

This study was initiated to demonstrate the feasibility of applying the state-of-the-art nondestructive testing methodology known as x-ray computed tomography (CT) to a ballistic damage assessment. Specifically desired is the capture, digitization, and display, in both two-dimensional (2-D) and three-dimensional (3-D) formats, of the actual mesocracking damage created in bulk ceramic targets following an interface defeat or dwell ballistic impact experiment. Dwell involves the delay, and interface defeat involves the prevention, of penetration by a long rod penetrator into the ceramic. In each mechanism, the penetrator material contacting the ceramic front face flows laterally. These mechanisms occur at or near the impacted front surface of a highly confined armor ceramic material and may result in considerable subsurface or interior damage. This study also reports on the development of a new capability to graphically represent the full assemblage of networked interior mesocracks by an isolated 3-D point cloud or wireform model which aids significantly in the visualization and understanding of the entire mesocracking damage network. Practical limits of image spatial resolution with this technique (≈400 μm for large volume samples) preclude the nondestructive characterization of the detailed microcracking damage at this time.

14. SUBJECT TERMS
x-ray computed tomography, TiC ceramic, ballistic impact, interface defeat, mesocracking, 2-D and 3-D visualization, multiplanar reconstruction, 3-D solid reconstruction, 3-D point cloud, wireform model

15. NUMBER OF PAGES
125

16. PRICE CODE

17. SECURITY CLASSIFICATION OF REPORT	18. SECURITY CLASSIFICATION OF THIS PAGE	19. SECURITY CLASSIFICATION OF ABSTRACT	20. LIMITATION OF ABSTRACT
UNCLASSIFIED	UNCLASSIFIED	UNCLASSIFIED	UL

INTENTIONALLY LEFT BLANK.